SERI/TP--211-3952

DE91 002112

SERI/TP-211-3952
UC Category: 273
DE91002112

High Efficiency Cadium and Zinc Telluride-Based Thin Film Solar Cells

Final Subcontract Report
1 March 1989 - 28 February 1990

A. Rohatgi
C. J. Summers
A. Erbil
R. Sudharsanan
S. Ringel
School of Electrical Engineering
Georgia Institute of Technology
Atlanta, Georgia

October 1990

SERI Technical Monitor: R. Mitchell

Prepared under Subcontract No. XL-7-06031-1

Solar Energy Research Institute
A Division of Midwest Research Institute

1617 Cole Boulevard
Golden, Colorado 80401-3393

Prepared for the
U.S. Department of Energy
Contract No. DE-AC02-83CH10093

NOTICE

Printed in the United States of America
Available from:
National Technical Information Service
U.S. Department of Commerce
5285 Port Royal Road
Springfield, VA 22161

Price: Microfiche A01
Printed Copy A05

Codes are used for pricing all publications. The code is determined by the number of pages in the publication. Information pertaining to the pricing codes can be found in the current issue of the following publications which are generally available in most libraries: *Energy Research Abstracts (ERA)*; *Government Reports Announcements* and Index (*GRA* and I); *Scientific and Technical Abstract Reports (STAR)*; and publication NTIS-PR-360 available from NTIS at the above address.

TABLE OF CONTENTS

1. INTRODUCTION

Recent advances in polycrystalline CdTe solar cells have generated a lot of interest in this area. CdTe cell efficiencies in excess of 12% have been verified with the potential of approaching 20%. However, in order to attain this potential, considerable amount of basic research needs to be done. More specifically, there is a need to understand the loss mechanisms including optical losses, bulk and interface recombination, grain boundary effects and resistance losses. Several different technologies have produced CdTe cell efficiencies in excess of 10%. However, different loss mechanisms are not understood well enough to make a precise comparison between the technologies and to provide guidelines for improvements. It may be necessary to develop new tools and models, and apply existing tools more prudently, in order to reveal and quantify loss mechanisms in CdTe solar cells.

The motivation for developing a wide bandgap photovoltaic material stems from the fact that the optimum two cell tandem design consists of 1.7 eV bandgap cell on top of a 1 eV bandgap cell. A high efficiency wide bandgap cell on top of a 15% efficient low bandgap cell can give tandem cell efficiency on the order of 20%. Considerable progress has been made on the bottom cell, particularly $CuInSe_2$ which has given a small area cell efficiency > 14%. But the 1.7 eV bandgap material based on II-VI elements for the top cell has not yet been discovered.

There are two ways of realizing ~20% efficient polycrystalline tandem solar cells. The first approach involves improving the CdTe cell efficiencies in excess of 15% and utilizing only a small amount of power from the bottom cell because of 1.5 eV bandgap of CdTe. The second approach is to develop a high efficiency (>10%) 1.7 eV bandgap cell with significant subgap transmission and take greater advantage of the high efficiency (~15%) bottom cell. This research addresses both approaches by fabricating CdTe as well as 1.7 eV bandgap CdZnTe solar cells.

The overall goal of this program is to improve basic understanding of CdTe and ZnTe alloys, by growing and characterizing these films along with cell fabrication. The major objective is to develop wide bandgap (1.6-1.8 eV) material for the top cell, along with compatible window material and transparent ohmic contact, so that cascade cell design can be optimized.

In this program, front wall solar cells were fabricated with glass/SnO_2/CdS window with thin CdS

layer to maximize transmission and current. Wide bandgap absorber films (E_g = 1.75 eV) were grown by MBE and MOCVD techniques, which provide excellent control for tailoring the film composition and properties. CdZnTe and HgZnTe films were grown by MBE and CdMnTe is grown by MOCVD. CdTe films were also grown both by MBE and MOCVD techniques. All the as-grown films were characterized by several techniques like X-ray diffraction (XRD), Surface photovoltage spectroscopy (SPV), Infrared spectroscopy (IR), Raman and photoluminescence, and Auger electron spectroscopy (AES) for composition, bulk uniformity, thickness, film and interface quality. Front-wall type solar cells were fabricated in collaboration with AMETEK materials research laboratory using CdTe, CdZnTe, and CdMnTe polycrystalline absorber films. The effects of processing on ternary films were studied by AES and XPS measurements coupled with C-V and I-V measurements. Bias dependent spectral response and electrical measurements were used to test some models in order to identify and quantify dominant loss mechanisms.

2. TECHNICAL PROGRESS

The technical progress has been divided into five sections. The growth and characterization of CdZnTe, CdMnTe, and HgZnTe films are described in section 2.1 and 2.2. Section 2.3 deals with the processing related effects on MBE-grown CdZnTe films. CdTe, CdZnTe, and CdMnTe device measurements and analysis of the films and solar cells are described in section 2.4 and 2.5.

2.1 A STUDY OF POLYCRYSTALLINE Cd(Zn,Mn)Te/CdS FILMS AND INTERFACES

This paper will be published in the Journal of electronic materials March, 1990.

2.1.1. Introduction

In recent years, CdTe has become a strong candidate for photovoltaic applications due to its optimum bandgap, high absorption coefficient, and ease of deposition. Cell efficiencies of ~13% have been reported for single crystal CdTe solar cells (1) and greater than 12% for polycrystalline thin film CdTe cells (2). It has been projected (3) that thin film cell efficiencies in the range of 15-20% can be obtained by a tandem cell design consisting of two cells of different bandgap semiconductors on top of each other (1.7 eV on 1.1 eV). Semiconducting alloys such as $Cd_{1-x}Zn_xTe$ and $Cd_{1-x}Mn_xTe$ are good candidates for the top cell since their bandgaps can be tailored between 1.45 eV (CdTe) and 2.26 eV (ZnTe) or 3.0 eV (MnTe) by adjusting the film composition. However, very few attempts have been made to grow these films in polycrystalline form (4-6) and hence little is known about the properties of such films, particularly when grown on coated glass substrates that are suitable for solar cells. Good control of bulk composition and reduced or no interdiffusion at the Cd(Zn,Mn)Te/CdS interface is important for high performance devices based on these materials.

In this work, polycrystalline $Cd_{1-x}Zn_xTe$ and $Cd_{1-x}Mn_xTe$ films were grown by molecular beam epitaxy (MBE) and metalorganic chemical vapor deposition (MOCVD), respectively, on CdS/SnO_2/glass substrates to form frontwall solar cell structures. X-ray diffraction (XRD), electrochemical surface photovoltage (SPV), and Auger electron spectroscopy (AES) measurements were performed to determine the proper growth conditions for obtaining a uniform bandgap and composition throughout the film and an abrupt film/CdS

interface. In this paper we report growth-induced variations in the composition and interface quality of the heterojunctions formed by MBE and MOCVD grown polycrystalline ternary films.

2.1.2. Growth and Characterization of Films

Polycrystalline $Cd_{1-x}Zn_xTe$ and CdTe films were grown by MBE using a Varian Gen II MBE system. Elemental sources with a purity better than 5N were used for all constituents. The films were grown on CdS/SnO_2/glass and glass substrates which were cleaned in trichloroetyelene, acetone, methonol, deionized water, and blow dry, as a standard degreasing procedure. The substrates were baked in a vacuum of ~ $1x10^{-7}$ torr at 250 C for 2 hours prior to film growth. During film growth, the substrate temperature was kept at 275 C for 30 minutes to commence film growth and increased to 300 C for the remainder of the run. Growth rates were typically ~ 1um/hr for both the $Cd_{1-x}Zn_xTe$ and CdTe films.

Polycrystalline $Cd_{1-x}Mn_xTe$ films were grown by MOCVD on CdS/SnO_2/glass substrates using a Cambridge Instruments MR102 MOCVD system. The source materials for Cd and Te were dimethylcadmium (DMCd) and diisopropyltellurium, respectively. Two different Mn sources were used, tricarbonyl methylcyclopentadienyl manganese (TCPMn) and Bis (isopropylcyclopentadienyl) manganese (BCPMn) to study the effects of different sources on the film properties. Cadmium and tellurium source temperatures were maintained at 0° C and 20° C, respectively, while the manganese source temperature was varied in the range 80° C to 100° C for both TCPMn and BCPMn. In order to investigate the effects of the growth conditions, the reactor pressure was varied in the range of 50 to 250 torr and the substrate temperature was varied from 420° C to 450° C for $Cd_{1-x}Mn_xTe$ films. The substrate temperature was kept at 400° C for CdTe films. Typical growth rates for $Cd_{1-x}Mn_xTe$ and CdTe films were 0.5 um/hr and 1.5 um/hr, respectively.

X-ray diffraction studies were performed to estimate the film composition using a Phillips PW1800 automatic diffractometer with 1.504 A Cu-K_α radiation. The lattice constants, a, of the $Cd_{1-x}Zn_xTe$ films were determined from the XRD data by plotting the lattice parameter, a(Θ), against its angular dependence (Θ) and determining the intercept according to (7)

$$a(\Theta) = 0.5[(\cos^2\Theta/\sin\Theta) + (\cos^2\Theta/\Theta)] \qquad (1)$$

where 2 is the diffraction peak position. The film composition (x) was determined from the lattice constant according to (8,9)

$$a(x) = 6.481 - 0.381x \quad (A), \qquad \text{for } Cd_{1-x}Zn_xTe \qquad (2)$$

and

$$a(x) = 6.487 - 0.149x \quad (A), \qquad \text{for } Cd_{1-x}Mn_xTe \qquad (3)$$

where x is the atomic concentrations of Zn and Mn in the $Cd_{1-x}Zn_xTe$ and $Cd_{1-x}Mn_xTe$, respectively.

The absorption edge or bandgap of the films was estimated by a nondestructive electrochemical SPV measurement in which an electrolyte composed of 0.2M NaOH and 0.1M EDTA (ethylenediaminetetraacetic acid) forms a Schottky barrier contact with the film surface. This barrier separates the photogenerated carriers to produce the open circuit voltage as a function of incident wavelength. This technique is also capable of providing information about bandgap variations within the film because the electrolyte/semiconductor junction can be biased so that controlled etch-steps can be made between SPV measurements. Hence, compositional variations in the direction of film growth can be monitored. This technique has been discussed in more detail elsewhere. (10,11) Bandgaps of the films were estimated from the wavelength ( ) at the midpoint of the absorption edge (E_g(eV) = 1.24/ (um)) in the SPV response. It should be noted that in certain cases, the sharpness of the absorption edge can be influenced by the diffusion length and film thickness.

To gain further confirmation on the compositional uniformity of the ternary films, AES profile measurements were performed using a Physical Electronics Model 600 Scanning Auger Multiprobe. The angle between the sample normal and the electron beam was 45°. All AES data were taken using a 3 KeV electron beam with a current of 1.0 uA. Sputter profiling was performed using a normally incident 2 KeV Ar ion beam at a current density of 28 uA/cm^2.

2.1.3. Results and Discussion

A. MBE-grown polycrystalline $Cd_{1-x}Zn_xTe$ and CdTe films

In order to achieve optimal composition (x = 0.3-0.4) or bandgap (1.65-1.75 eV) for tandem solar cell applications, MBE films were grown with various Zn/(Cd + Zn) ratios. Figure 1 shows a comparison of XRD spectra of a CdTe film and a $Cd_{1-x}Zn_xTe$ film grown with a Zn/(Cd + Zn) beam flux ratio of 0.4 on CdS/SnO_2/glass substrates. A comparison of the peak positions and relative amplitudes in each diffraction pattern with the tabulated values (10) suggests that in both cases the CdTe cubic structure is the only detectable phase. By determining the lattice parameter ($a(\theta)$) associated with each major $Cd_{1-x}Zn_xTe$ diffraction peak, the lattice constant (a) of the film was determined according to equation (1). By combining this information with the measured bandgap from the SPV (Figure 3) for several films grown with various Zn/(Cd + Zn) beam flux ratios, a correlation was established between the growth conditions (Zn/(Cd + Zn) beam flux ratio), film composition, and bandgap for the MBE-grown polycrystalline $Cd_{1-x}Zn_xTe$ films and is shown in Figure 2. A linear dependence was found between these parameters for the composition range investigated which indicates proper substitution of Zn for Cd in the MBE films. This result is consistent with data reported for single crystal $Cd_{1-x}Zn_xTe$ films grown by other techniques [6,8], suggesting that grain boundaries do not influence the reproducibility and control of film composition. Furthermore, this linear relationship was found to be independent of growth rate and Te flux.

Figure 3a shows an SPV spectrum of a $Cd_{1-x}Zn_xTe$ film grown on the CdS/SnO_2/glass substrate. The sharp absorption edge indicates that the film has uniform composition and negligible sub-bandgap absorption. The compositional uniformity in the direction of film growth was investigated in more detail by Auger depth profiling. Figure 3b shows a uniform distribution of Cd, Zn, and Te throughout the film thickness, consistent with the sharp SPV cutoff. The $Cd_{1-x}Zn_xTe$/CdS interface was found to be much sharper than the $Cd_{1-x}Mn_xTe$/CdS interface grown by MOCVD (discussed in the following section) indicating less interdiffusion between MBE-grown films and the substrate.

B. MOCVD-grown Polycrystalline $Cd_{1-x}Mn_xTe$ Films on CdS/SnO_2/glass Substrates

Two different Mn sources, TCPMn and BCPMn, were used to grow $Cd_{1-x}Mn_xTe$ films by MOCVD. We were not able to obtain compositionally uniform films using the TCPMn source. This is reflected in the SPV spectra and Auger depth profile (Figure 4) for a $Cd_{1-x}Mn_xTe$ film grown on CdS/SnO_2/glass substrates using the TCPMn source maintained at 80° C. The SPV response has a broad absorption edge (which can result from nonuniform composition and/or low diffusion length) which makes it difficult to accurately

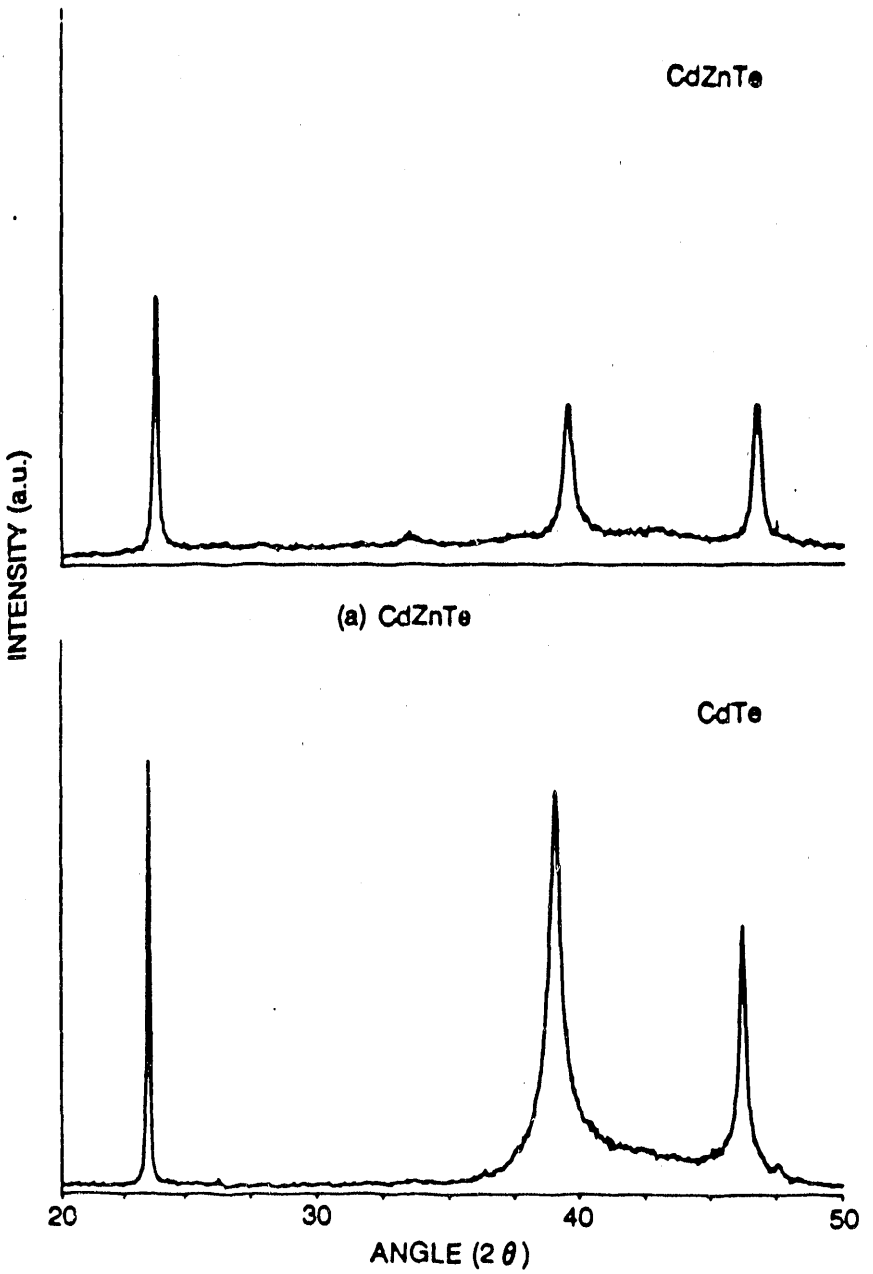

Figure 1. X-ray diffraction spectra of MBE-grown polycrystalline

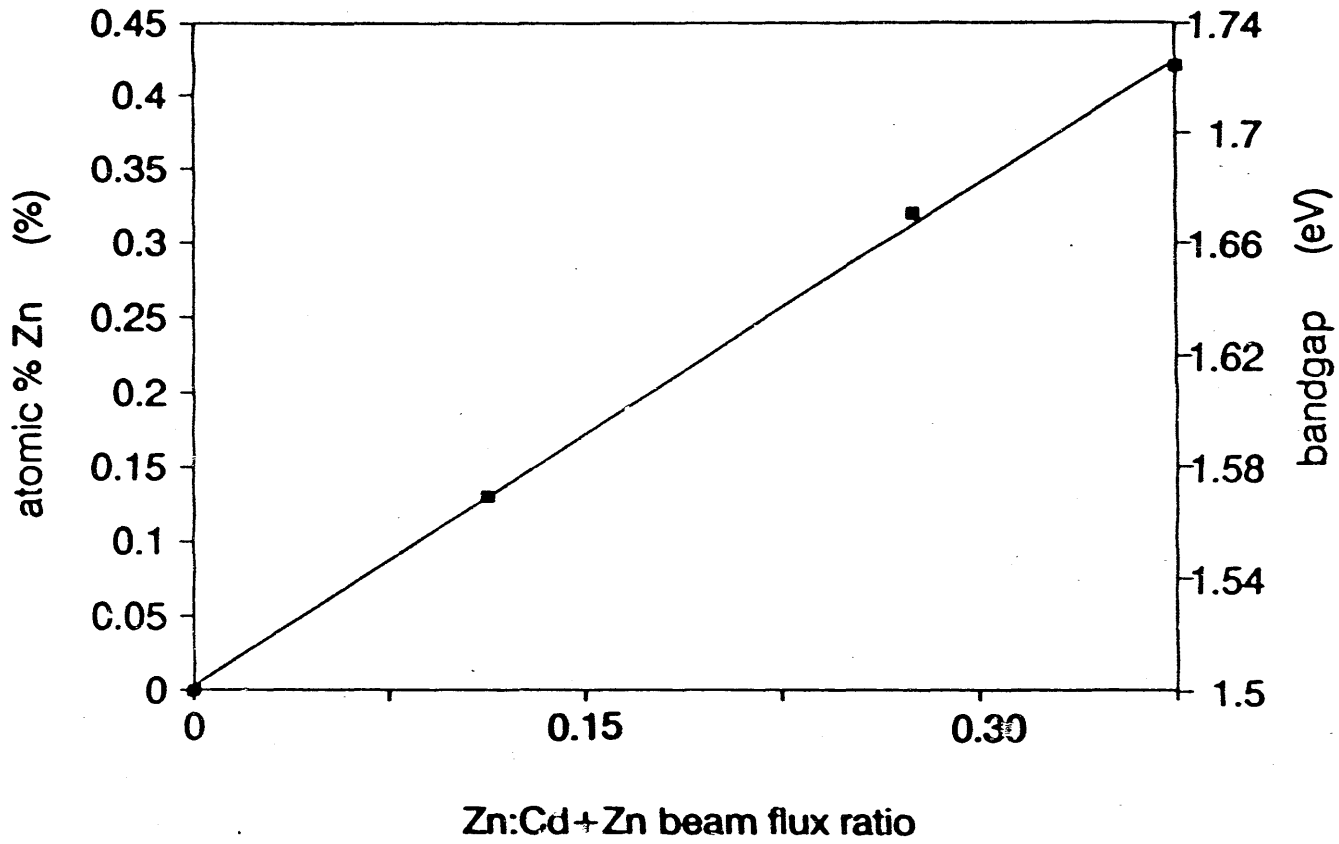

Figure 2. Concentration of Zn calculated from x-ray data and eq. (2), and bandgap measured by surface photovoltage for MBE-grown CdZnTe films grown using various Zn:Cd + Zn beam flux ratios as shown.

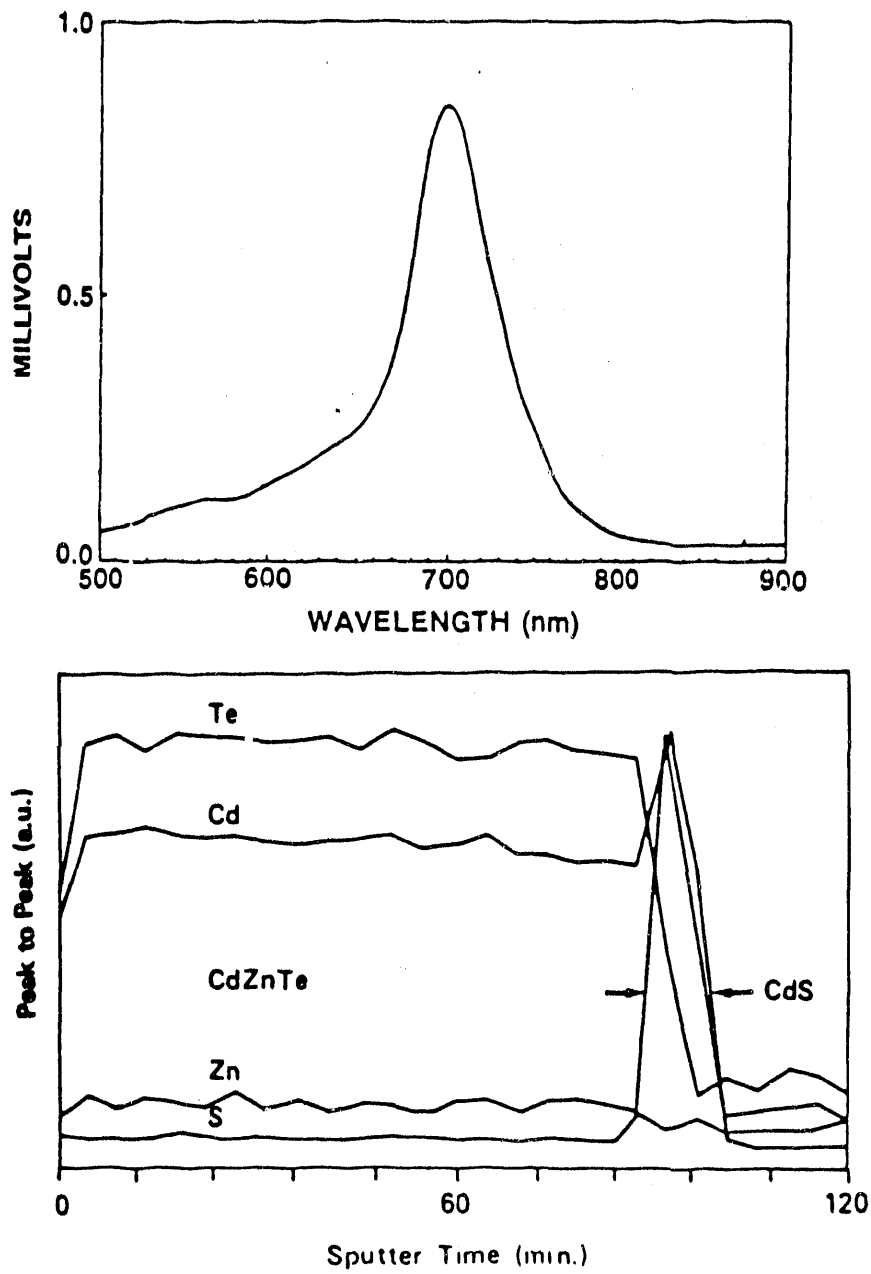

Figure 3. (a) SPV spectra and (b) Auger depth profile of an MBE-grown CdZnTe film with a bandgap of 1.7 eV on a CdS/SnO_2/glass substrate.

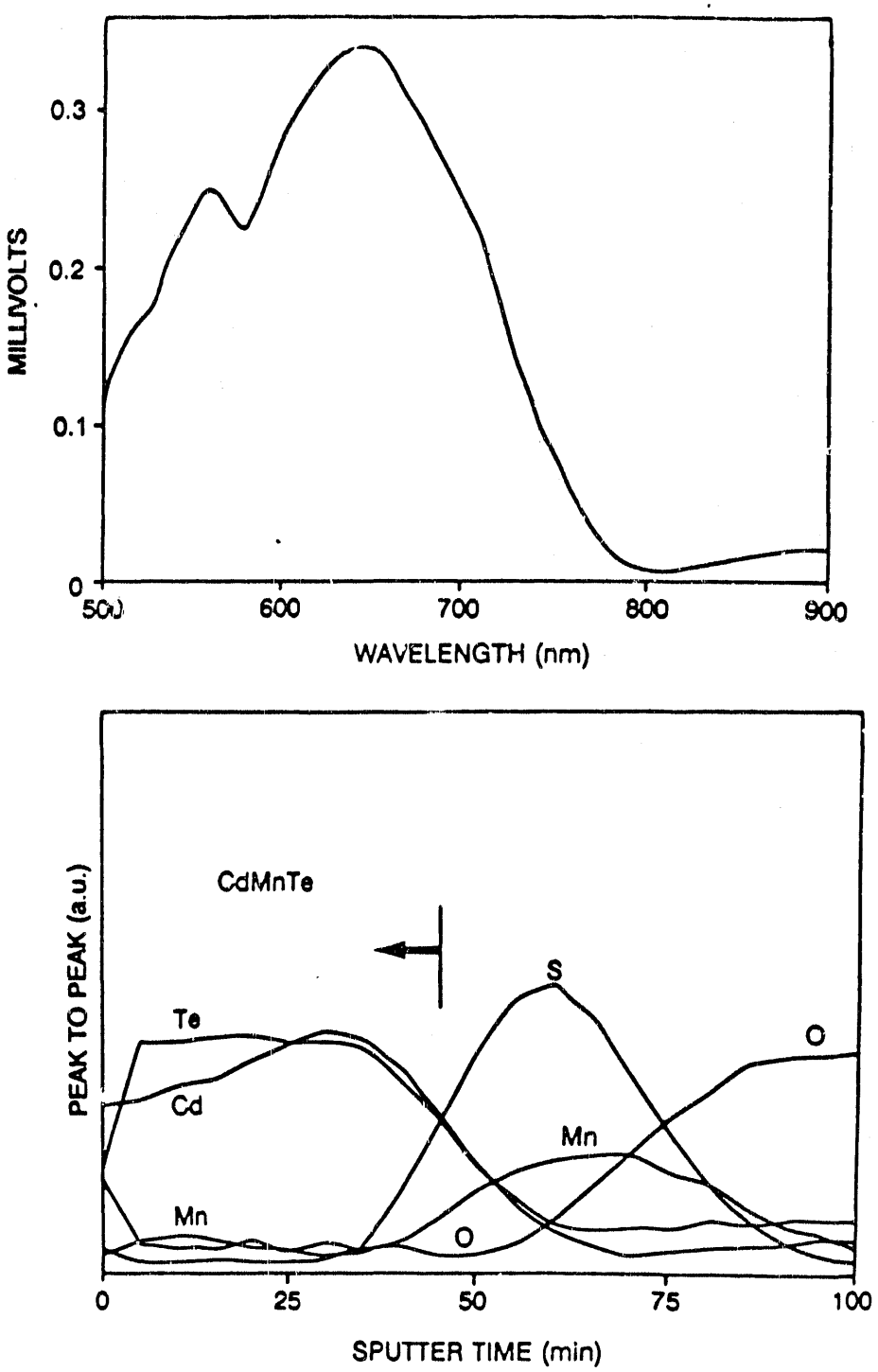

Figure 4. (a) SPV spectra and (b) Auger depth profile of an MOCVD-grown CdMnTe film on a CdS/SnO_2/glass substrate using the TCPMn source.

determine a single bandgap. If we take an average of the absorption cutoff at 1.74 eV, the average Mn concentration is estimated to be ~ 16% for this film using the relationship E_g = 1.50 + 1.34x eV at room temperature. (9) Considering the significant nonuniformity of the film, this is in reasonable agreement with the XRD value of 11% obtained from equation (3). In contrast to the TCPMn source, we had more success in growing relatively uniform $Cd_{1-x}Mn_xTe$ films using the BCPMn source as depicted by the more uniform Auger depth profile and sharper SPV cutoff, Figure 5. These films were grown with a source temperature of 100° C (rather than 80° C for the TCPMn source) and a reactor pressure of 50 torr (instead of 250 torr for TCPMn). The higher Mn source temperature transports more Mn due to its higher vapor pressure which may help Mn incorporation into the $Cd_{1-x}Mn_xTe$ film. Low reactor pressure increases the velocity of all alkyls, which reduces the residence time inside the reactor thus avoiding unwanted reactions and possible Mn pileup. Thus, the above two factors may help but cannot fully account for uniform composition of the films grown with the BCPMn source because $Cd_{1-x}Mn_xTe$ films grown with the TCPMn source under similar conditions did not produce uniform films. These results suggest that further optimization of growth conditions is necessary to obtain uniform films using the TCPMn source. Recently, atttempts were made [12] using a TCPMn source to grow Mn-doped ZnS films which resulted in poor electroluminescent properties of the film due to .he formation of $MnOCO_2$ compounds.

The compositional uniformity in the direction of film growth (normal to the substrate) was investigated for $Cd_{1-x}Mn_xTe$ films grown using both TCPMn and BCPMn sources. Use of the BCPMn source resulted in a more uniform film but did not prevent the interdiffusion of Mn at the $Cd_{1-x}Mn_xTe$ interface as shown by Auger depth profile data (Figure 5) as compared to the films grown using the TCPMn source. In the case of non-uniform films grown with the TCPMn source, significant interdiffusion led to Mn pile-up near the interface which was further verified by Auger measurements made on a cleaved cross-section of the sample. However, the amount of Mn pile-up for the film grown using the BCPMn source was significantly lower. In order to gain better understanding of the interdiffusion and Mn pile-up near the interface region, Auger depth profile analysis was performed on a single crystal $Cd_{1-x}Mn_xTe$ grown on GaAs (111) under the same conditions using both Mn sources to determine the influence of the substrate. No accumulation of Mn was detected near the $Cd_{1-x}Mn_xTe$/GaAs interface, suggesting that the substrate temperature of 420° C is not the reason for the observed Mn interdiffusion, instead the interdiffusion in the polycrystalline case may

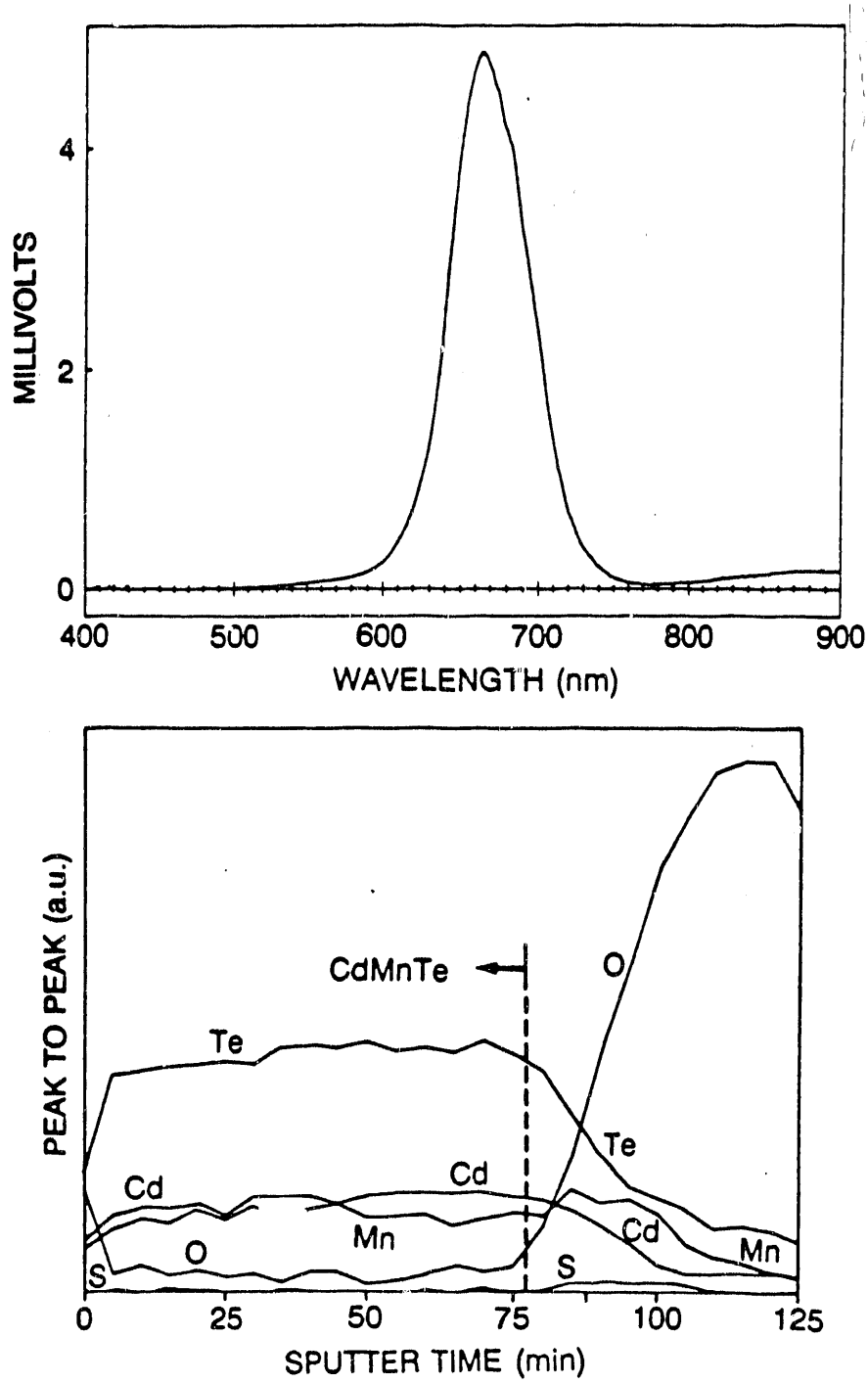

Figure 5. (a) SPV spectra and (b) Auger depth profile of an MOCVD-grown CdMnTe film on a CdS/SnO_2/glass substrate using the BCPMn source.

be due to an exchange reaction between the Cd in the underlying CdS film and the Mn in the $Cd_{1-x}Mn_xTe$ film. This suggests that the stability of the $Cd_{1-x}Mn_xTe$/CdS interface influences the uniformity of the films in the growth direction. This is probable because the Mn-S bond is stronger than the Mn-Te bond (13) from thermodynamic considerations, which may drive Mn into the CdS where it replaces Cd. Further measurements are necessary to confirm the mechanism of interdiffusion between CdS and $Cd_{1-x}Mn_xTe$ films.

Finally, even the MOCVD-grown CdTe/CdS interface was found to be somewhat broader than MBE-grown CdTe/CdS and $Cd_{1-x}Zn_xTe$/CdS interfaces, Figure 6. This may be the result of higher MOCVD growth temperatures. In spite of the broad interfaces we were able to achieve 9.7% efficient CdTe/CdS solar cells from MOCVD (14). The best MBE CdTe solar cell efficiencies are ~10.5%. (14) Ternary based cells are being investigated and will be reported in the future.

2.1.4. Conclusions

Polycrystalline $Cd_{1-x}Zn_xTe$ and $Cd_{1-x}Mn_xTe$ films with a bandgap of 1.7 eV were successfully grown on glass/SnO_2/CdS substrates by MBE and MOCVD techniques, respectively. Polycrystalline $Cd_{1-x}Zn_xTe$ films grown by MBE resulted in uniform composition and sharp interfaces, which are important for high performance devices. No new phase was detected as a result of introducing Zn ($x<0.4$) in the CdTe structure. A linear relationship was found between the Zn/(Cd+Zn) beam flux ratio and bandgap for the MBE-grown $Cd_{1-x}Zn_xTe$ films. However, polycrystalline $Cd_{1-x}Mn_xTe$ films grown by MOCVD had nonuniform composition and showed evidence of Mn accumulation at the $Cd_{1-x}Mn_xTe$/CdS interface. It was found that Mn interdiffuses and replaces Cd in the CdS film. The degree of interdiffusion was also found to be a function of the Mn source with the TCPMn source producing an inferior interface compared to the BCPMn source for the growth conditions used here.

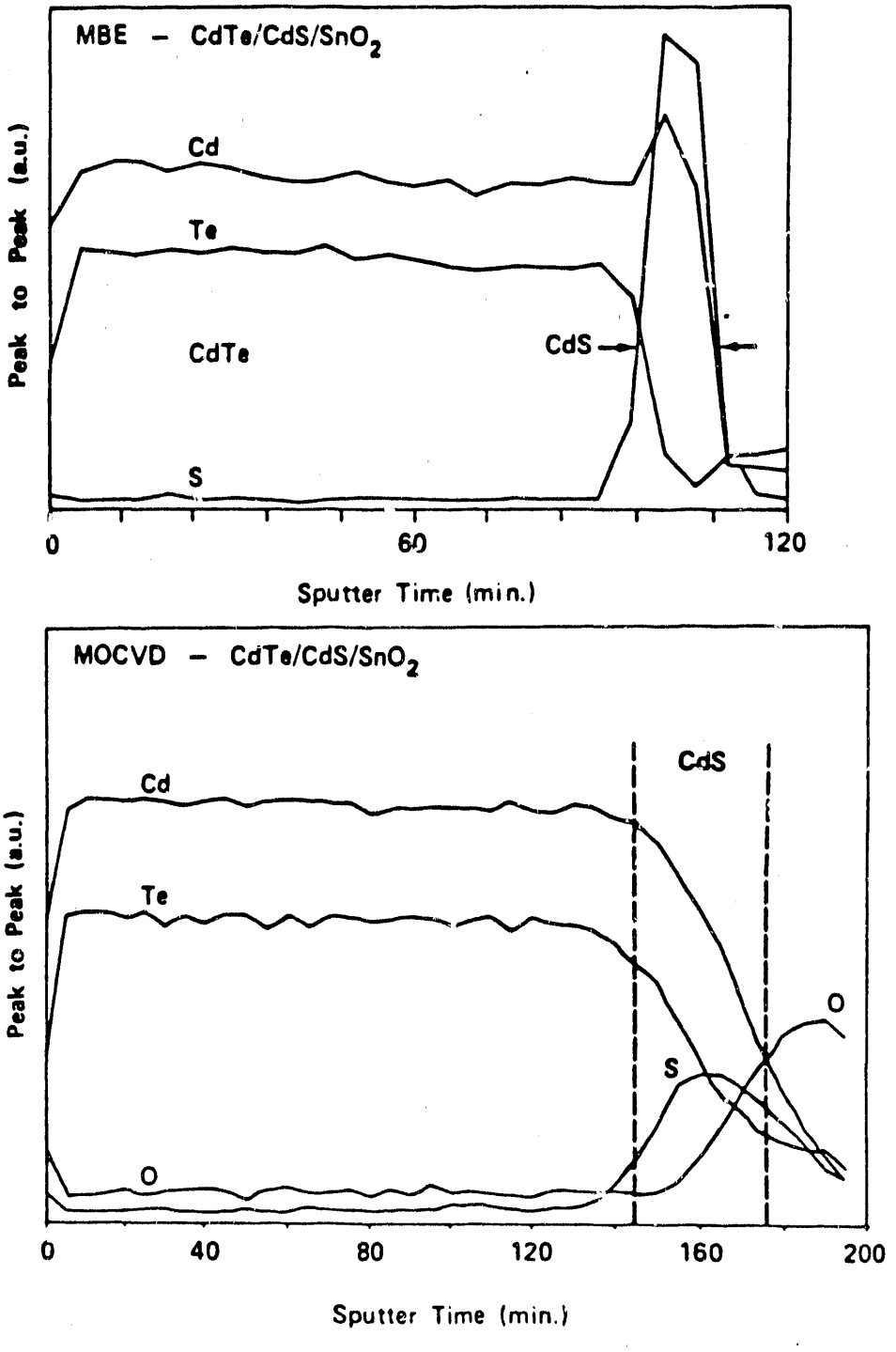

Figure 6. Auger depth profiles of (a) MBE-grown and (b) MOCVD-grown CdTe on CdS/SnO_2/glass substrates.

2.2. GROWTH OF CdTe AND Hg-BASED ALLOYS BY CHEMICAL BEAM EPITAXY

(This paper will appear in J. Vac. Sci. Tech. 1990).

2.2.1. INTRODUCTION

We describe in this paper the development of a chemical beam epitaxial (CBE) growth technique for HgCdTe and related alloys. As discussed in detail below, this technique offers many significant advantages over current growth technologies and is well suited to grow new detector designs for enhanced long-wavelength detection. (1)

Currently, the flexibility of conventional MBE is limited because little control is possible over the atomic species applied to the growth surface. The evaporation of group VI and V species produce dimer and tetramer molecules which are difficult to effectively incorporate at the growth surface. (2) Also, although the evaporation of the Li and Ag (p-type) and the Ga and In (n-type) dopants produce monomer species, their high diffusion rates on the cation sublattice prevent precise dopant profiles from being obtained. (3-5) Consequently, n- and p-type doping of HgCdTe alloys is still mostly accomplished by stoichiometric adjustment.

In chemical beam epitaxy, the use of hydride or metalorganic sources enables greater flexibility and more precise control to be achieved over the chemical reactions occuring during growth. Monomer, dimer, or tetramer species can be supplied to the growth surface depending on which species is found to optimize the nucleation and growth process. Additionally, the application of an incident photon flux can be used to supply additional kinetic energy to the growth surface and enables the selective photon enhancement of specific chemical reactions. The reduction of the desorption activation energy for Te which enhances Sb and As incorporation into CdTe is an example of the power of the photo-assisted technique. (6,7) Also, the role of monomer Te, produced by high temperature laser evaporation, in reducing the kinetic hinderance to growth has recently been demonstrated by Cheung. (8)

2.2.2. EXPERIMENTAL

Growth was performed in a Varian GEN II MBE system equipped with a reflection high energy electron diffraction (RHEED) system. Extensive modifications to the MBE system have been made to convert

it to a CBE system. These modifications and their justification are presented below in some detail.

Both (001) oriented CdTe and HgTe were grown on chemically polished (001) CdTe substrates (supplied by Galtech and II-VI Inc.) while (001) HgZnTe growth was achieved on (001) GaAs substrates. The HgTe was grown on CdTe buffers and the HgZnTe on ZnTe buffers. The Hg based layers were grown at a substrate temperature of 185 C and the CdTe layers were grown at substrate temperatures ranging from 185 to 320 C. Substrate surface temperatures below 230 C were measured by a recently developed Te-condensation technique. (9) Growth was carried out using elemental Zn, Cd, and Hg sources. The Hg flux was supplied by a Hg pressure controlled vapor source described previously. (10) The Te flux was supplied by a direct injection flow controller using diisopropyltelluride (DipTe) as the source gas. DipTe was chosen in order to minimize any possible carbon doping effects. (11) The detailed characteristics of these flow controllers and the injectors used to precrack the organometallics are also described below.

2.2.2a. Pumping System

Because of the relatively high gas loads and toxic gases used in CBE, a specially designed pumping system was implemented. This system, shown in Figure 1, was designed to handle the potentially hazardous and corrosive organometallics and hydrides as well as Hg vapor. Figure 1 shows a schematic representation of the pumping system. The main component of the system is a Balzers MBE Series turbomolecular pump. This pump has a pumping speed of 1400 l/s for N_2 and approximately 1000 l/s for Hg. (The turbomolecular pump was originally mounted horizontally on the growth chamber in order to maximize the conductance to the pump. However, in order to increase the bearing life, it has since been mounted vertically.) In case of a power or other type of failure, the turbomolecular pumping system is automatically isolated from the growth chamber by an 8" I.D. gate valve and vented with N_2 to prevent oil contamination. The MBE Series pump has features designed to minimize wear and contamination of the pump due to the particular nature of the process gases. These features include the use of inert Fomblin oil for lubrication, a large oil reservoir and oil pump to increase bearing life, and an inert gas purge of the bearings. Only stainles steel and an aluminum alloy are in contact with the process gases. The pump is also heated to prevent any condensation on these metallic surfaces and, thus, any reaction of Hg with the aluminum alloy is prevented.

Gas exhausted from the turbomolecular pump passes directly through an isolation valve into a

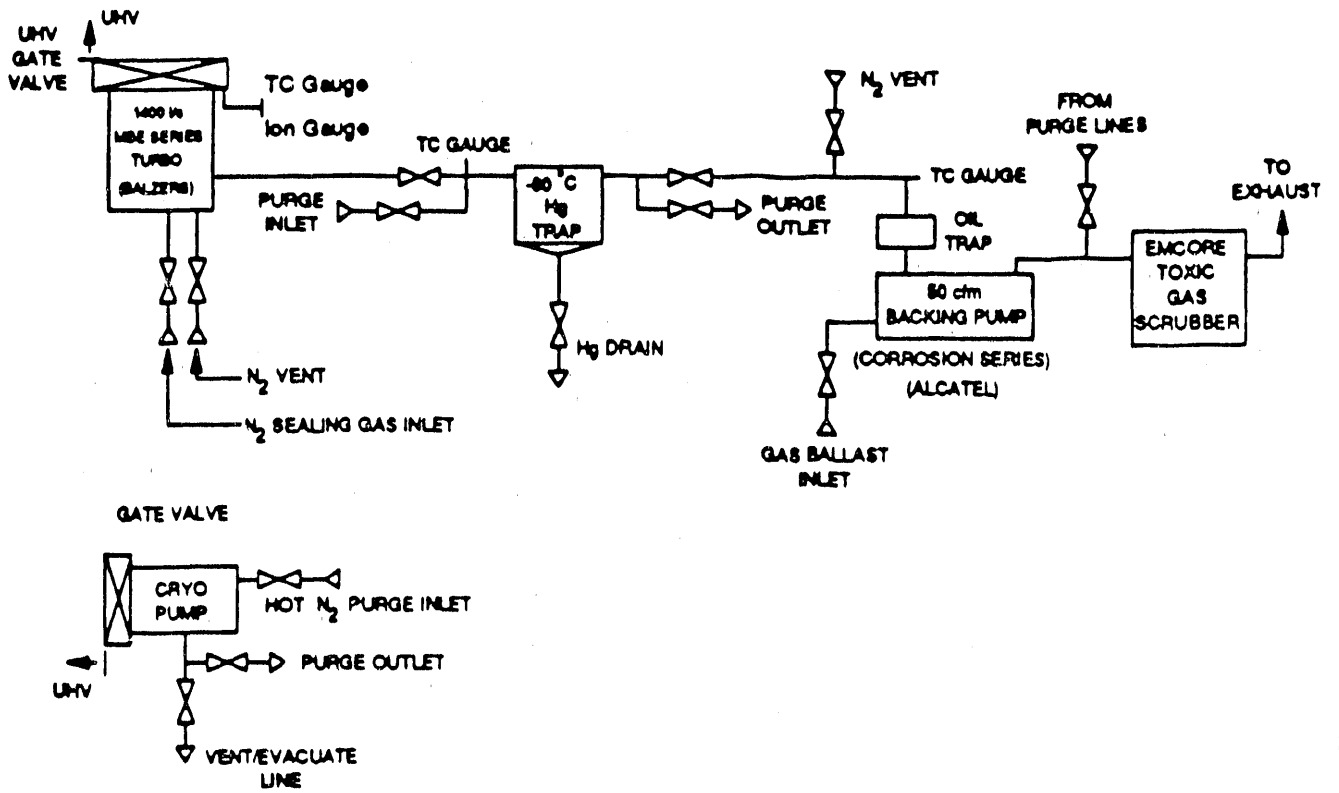

Figure 1. Schematic representation of CBE pumping system.

specially designed cold trap operated at -60 C. This trap condenses most of the Hg vapor and significantly minimizes the amount of Hg entering the mechanical backing pump. Valves on either side of the trap enable it to be isolated and warmed for removal of the condensed vapors. A micromaze oil vapor trap is included on the inlet of the backing pump to minimize contamination due to hydrocarbon backstreaming.

The backing pump, an Alcatel 50 cfm Corrosion Series Pump, is also designed such that process gases only come into contact with stainless steel and viton. The pump also uses inert gas ballasting to dilute and prevent condensation of the pumped vapors.

The exhaust line from the mechanical pump has inlets allowing atmospheric pressure purging of the various pumping and gas source lines. The Alcatel pump exhaust enters an Emcore toxic gas scrubber filled with a sulfur impregnated activated charcoal capable of absorbing up to 40 percent of its weight in Hg. This feature has no effect on the charcoal's ability to absorb organometallics and hydrides which can then be oxidized and disposed of in a controlled manner.

A Varian cryopump is also attached to the system and is capable of removing both Hg and organometallics from the growth ambient. Provisions are made for hot gas purging of the cryopump using the system described above.

Gas Sources

The gas sources utilized in the CBE system are of the pressure controlled variety rather than the conventional mass flow type. Mass flow controllers typically require inlet pressures of 50 torr to operate. However, due to the low vapor pressures of many organometallics, it is necessary to mix the source gas with a carrier gas such as hydrogen and, thus, carefully control the organometallic bubbler temperature. The pressure controlled vapor sources, however, require inlet pressures on the order of only one torr and hence are able to directly inject the source gases without a carrier gas. This not only simplifies the gas source construction, but also minimizes the gas load on the CBE system while maintaining the beam fluxes in the molecular flow regime. This is especially important in the growth of Hg-based materials because of the large Hg fluxes required.

The pressure controlled vapor sources operate on the principle of choked viscous flow through an orifice. This type of flow has the important properties that the flow is directly proportional to the pressure upstream of the orifice (note that the flow is quite insensitive to downstream pressure) and has only a square

root dependence on the gas temperature. A Hg source of this type has been designed and implemented in our laboratory. (10) For a more complete discussion of choked flow see Ref. 12. The Te, Cd, and Zn flow controllers operating on this principle have been obtained from MKS Instruments (Type 1150B) and use diisopropyltelluride (DipTe), diethylcadmium (DeCd), and diethylzinc (DeZn) as the source gases. These gases are the adduct purified grade obtained from Air Products Inc. The DipTe (10 sccm f.s.), DeCd, and DeZn (5 sccm f.s.) flow controllers have repeatabilities of 0.2%. These flow rates are estimated to produce growth rates of up to 2 fm/hr. The stability of the flow controllers is calculated to produce a stability in the Cd to Te ratio of approximately 0.1%. For $Hg_{1-x}Cd_xTe$ alloys with x=0.2, this stability corresponds to a deviation in the x value of 0.0002, a factor of 5-10 better than currently available with conventional thermal sources.

2.2.2b. Dopant Source

A p-type gas dopant source was also designed which operates on the same principle as the host gas sources. However, the dopant source is able to accurately regulate flow rates at four to eight orders of magnitude less than the host gas flow controllers. Arsine was chosen as the dopant gas although any of the organometallic As gases could be substituted when more fully developed. The pure arsine is contained in a small volume, low pressure bottle with a built-in flow limiting orifice thus minimizing the safety hazards usually associated with arsine. An absolute pressure regulator is utilized allowing control of the arsine at less than atmospheric pressure. The reduced pressure arsine is then fed through a stepper motor driven leak valve which maintains the downstream pressure as measured by a high accuracy capacitance manometer. This controlled pressure exits through another leak valve (which acts as an variable orifice) and enters the CBE growth chamber. The sensitivity of the manometer and valve feedback system gives the dopant source a four order of magnitude dynamic range for a fixed orifice setting. Changing the orifice setting allows the system to achieve an even greater dynamic range. Figure 2 shows a schematic of the dopant gas source.

2.2.2c. Injectors

In order to remove the cracking dependence from the substrate temperature, the source gases are precracked in a high temperature injector. To prevent gas phase reactions, two separate injectors are

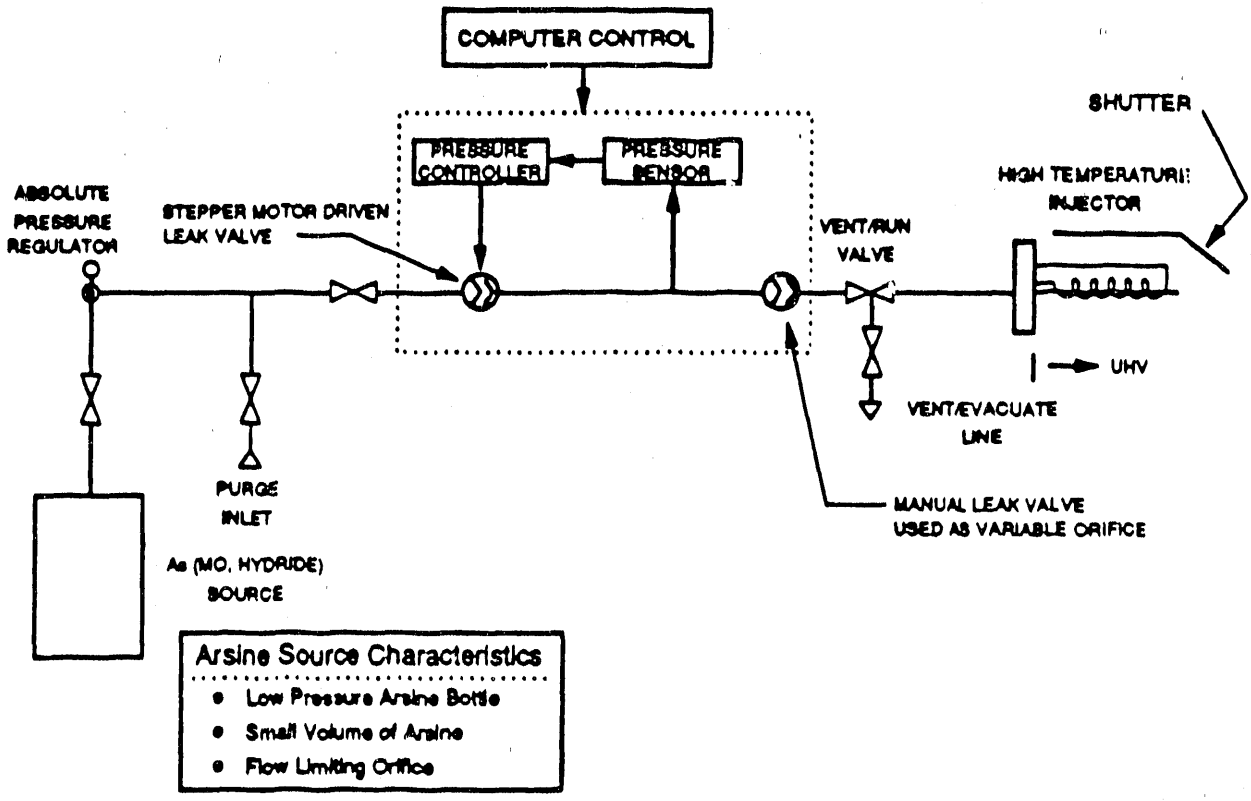

Figure 2. Schematic of arsine gas dopant source.

utilized. One for the group II elements and one for the group VI elements. This also allows optimization of the cracking conditions for each source gas. Both injectors have dual thermocouples to monitor the hot and cold zone temperatures. Each injector also has a specially designed boron nitride diffuser/nozzle element to enhance cracking and increase flux uniformity. The group II injector uses a 3/4 in. o.d. high purity Ta delivery tube while the group VI utilizes a pyrolitic boron nitride (PBN) delivery tube to avoid any reaction of Te and Ta. The diffuser element design is also different for each injector. More specifically, the group VI nozzle is designed to avoid recombination of monomer Te into its dimmer form.

2.2.3. RESULTS

A preliminary study was initiated to determine the DipTe cracking products and their dependence on the injector temperature. Data was taken with a UTI 100C quadrapole mass spectrometer (QMS) with particular attention to the production of monomer Te. Figure 3 shows the ratio of the Te^+ peak current to the $DipTe^+$ current as a function of injector temperature. It should be pointed out that with this particular injector, the temperature is measured outside the hot zone and, thus, only gives a relative indication of the actual cracking temperature.

Next, CdTe growth was undertaken using DipTe and a solid Cd source. While under a constant flux of Cd, growth was initiated and terminated using the DipTe vent/run valve. However, it was determined from RHEED intensity oscillation measurements that flux transients occurred when initiating the DipTe flux this way. Because of these transients, the MBE shutter was used to terminate and initiate the DipTe flow while the flow controller was used as a soft shut-off. No growth was observed with the DipTe flow on and the shutter closed. This shuttering method not only eliminates flux transients, but has the further advantages of minimizing the organometallic consumption and the gas load on the pumping system. If the flow controller only was used as the shuttering mechanism, the flow could be ramped off or on within 5 seconds. This corresponds to approximately 3 monolayers at a 0.5 fm/hr growth rate.

Growth rate measurements were obtained using RHEED intensity oscillations (Figure 4). Figures 5a and b show CdTe growth rates for a constant Cd flux as a function of DipTe flow for substrate temperatures of 250 and 300 C, respectively. At the low flows, the growth rate is limited by the Te arrival rate while at the higher flows, the growth rate saturates and is limited by the Cd flux. These curves

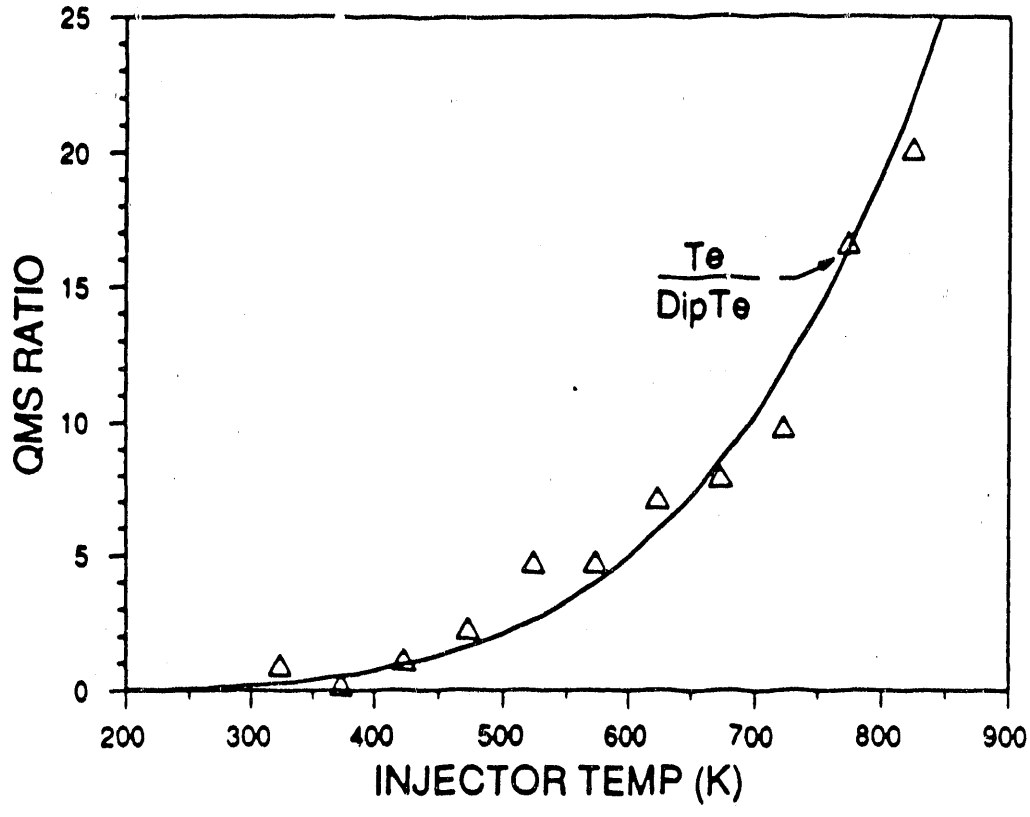

Figure 3. Ratio of QMS Te^+ current to DipTe$^+$ current as function of injector temperature.

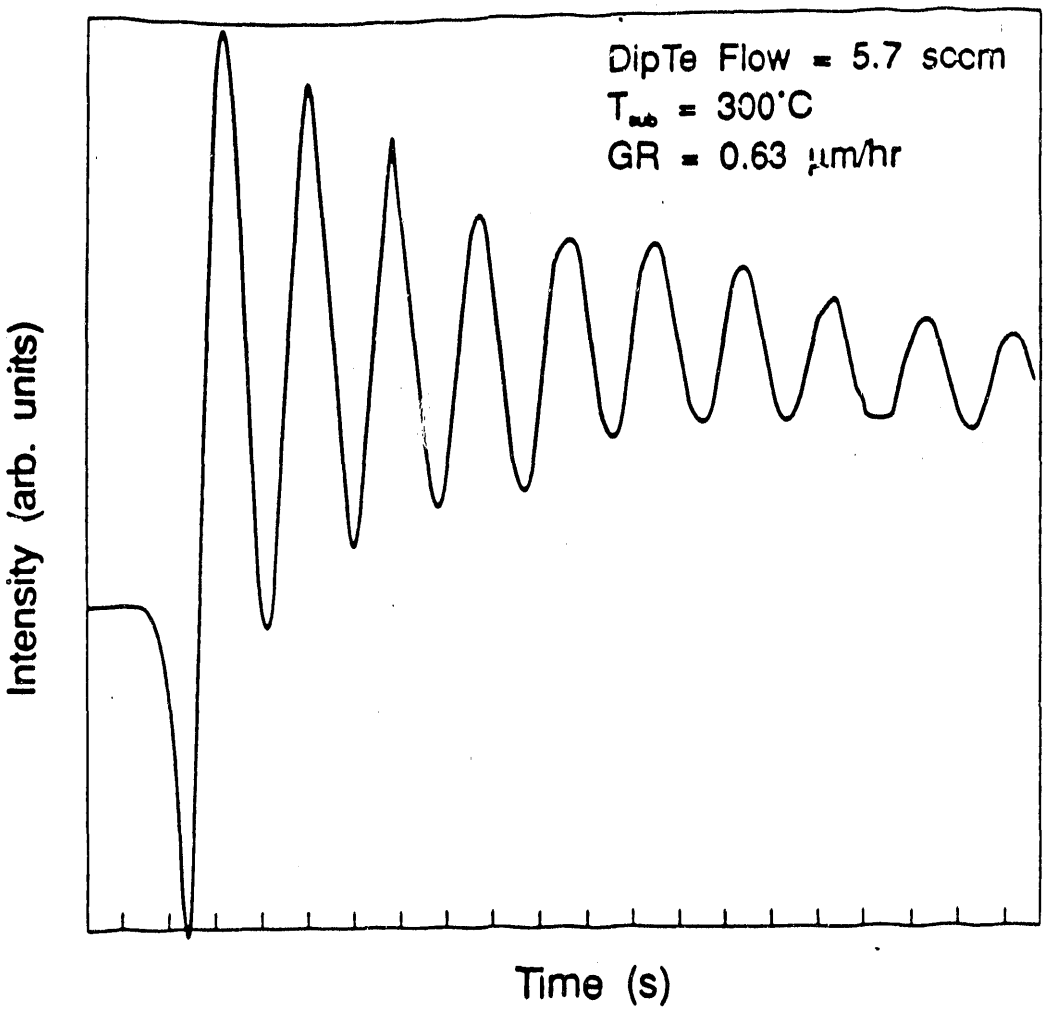

Figure 4. RHEED intensity oscillations for CdTe growth using elemental Cd and DipTe fluxes.

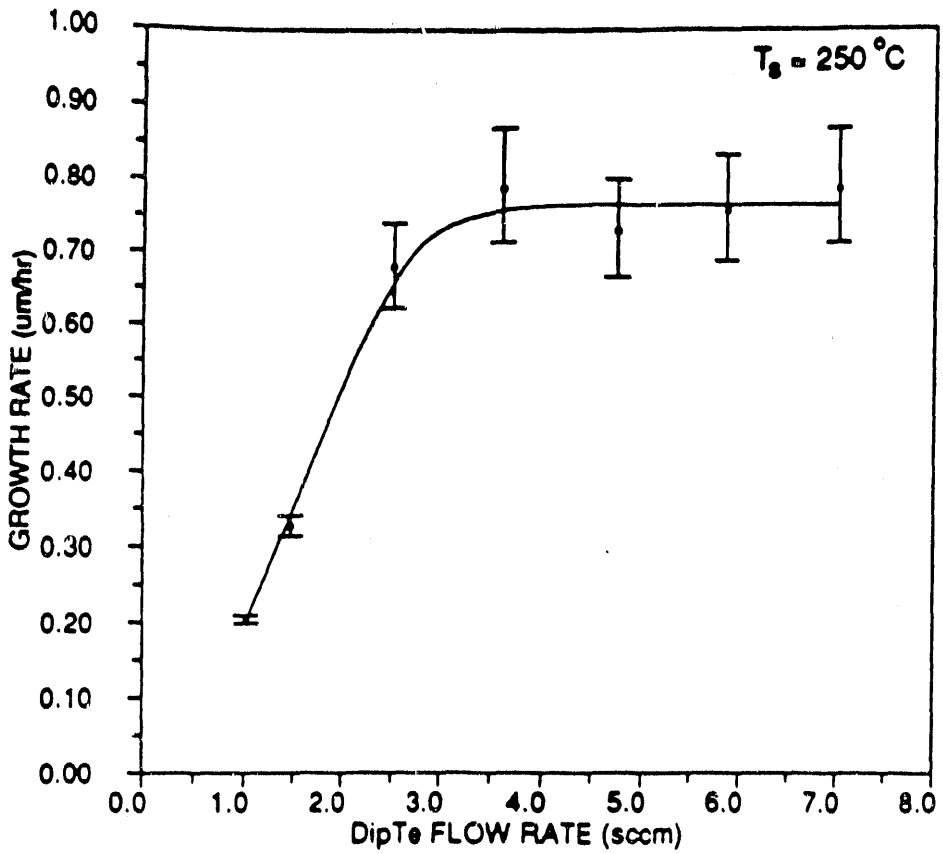

a) T_{sub} = 250 °C;

Figure 5. CdTe growth rate as function of DipTe flow rate:

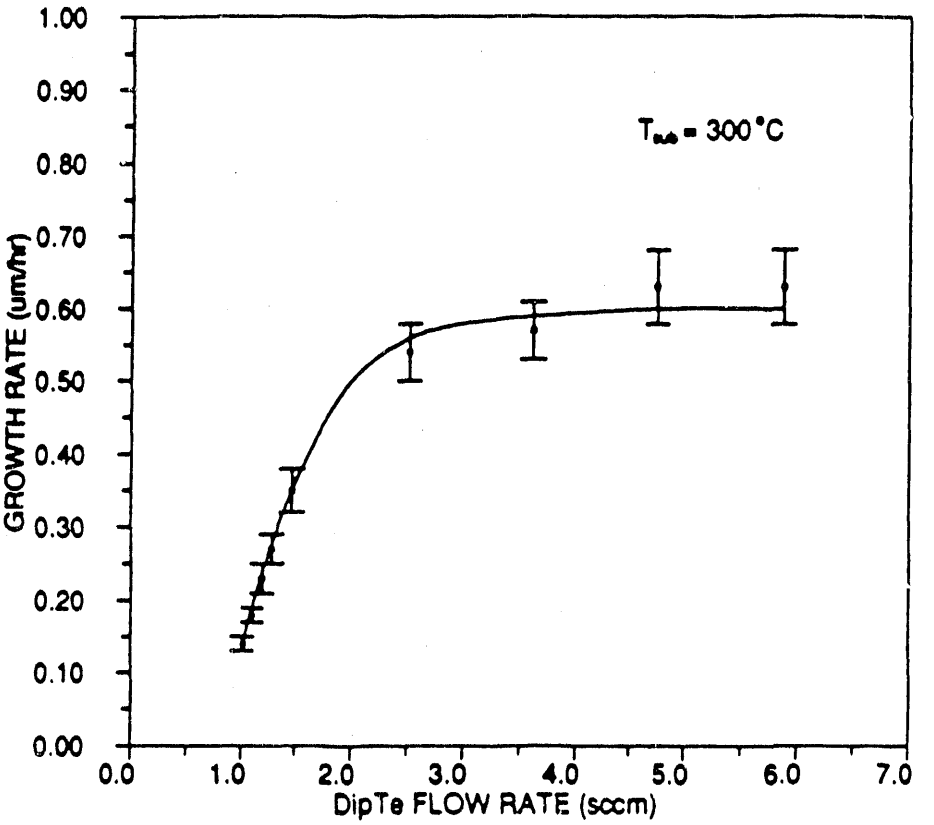

b) T_{sub} = 300 °C.

Figure 5. CdTe growth rate as function of DipTe flow rate

demonstrate the flexibility of the CBE technique for adjusting the stoichiometry of the growth rate.

Growth of HgTe and HgZnTe using DipTe and elemental Hg and Zn fluxes was also performed. Figure 6 shows typical RHEED patterns during the recent growth of HgTe. Room temperature infra-red transmission spectra were taken of the $Hg_{1-x}Zn_xTe$ layers. The Zn content in the layers (x=0.33,0.59) was estimated by the cut-off wavelength and bandgap energy versus x value data from reference 13. Figure 7 shows the transmission spectrum of a 5.6 um thick $Hg_{.67}Zn_{.33}Te$ layer.

2.2.4. CONCLUSION

A CBE system for the growth of II-VI compounds has been designed and constructed. The system features include direct injection flow controllers, separate cracking injectors for the group II and VI elements, a Hg-PCVS, and a specifically designed pumping and purging system. The growth of CdTe, HgTe and HgZnTe has been demonstrated.

CBE has the potential to solve many of the problems current experienced by conventional growth technologies in obtaining abrupt heterointerfaces, compositionally graded structures, precise stoichiometric adjustment and complex n- and p-type extrinsic doping profiles. This potential along with a possible increase in Hg incorporation rate through the use of monomer Te make CBE an important growth technology for II-VI materials.

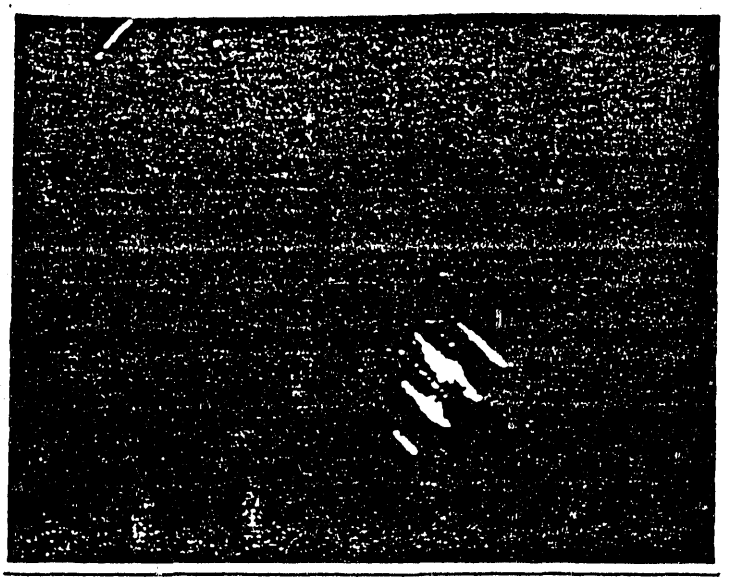

(a)

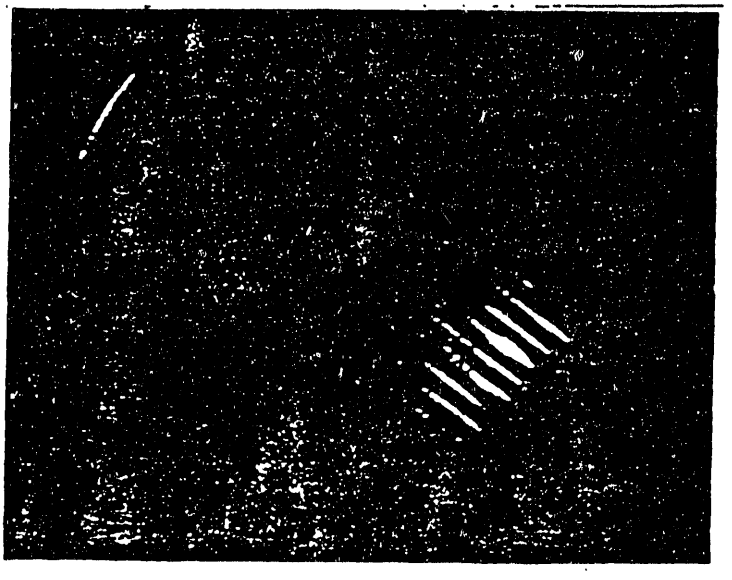

(b)

Figure 6. RHEED patterns during growth of HgTe (T_{sub} = 185°C) using elemental Hg and DipTe: a) [110] azimuth; b)[100] azimuth.

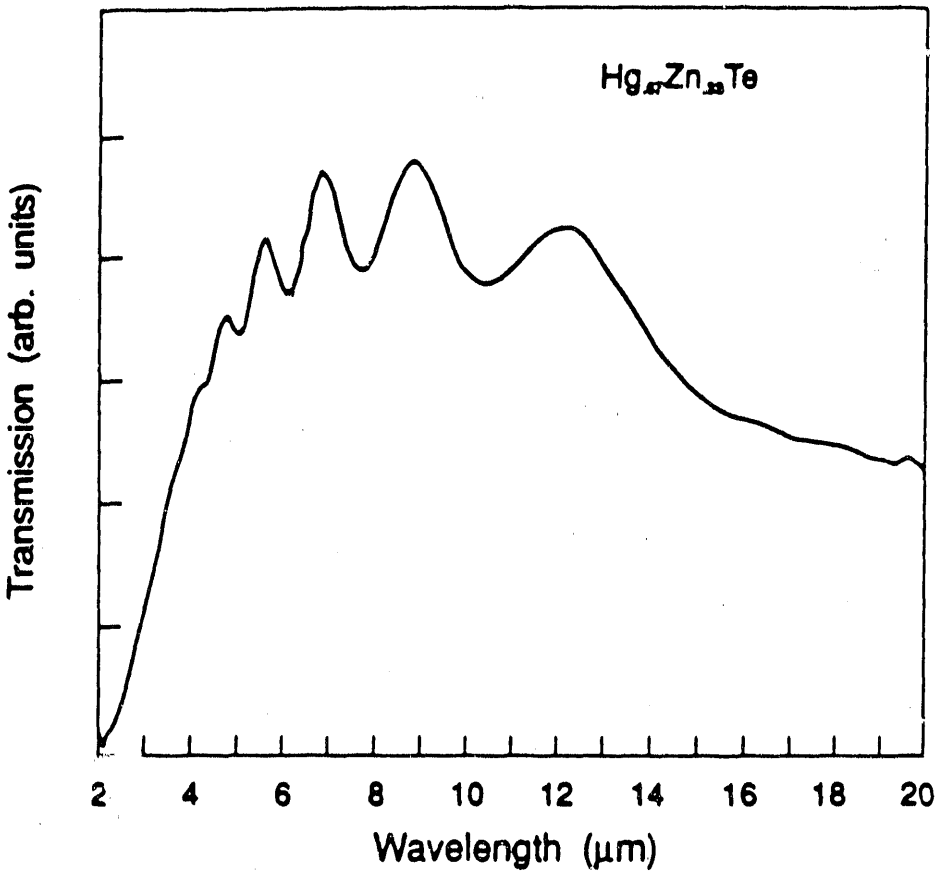

Figure 7. IR transmission spectrum of $Hg_{.67}Zn_{.33}Te$ layer.

2.3. EFFECTS OF ANNEALING AND SURFACE PREPARATION ON THE PROPERTIES OF MBE-GROWN POLYCRYSTALLINE CdZnTe FILMS

(This paper was published in J. Vac. Sci. Tech. A 8, pp. 2012-2019, 1990).

2.3.1. INTRODUCTION

Solar cells based on CdTe have shown great promise due to its optimum 1.45 eV bandgap, ease of manufacturing CdTe thin film polycrystalline devices, and conversion efficiencies in excess of 12% for heterojunctions formed on n-CdS/SnO_2/glass substrates. (1) The performance of these devices is a strong function of the processing steps used in the device fabrication which generally consist of a post-deposition anneal in air followed by a chemical etch prior to ohmic contact formation, both of which are necessary to achieve high performance solar cells. (2) The purpose of the anneal is to enhance the p-type conductivity of the as-grown CdTe to form a proper heterojunction with the n-type CdS. The etch step is necessary to remove the surface oxide resulting from the anneal and to deplete the surface of Cd (enrich in Te), both of which are necessary to facilitate good ohmic contacts. This is generally achieved by using either a dichromate etch consisting of $K_2Cr_2O_7$:H_2SO_4 or a Br_2:CH_3OH etch on the CdTe surface. Low contact resistance has been achieved on CdTe with either etch, however studies have shown that the dichromate etch results in superior ohmic contacts by virtue of a thicker and more Te-rich surface layer. (2,3)

Proper annealing and etching in fabrication have led to CdTe/CdS solar cell efficiencies in the range of 10-12% for CdTe grown by many techniques, including electrodeposition (4), screen printing (5), close-spaced vapor transport (6), molecular beam epitaxy (MBE) (7), and metalorganic chemical vapor deposition (MOCVD). (7) The efficiencies of these devices can decrease dramatically if the fabrication process is not optimized, regardless of the growth technique. While further performance improvement can come from material and process optimization, an alternative approach to achieving high efficiency in polycrystalline thin film cells is to make better use of the solar spectrum by utilizing a tandem cell design in which a 1.65-1.75 eV bandgap cell is stacked on top of a 1.0 eV bandgap bottom cell. Efficiencies of 18-20% are predicted for this design if a 10% efficient top cell with ~ 80% subgap transmission can be fabricated on top of a 15% bottom cell. (8) While $CuInSe_2$/CdS cells are well suited for the bottom cell with a 1 eV bandgap and efficiencies exceeding 14% (9), there is no clear choice for the wider bandgap top cell. Polycrystalline

$Cd_{1-x}Zn_xTe$ is a promising candidate for top cell application since its bandgap is adjustable between 1.45 eV and 2.26 eV by tailoring the composition between CdTe and ZnTe, respectively. Preliminary MBE-grown polycrystalline $Cd_{1-x}Zn_xTe$/CdS solar cells made by us have recently yielded efficiencies in the range of 4-5% for 1.55 eV bandgaps and 1-2% for 1.7 eV bandgaps using the standard CdTe processing sequence. (7) In contrast, MBE-grown polycrystalline CdTe/CdS cells, which have undergone identical processing treatments, have resulted in efficiencies in excess of 10%. Hence the standard CdTe processing procedure may not be optimum for good ternary cell performance. While a number of investigations have been carried out on annealing and etching properties of CdTe which have guided the development of polycrystalline CdTe solar cells (2-3,10-13), no such study has yet been performed on $Cd_{1-x}Zn_xTe$. In view of the importance of annealing and etching on the ultimate performance of CdTe/CdS devices, it is expected that better understanding of the properties of processed $Cd_{1-x}Zn_xTe$ is necessary for improving device performance.

In this paper, we present the first such study on polycrystalline $Cd_{1-x}Zn_xTe$ films grown by MBE. The surface properties are investigated after heat treatments in air, hydrogen, and argon, and after subsequent etching in dichromate solutions of various concentrations and Br_2:CH_3OH etchants. Auger electron spectroscopy (AES) and x-ray photoelectron spectroscopy (XPS) techniques are used to determine compositional and chemical changes in the surface and near-surface regions of treated $Cd_{1-x}Zn_xTe$ films. Attempts have been made to correlate the properties of annealed and etched $Cd_{1-x}Zn_xTe$ surfaces with the electrical properties (barrier heights) of In/$Cd_{1-x}Zn_xTe$ Schottky barriers formed on treated surfaces in an effort to reduce the high contact resistance present in $Cd_{1-x}Zn_xTe$ solar cells.

2.3.2. EXPERIMENTAL

2.3.2a. Film Growth and Preparation

Polycrystalline $Cd_{1-x}Zn_xTe$ and CdTe films were grown by MBE on CdS/SnO_2/glass substrates suitable for solar cell applications as described previously. (14) The film thickness used in this study was in the range of 1.5-2.5 um. Post-deposition anneals in breathing grade air, forming gas (10% H_2 + 90% N_2), and argon, were performed at 350 C for 30 minutes. The etching procedures involved a 10 second dip in < 0.1%Br_2:CH_3OH (B-M etch)or a 3 second dip in saturated $K_2Cr_2O_7$:H_2SO_4 (in a 1:1 ratio) (dichromate etch)

followed by a 30 second DI water rinse and a blow-dry in N_2. The effects of diluting the dichromate etch to 50%, 10%, and 1% concentrations in H_2O were investigated.

2.3.2b. Surface Spectroscopy and Depth Profiling

AES measurements were made using a Physical Electronics Model 600 Scanning Auger Multiprobe. The angle between the sample normal and the electron beam was 45°. All AES data were taken using a 3 KeV electron beam with a current of 1.0 uA. Sputtering for depth profiling was done using a 2 KeV Ar ion beam at a current density of 28 uA/cm^2 at normal incidence.

XPS measurements were performed using a Surface Science Labs SSX-100 monochromated XPS system. Al K-alpha radiation at 1486.6 eV was used as the excitation source. The system had a base pressure of ~ $5x10^{-9}$ torr. All samples were loaded from atmosphere into the instrument. Sample sputtering was accomplished using an Ar ion beam at 4 KeV with a background pressure of $3.5x10^{-7}$ torr. All reported binding energies were calibrated to the Au $4f_{7/2}$ = 83.8 eV and C 1s = 286.6 eV photoelectron lines. Quantitative compositional information was determined from the peak areas and elemental sensitivity factors using standard curve-fitting procedures.

2.3. Electrical Characterization

In/CdZnTe Schottky barrier diodes were fabricated on the surface of the CdZnTe film to facilitate I-V and C-V (1 MHz) measurements. Ring Schottky barrier contacts were formed on the surface with a spacing of 10 um between the two contacts. This arrangement allows the probing of the near surface properties utilizing two surface contacts. A lift-off photoresist process was used to fabricate small area contacts (0.635 mm^2) with a 10 um spacing between the small area contact and a much larger area (19.6 mm^2) concentric contact. The I-V and C-V measurements were made between these two contacts. For C-V measurements, even though both contacts are Schottky contacts, the capacitance and impedance are dominated by the small area contact in the series arrangement. C-V measurements were also made on the CdS/CdZnTe junction by depositing Cu doped p^+ ZnTe followed by Ni evaporation on the CdZnTe surface to facilitate a back contact. All C-V and I-V measurements were made at 300 K under dark conditions.

2.3.3. RESULTS AND DISCUSSION

2.3.3a. Annealing and Etching Studies by Surface Spectroscopy and Depth Profiling

Annealing Effects on MBE-grown Polycrystalline $Cd_{1-x}Zn_xTe$

Annealing of the $Cd_{1-x}Zn_xTe$/CdS structure (referred to as CdZnTe/CdS where x = 0.35), was necessary to obtain measurable solar cell data. Anneals were performed in air, forming gas, and Ar ambients. Air anneals gave the best cell performance. C-V measurements of the Ni/p^+ ZnTe/CdZnTe/n-CdS/SnO_2/glass heterojunction diodes as a function of annealing time in air suggest that the air anneal enhances the uniformity of the p-type character of the CdZnTe films. This is demonstrated in Figure 1 (the applied bias sign is with respect to the CdZnTe) which shows the evolution to a typical reverse-biased C-V curve that obeys the inverse square law relation,$(1/C^2 \sim V)$ and is indicative of uniform p-type doping distribution throughout the CdZnTe. The p-type doping density after the 30 minute anneal was found to be $\sim 3\times10^{15}$ cm^{-3} from $N_a = (2/q\ \ )[d(A^2/C^2)/dV]^{-1}$. The one-sided depletion approximation should be valid since N_d of the CdS ($> 1\times10^{17}$ cm^{-3}) is much greater than the CdZnTe doping level. The enhanced p-type character of the CdZnTe allows the formation of the p-CdZnTe/n-CdS anisotype heterojunction. Similar air annealing and subsequent p-type enhancement was found to be necessary to obtain high efficiency CdTe/CdS solar cells. (2) However, CdZnTe/CdS cell performance was poor in comparison to CdTe cells which suggests that the properties of annealed CdZnTe must be investigated and optimized to improve device performance.

The effects of annealing on the surface properties of CdZnTe were investigated by both XPS and AES. The Te $3d_{5/2}$ and $3d_{3/2}$ electrons, the Cd $3d_{5/2}$ and $3d_{3/2}$ electrons, and the Zn $L_3M_{45}M_{45}$ (referred to as LMM) Auger electrons were used in the XPS analysis. The Zn $2p_{3/2}$ and $2p_{1/2}$ electron binding energies were also determined but since little binding energy shift has been reported for the different Zn bonding configurations they were not used to distinguish chemical states of Zn. Table 1 lists a representative set of relevant binding energies from the literature for the above electrons. All energies were adjusted to the same carbon 1s line of 284.6 eV. The Zn LMM electron energies were tabulated as electron kinetic energy (K.E. = 1486.6 - binding energy in eV).

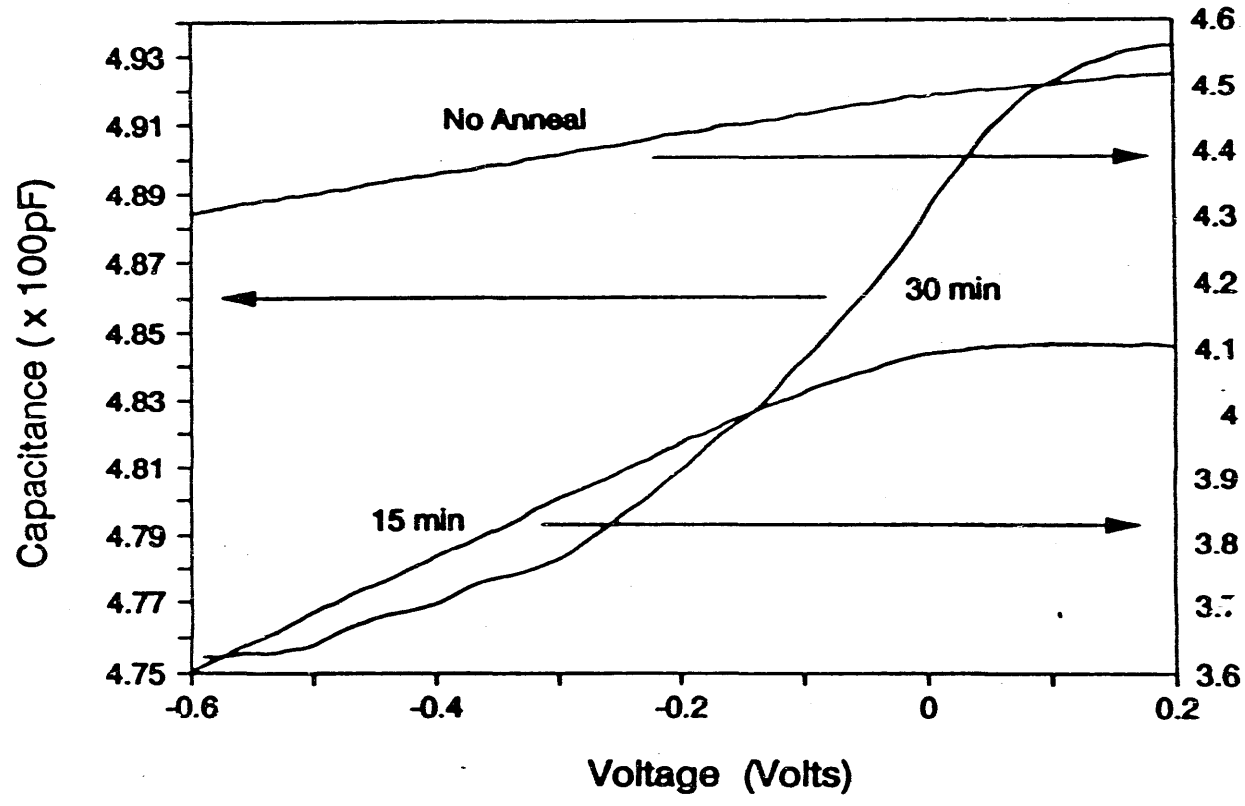

Figure 1. 1 MHz C-V data measured on Ni/p^+ ZnTe/CdZnTe/n-CdS/SnO_2/glass diodes with post CdZnTe growth anneals of (a) 0 minutes, (b) 15 minutes, and (c) 30 minutes. The sign of the applied bias is with respect to the Ni contact.

Material	Cd $3d_{5/2}$	Te $3d_{5/2}$	Zn LMM
CdTe	405.0	572.5	
ZnTe		———	991.1
Cd	405.1		
Te		572.7	
Zn			992.0
CdO	404.0		
TeO_2		575.9	
ZnO			988.4

Table 1. Library of binding energies of Cd and Te $3d_{5/2}$ core level, and kinetic energies of Zn $L_3M_{45}M_{45}$ Auger electrons from reference 15. All energies are adjusted to the C 1s = 284.6 eV line and are listed in eV.

Table 2 lists the binding energies of the Te $3d_{5/2}$ and Cd $3d_{5/2}$ electrons and the Zn LMM Auger kinetic energy for the processed CdZnTe films. Also listed are the Cd:Zn:Te ratios determined from XPS peak areas. A representative set of XPS data is shown in Figure 2 for the Te 3d photoelectrons as a function of annealing and etching conditions as indicated. It is apparent that Te-O bonding is present at the as-grown and air-annealed surfaces as indicated by the peaks at ~ 576 eV and 586 eV along with the expected Te peaks at ~ 573 eV and 583 eV for the CdZnTe. Some investigators have recently shown that for annealed CdTe and ZnTe, complex oxides such as $CdTeO_3$ (16) and $ZnTeO_3$ (17), respectively, are thermodynamically favorable and hence cannot be ruled out at this time. The air-annealing greatly enhances the percentage of Te in the Te-O state at the surface relative to the unannealed surface, as can be seen from the increase in the Te-O/Te-Cd peak height ratios in Figure 2. Quantitative compositional analysis using XPS peak areas indicate that air-annealing converts ~ 70% of the surface Te into the Te-O state whereas the as-grown CdZnTe surface has ~ 40% Te-O, Table 2. XPS data indicate that neither forming gas nor Ar anneals result in additional Te-O formation over the as-grown value, suggesting that laboratory air exposure prior to sample loading is responsible for the ~ 40% Te-O.

Depth resolved XPS analysis showed that in all annealed and unannealed CdZnTe films, Te-O was completely removed by a 30 second Ar^+ sputter etch, indicating that the detectable Te oxide is present only very close (< 5 nm) to the surface. Similar results were found for Cd where XPS measurements made on as-grown and annealed surfaces showed a Cd $3d_{5/2}$ binding energy of ~ 404.5 eV, indicative of Cd-O (Tables 1 and 2), but after a 30 second sputter etch, shifted to ~ 405.2 eV, indicative of predominantly Cd-Te bonding, revealing a thin Cd oxide surface layer. However, Zn behaved quite differently from Cd and Te. The kinetic energy of the Zn LMM Auger transition was used to monitor the changes in the chemical state of Zn. The surfaces of as-grown and annealed (all ambients) films showed a broad Zn LMM lineshape which was deconvoluted into two distinct peaks indicative of Zn-O (~989 eV) and Zn-Te or Zn° (991-992 eV) chemical states. More than 50% of the Zn was found to be oxidized in as-grown, Ar and forming gas annealed films but air annealing resulted in ~ 80% of the total Zn in the Zn-O state at the film surface. A 30 second Ar^+ sputter etch revealed two changes in as-grown, forming gas annealed, and Ar annealed films compared to air annealed films. First, the Zn-O peak at ~989 eV was completely removed and secondly, the higher energy peak at ~992 eV shifted slightly to ~991 eV indicative of pure Zn-Te rather than the Zn-

Process	$Te3d_{3/2}$ (eV) Surf	Sputt	$Cd3d_{3/2}$ (eV) Surf	Sputt	Zn $L_3M_{4,5}M_{4,5}$ (eV) Surf	Sputt	Zn:Cd:Te
As-Grown (AG)	572.5 575.7 (40%)	572.6	404.6	405.3	992.7 989.4 (30%)	990.9	.35:.65:1.0
Air Anneal	572.8 575.8 (72%)	572.8	404.4	405.3	992.8 989.4 (80%)	992.8 989.5 (80%)	0.7:0.3:0.6
AG + B-M	572.7	572.7	405.2	405.3	991.5 989.7 (7%)	990.9	.35:.65:1.3
AIR + B-M	572.8	572.8	405.1	405.1	991.2 988.8 (33%)	988.9 (75%)	0.4:0.6:1.4
AG + 100% K-D	572.8	572.8	---	---	---	---	---
AIR + 100% K-D	572.8	572.8	405.2*	405.2*	---	---	---
AG + 50% K-D	572.3	572.2	404.8	405.0	991.0	991.0	0.2:0.8:1.3
AIR + 50% K-D	572.3	572.3	404.7	405.0	991.3	991.0	0.2:0.8:1.3
AG + 10% K-D	572.0 575.6 (10%)	572.3	404.6	405.0	991.5	991.0	0.3:0.7:1.1
AIR + 10% K-D	572.2 575.6 (15%)	572.3	404.6	405.0	991.3	991.1	0.3:0.7:1.4
AG + 1% K-D	572.0 575.6 (20%)	572.3	404.5	405.0	991.7	991.0	0.3:0.7:1.0
FG Anneal	572.0 575.7 (40%)	572.5	404.5	405.3	992.5 989.4 (69%)	990.7	0.5:0.5:1.0
Ar Anneal	572.0 575.8 (35%)	572.5	404.5	405.3	992.5 989.5 (66%)	990.7	0.5:0.5:1.0

Table 2. Summary of Cd and Te $3d_{3/2}$ core level binding energies, and Zn $L_3M_{45}M_{45}$ Auger kinetic energies for both unsputtered and sputter etched (30 seconds) surfaces. The Cd:Zn:Te ratios listed were calculated after the sputter etch. The percentages of oxidized Te and Zn are noted in parentheses beside the oxide peaks where possible. All energies are referenced to the C 1s = 284.6 eV line and are given in eV. AG refers to as-grown CdZnTe and FG refers to forming gas anneal and K-D refers to the potassium dichromate etch. Starred (*) entries were detected in trace amounts.

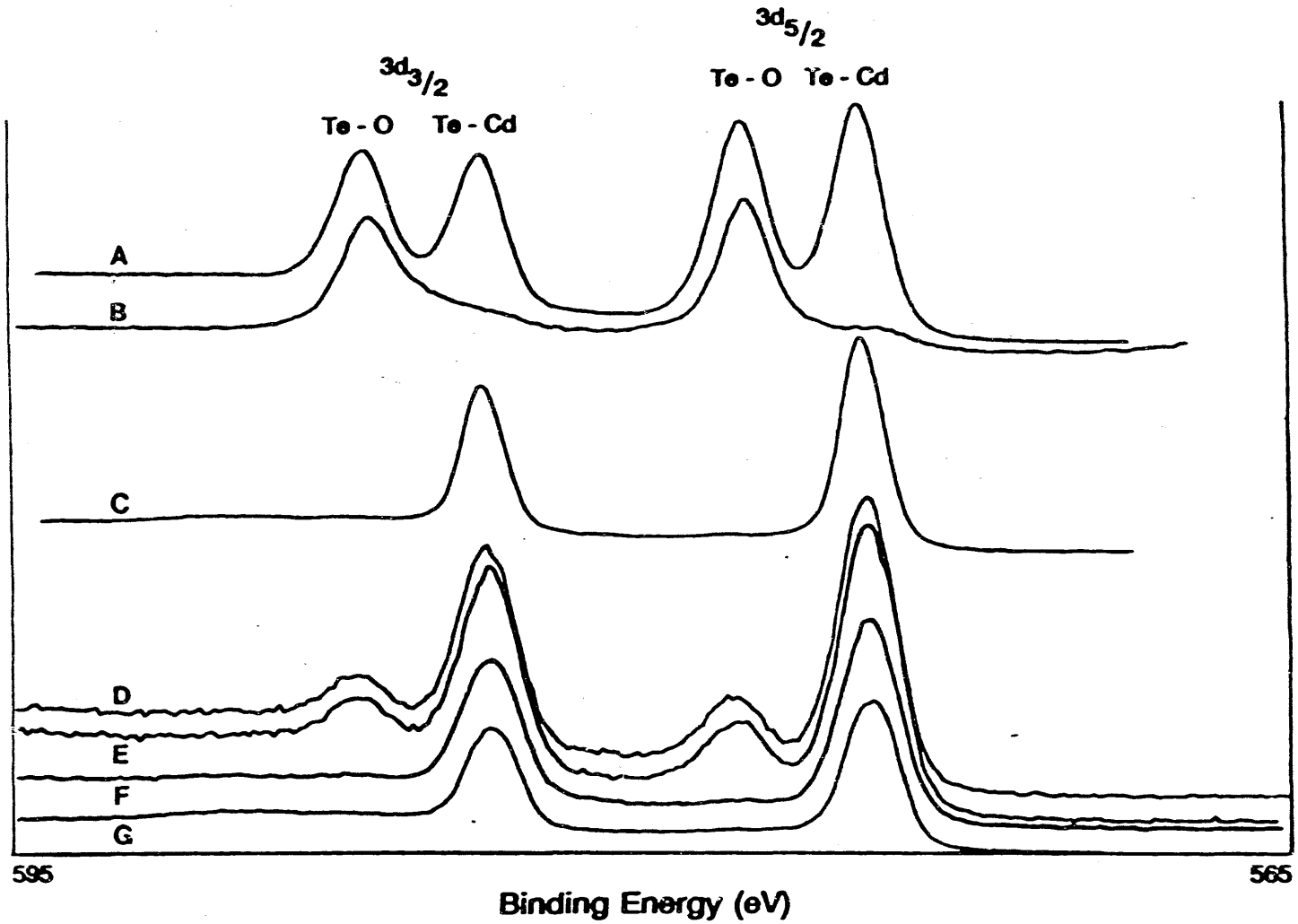

Figure 2. High resolution XPS spectra of the Te 3d core levels for CdZnTe processed as indicated. The scans are of CdZnTe after (a) film growth, (b) air anneal, (c) air anneal + B-M etch, (d) air anneal + 1% dichromate etch, (e) air anneal + 10% dichromate etch, (f) air anneal + 50% dichromate etch, and (g) air anneal + saturated (100%) dichromate etch. Forming gas and Ar annealed CdZnTe behaved similar to the air annealed cases. All data shown were taken on the as-processed surfaces.

Te/Zn° mixture present at the surface. In contrast, neither the 30 second nor a 60 second sputter etch (~ 10 nm into the film) could remove the Zn-O peak from the air-annealed CdZnTe film. It was found that even after the 30 sec. sputter etch, ~80% of the total Zn concentration was still in the Zn-O state. It should be noted that the surface of the annealed polycrystalline CdZnTe consists of a mixture of oxidized Cd, Te, and Zn, along with CdZnTe and is not a homogenous film of any particular compound.

Besides causing oxidation of the surface region, the annealing step also tends to redistribute the constituent elements of the CdZnTe film. XPS studies showed that a Zn-rich surface region was formed after annealing which resulted in a Zn:Cd:Te ratio of ~ 0.5:0.5:1 for forming gas and Ar annealed films compared to a ratio of ~ 0.35:0.65:1 in the as-grown CdZnTe. However, annealing in an air ambient resulted in a more heavily Zn-enriched surface with a Zn:Cd:Te ratio of ~ 0.7:0.3:1 for identical annealing time and temperature. Furthermore, the heavily Zn-rich region in the air annealed films extends ~ 0.1 um into the CdZnTe film seen by the Auger depth profile in Figure 3. Similar results have been reported for single crystal CdZnTe grown by close-spaced-vapor-transport (CSVT) but annealed in hydrogen. (18) The Zn pile-up near the surface in this CSVT-grown CdZnTe was attributed to the expected lower partial pressure of Zn over CdZnTe as compared to either Cd or Te which results in a slower rate of evaporation of Zn from the surface and hence an accumulation of Zn at the surface. In this model, the amount of Zn accumulation should be essentially independent of annealing ambient. This argument does not completely explain the additional increase in Zn pile-up at the surface of air-annealed films compared to forming gas and Ar annealed films in our study. Oxygen preferentially bonds to Zn over Cd and Te in the near-surface region of oxygen in-diffusion. This is consistent with XPS sputter profile data, Table 2, which clearly showed that only Zn-O bonds, and not Cd-O or Te-O bonds, exist beneath the annealed surface. Furthermore, this was supported by the Auger profile in Figure 3 which showed that the profiles of oxygen and Zn track each other. It is likely that the oxygen diffusion and Zn oxidation processes are enhanced in polycrystalline CdZnTe compared to single crystal CdZnTe due to diffusion and segregation along grain boundaries. It is apparent that the Zn accumulation near the surface is the result of Zn gettering caused by the indiffusion of oxygen. This mechanism is suggested by: (1) the depletion of Zn in the CdZnTe bulk associated with the pile-up of Zn near the surface, (2) the decreasing profile of oxygen into the film, (3) the formation of Zn-O at and beneath the surface, and (4) the thermodynamically preferred formation of Zn-O bonds over Cd-O and Te-

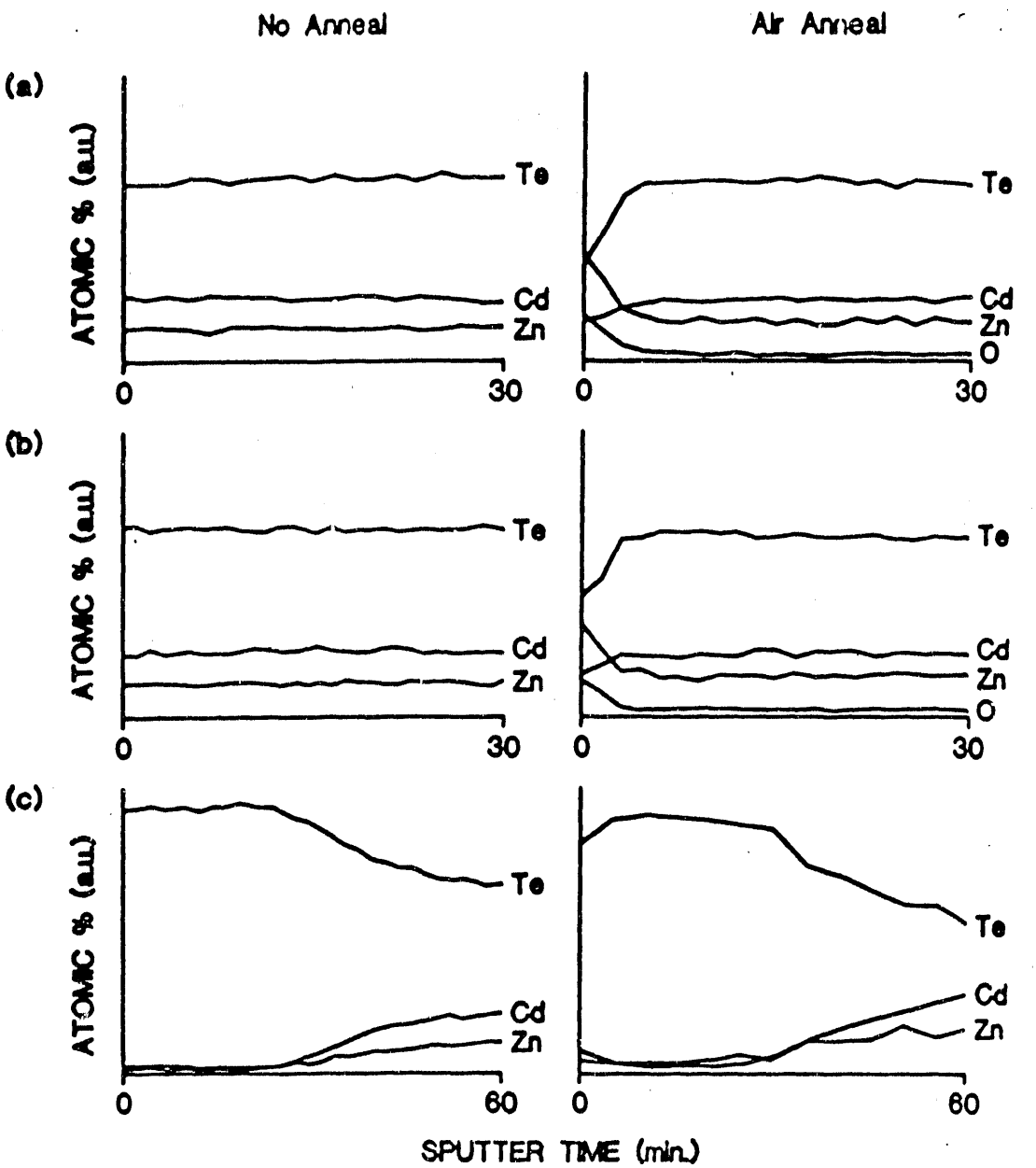

Figure 3. Auger depth profiles of as-grown and air annealed CdZnTe after (a) no etch, (b) B-M etch, and (c) saturated dichromate etch. Etch rates for all profiles were ~ 0.01 um/min.

O bonds.

A possible model for the gettering process can be constructed by analogy to Au impurity gettering in Si by phosphorous, which is highly reactive with Au. (19) As oxygen diffuses into the CdZnTe film during the air-anneal, it reacts with the Zn to form Zn-O resulting in depletion of Zn in the CdZnTe phase near the surface. This serves as the driving force for diffusion of Zn from the bulk since a concentration gradient is established which favors the diffusion of Zn in the Zn-Te phase to the surface. The amount of Zn-O formed is proportional to the oxygen content of the film, therefore, the greatest Zn accumulation occurs at the surface with a decreasing profile into the film, similar to the observed oxygen profile (Figure 3). Identical results were reported (19) in the phosphorous-diffused layer of Au-containing Si wafers where Au pile-up toward the surface was dictated by the phosphorous in-diffusion profile. Hence it appears that the rate limiting step for Zn accumulation is the diffusion of oxygen into the film whose kinetics can be described by a constant source diffusion model. By solving the one-dimensional diffusion equation,

$$d^2[N(x,t)]/dt^2 = D[d^2[N(x,t)]/dx^2] \qquad (1)$$

with the following boundary conditions,

$$N(x = 0,t) = N_s$$

$$N(x = \infty,t) = 0$$

$$N(x,t = 0^-) = 0$$

the oxygen concentration profile can be expressed in the form

$$N(x,t) = N_s \mathrm{erfc}\{x/[2(Dt)^{1/2}]\} \qquad (2)$$

Using the Auger profile of Figure 3, the surface concentration of oxygen, N_s, was found to be ~ 7×10^{21} cm^{-3}. Substituting this in equation (2) and matching the experimental data for the oxygen concentration profile, the diffusivity of oxygen in the polycrystalline CdZnTe film was determined to be ~ 1×10^{-15} cm^2/sec for a 350° C air anneal for a number of points along the oxygen concentration profile. Similar calculations were made for CdZnTe annealed at 400° C in air for 30 minutes, which is the optimum condition for high

performance (~10% efficient) MBE-grown CdTe devices, and resulted in a diffusivity of ~ $6x10^{-14}$ cm^2/sec.

As shown above, the annealing step in the processing of polycrystalline CdZnTe cells has both beneficial and deleterious effects on the CdZnTe properties. Annealing enhances the desired p-type character of the CdZnTe but, it also induces Zn pile-up near the surface of the film and the formation of undesirable Te, Cd,and Zn oxides with the Zn-O present beneath the CdZnTe surface.

2.3.3b. Effects of Chemical Etching on MBE-Grown Polycrystalline CdZnTe

The formation of Te-O, Cd-O, and Zn-O in the p-type CdZnTe can result in high contact or series resistance which will degrade the device performance. Therefore, a surface etch is necessary to remove the oxidized surface layer and create a Te-rich (depleted in Cd and Zn) p^+ surface layer. This step has been found to be critical for obtaining high efficiency CdTe solar cells since a poor ohmic contact has been shown to result in greatly increased series resistance and decreased fill factor contributing to poor cell efficiency. (2,3) In the case of polycrystalline CdTe solar cells, investigators have opted for surface etches such as dichromate ($K_2Cr_2O_7$:H_2SO_4) or B-M (Br_2:CH_3OH) solutions to provide p^+ surfaces. Compared to the B-M etch, the dichromate etch on CdTe has been shown to result in lower series resistance which depends not only on the Te:Cd ratio at the surface, but also on the thickness of the Te-rich layer, with layers > 30 nm giving lowest resistances. (2) In this section, we report for the first time, the comparative merits of using B-M and dichromate etches on annealed polycrystalline CdZnTe films.

Figure 3 shows the Auger depth profiles of annealed and unannealed CdZnTe films after B-M and 100% dichromate etching. It is apparent from this figure that the B-M etch does little to increase the Te concentration relative to the Cd + Zn concentration at the air annealed surface. Similar results were found for Ar and forming gas annealed films. XPS data showed that the Te:(Cd + Zn) ratio was only ~ 1.2-1.4 in all cases, which is lower than the Te:Cd ratio of ~ 1.5-2 found for B-M etched MBE-grown CdTe. Figure 2 and Table 2 indicate that the B-M etch completely removed the Te-O $3d_{5/2}$ peak at ~ 576 eV leaving only Te either as an element or in a CdTe state (the binding energies are too close to distinguish in our measurements). Table 2 also shows that the B-M etch removes the Cd-O from the surface of the CdZnTe since the Cd $3d_{5/2}$ binding energy shifts from ~404.5 eV to ~ 405.2 eV after the etch. Removal of oxidized Te and Cd at the surface occurred for all films. In contrast to Cd and Te, the B-M etch did not remove the

Zn-O peak at ~ 989 eV for any CdZnTe film, Table 2, although the total Zn concentration and percentage of Zn in the Zn-O state was reduced at the surface. The B-M etch also shifted the higher energy Zn peak from ~ 992 eV to ~ 991 eV, indicating the removal of metallic Zn° formed by the anneal. Thus, the B-M etch leaves Zn in the form of lattice Zn (Zn-Te) and Zn-O at the surface. A 30 second Ar ion sputter etch removed the Zn-O peak from the XPS spectra for the unannealed, forming gas annealed, and Ar annealed CdZnTe films, leaving only lattice Zn (~ 991 eV), but it could not remove the Zn-O peak from the air-annealed CdZnTe. In fact, table 2 shows that after the 30 second sputter of the air annealed film, ~ 75% of the remaining Zn is still in the Zn-O state. This indicates that the B-M etched away only a very thin (< 5 nm) surface layer of the film which was enough to remove oxidized Cd and Te but not enough to remove the more deeply diffused Zn-O. Slightly higher concentrations of the B-M solution failed to remove the Zn-O from the XPS spectrum. Hence, the standard B-M etch used successfully for CdTe solar cell processing was neither able to remove Zn-O nor result in Te-enrichment near the surface, therefore we conclude it is not a suitable etch for processing polycrystalline CdZnTe for solar cell applications.

In an attempt to achieve the proper surface conditions for good ohmic contacts on CdZnTe, a dichromate etch was investigated. Figure 3 shows the effect of a saturated dichromate etch on the depth profile of polycrystalline CdZnTe which, unlike the B-M etch, gives a Te° surface layer with little or no trace of Zn, Cd, or oxygen. The Te-rich surface was estimated to be ~ 0.3 um thick. This was confirmed by XPS in Table 2 which shows that the film is virtually all elemental Te° with no trace of oxides. The oxidation of lattice Te^{2-} to Te° has been shown to be thermodynamically favorable during the dichromate etch in CdTe. (10) In an attempt to better control the very rapid etch rate of the saturated dichromate etch, the etch was diluted in H_2O to obtain 50%, 10%, and 1% concentrations as described earlier. The 50% dichromate solution resulted in a Te-rich layer thickness of ~ 25 nm compared to less than 5 nm for the 10% and 1% dichromate solutions. The Te:Cd+Zn ratios for all of the diluted dichromate etches were ~ 1.0-1.4. Furthermore, while there is no evidence of Zn oxidation for any of the dilute etches, Te and Cd became more oxidized as the concentration decreased from 50% to 10% to 1%, Table 2 (which is in contrast with the B-M etch which always removed Te-O and Cd-O but not Zn-O). This is reflected by the shift of the Cd $3d_{5/2}$ peak to higher binding energies and the growth of the Te 3d peaks at ~ 576 eV and ~ 586 eV with lower concentration, Figure 2. An identical trend was previously found for CdTe surfaces where it was shown that

the dichromate solution must have sufficient acid content to avoid the oxidation of Te by the dilute dichromate etch itself. (2,10) Thus, from the point of view of CdZnTe post-anneal surface properties for solar cell applications, a dichromate etch with concentration of > 50% is recommended because it gives adequate Te-richness, Te-rich layer thickness, and an oxide-free surface, all of which help the formation of good ohmic contacts.

2.3.4. Electrical Characterization of In/$Cd_{1-x}Zn_xTe$ Schottky Barriers

To determine the ultimate effects of annealing and chemical etching on the electrical properties of the polycrystalline CdZnTe surface, In/CdZnTe Schottky barrier diodes were fabricated on the CdZnTe structures. Figure 4 shows the dramatic change in the dark I-V characteristics of various annealed and chemically etched CdZnTe surfaces. The built-in-voltage shifted from ~ 1.5 V to ~ 0.3 V for In junctions made on air annealed CdZnTe surfaces followed by a B-M etch and a saturated dichromate etch, respectively. This indicates a substantial reduction in effective barrier height for saturated dichromate etched CdZnTe, which was accompanied by a large decrease in resistance. Diodes fabricated on the air annealed CdZnTe with no etch essentially showed a resistance-dominated I-V behavior. To further confirm the barrier height reduction, an attempt was made to fit the dark I-V characteristics to the Schottky diode equation,

$$J = J_o[\exp((q/nkT)(V - JR_s)) - 1] \qquad (3)$$

where n is the diode ideality factor, R_s is the series resistance. The dark saturation current density, J_o, can be expressed as

$$J_o = A^*T^2\exp[(-\phi_{en}/nkT)] \qquad (4)$$

where A^* is the effective Richardson constant and ϕ_{en} is the effective barrier height which is equal to the actual barrier height ($E_G - (\phi_m - \chi)$) for ideal Schottky diodes with thermionic emission the dominant current transport mechanism. Dark I-V characteristics of In junctions made on annealed but not etched CdZnTe surfaces could not be fit to equation (3) supporting that the transport was modified by the presence of the Te, Cd, and Zn oxidized surface region and was probably dominated by series resistance. The I-V behavior

of the In/B-M etched CdZnTe junctions were well described by equation (3) and typically gave a dark saturation current density of ~ $8x10^{-9}$ A/cm^2 with a diode factor of ~ 1.3, indicating that there are possibly other current transport mechanisms operating in parallel with thermionic emission. Saturated dichromate etched CdZnTe surfaces exhibited dark saturation current densities of ~ $1x10^{-5}$ A/cm^2 with diode factors of ~ 1. The large increase in J_o for dichromate etched CdZnTe without a substantial change in the ideality factor suggests a significant reduction in the barrier height. The barrier height for the saturated dichromate etched In/CdZnTe junction was estimated from equation (4) to be ~ 0.65 eV using an A^* value of 92 A/cm^2/K^2, a hole effective mass of 0.77m_o (20), and a value of n = 1 at 300 K for the best fit to the data. Similarly, the effective barrier height for the B-M etched CdZnTe was found to be ~ 1.2 eV with an ideality factor of 1.3.

The observed reduction of the effective barrier height and decrease in resistance for saturated dichromate etched CdZnTe compared to both annealed and B-M etched CdZnTe results from both the removal of the surface region consisting of oxidized Te, Cd, and Zn, and the subsequent formation of a Te-rich p^+ surface layer, suggested by both Auger profiling (Figure 3) and XPS data (Table 2). The reduction in the effective barrier height and series resistance from the annealed CdZnTe surface to the B-M etched CdZnTe surface (Figure 4) can be attributed to the removal of both Te and Cd oxides, but further decrease in barrier height and resistance was not possible due to the presence of the thicker Zn-oxidized CdZnTe layer and the persisting Te-deficiency (see Figure 3). This is in contrast to the effects of the B-M etch on CdTe surfaces where the B-M etch not only removes the surface oxide layer, but forms a Te-rich surface resulting in a lower effective barrier height. Our study clearly shows that oxide removal, Te-richness and barrier lowering in CdZnTe films can only be accomplished by a dichromate etch (>50% concentration) and not by the standard B-M etch. C-V profiling of the In/CdZnTe junctions confirmed that the dichromate etching resulted in a ~ 0.15 um p^+ surface layer which had a net doping of ~ $2x10^{17}$ cm^{-3}, compared to bulk CdZnTe doping levels of ~ $3x10^{15}$ cm^{-3} beneath the Te-rich layer extracted from the C-V characteristics of the CdS/CdZnTe heterojunction, Figure 1. Therefore, it is expected that the dichromate treatment of sufficient concentration will result in greatly improved ohmic contacts for solar cell applications since in these devices a higher work function metal such as Au or Ni are typically used. In addition, since the dichromate treatment results in a surface that is much more heavily p-type compared to the bulk of the CdZnTe, possible

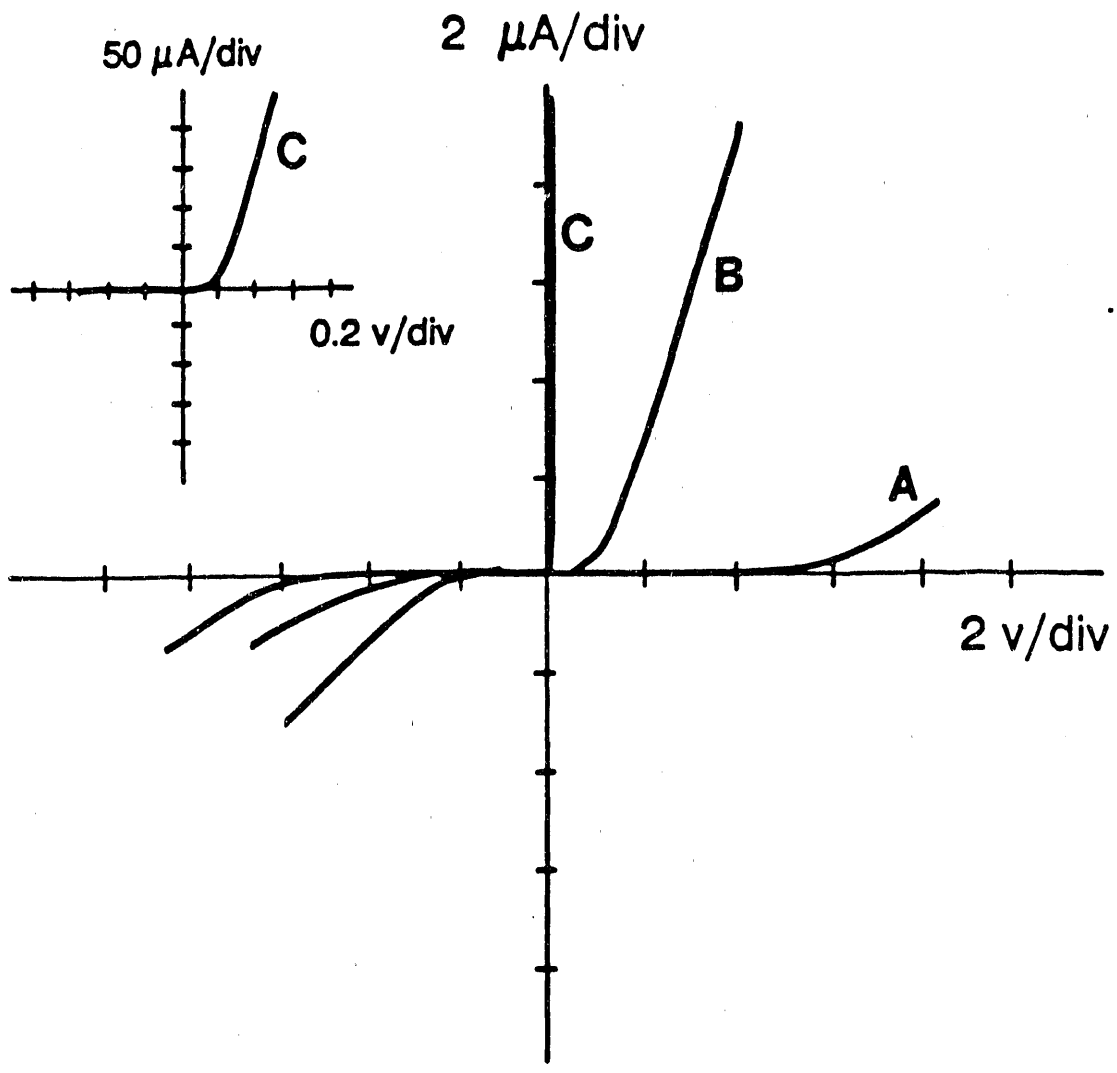

Figure 4. Dark I-V characteristics of In/CdZnTe junctions made on (a) air annealed, (b) air annealed + B-M etched, and (c) air annealed + saturated dichromate etched CdZnTe surfaces. Curve (c) is shown at a larger scale in the inset for clarity.

back surface field action is possible which enhances the collection of the photogenerated minority carrier electrons by the CdS/CdZnTe heterojunction. The effects of the annealing and etching on the properties and performance of polycrystalline CdZnTe/CdS solar cells are presently being investigated.

2.3.5. CONCLUSIONS

Standard processing procedures used in the successful fabrication of high efficiency polycrystalline CdTe solar cells such as air annealing were found to provide the desired p-type enhancement of the CdZnTe bulk, however it resulted in extensive oxidation of Zn into the bulk and accumulation of Zn near the film surface. It was found that the air anneal (specifically oxygen), while necessary to achieve uniform p-type conductivity, triggered the outdiffusion of Zn from the bulk as more of the Zn at the surface became oxidized. Subsequent etching in a standard B-M etch which was successfully used for CdTe cells removed only the surface oxides of Te and Cd but did not remove neither the Zn-O or the Zn-rich surface region nor create a p^+ Te-rich surface which is necessary for low contact resistance to the CdZnTe surface. It was found that the removal of the thin surface layer of oxidized Te and Cd by the B-M etch reduced the series resistance of In/CdZnTe Schottky barrier diodes and yielded a diode-like I-V characteristic with a barrier height of ~ 1.2 eV. An alternate etch consisting of a concentrated dichromate solution was found to remove all oxides and resulted in a highly Te-enriched surface with a thickness of ~ 0.25 um and with a doping level of ~ $2x10^{17}$ cm^{-3} compared to ~ $3x10^{15}$ cm^{-3} doping concentration within the bulk of the CdZnTe film. Concentrations of less than 50% dichromate resulted in the oxidation of both Te and Cd but not Zn. In/CdZnTe Schottky diodes fabricated on concentrated dichromate etched surfaces showed both a large decrease in barrier height (~ 0.65 eV) compared to the B-M etched CdZnTe surface (~1.2 eV), and a large decrease in the series resistance. These results suggest that an air anneal followed by a dichromate etch of the CdZnTe solar cell structure should significantly improve the ohmic behavior of the back contact which is necessary to increase present-day CdZnTe cell efficiency.

2.4. INVESTIGATION OF MOCVD-GROWN CdTe/CdS SOLAR CELLS

(This paper is submitted to J. Appl. Phys.).

2.4.1. Introduction

Thin film polycrystalline CdTe solar cells have the potential to reach efficiency greater than 20%. There are many properties of CdTe, like optimal bandgap of 1.45 eV, high absorption coefficient, ease of deposition, and feasibility of p and n type doping, which make CdTe an attractive material for terrestrial solar cell applications. To date, efficiency as high as 12% has been achieved on CdTe/CdS solar cell prepared by spray pyrolysis (1). Theoretical calculations suggest that the maximum possible efficiency for polycrystalline CdTe/CdS solar cells is 27% (2), although some investigators estimate that practically achievable efficiency is ~22% (3). In order to realize this efficiency, further improvement in CdTe film quality, CdTe/CdS interface quality, and design modifications are necessary. An alternate approach to obtain efficiency greater than 20% is to use a tandem cell design, in which a wide bandgap cell is stacked over a narrow bandgap cell (4). The optimum bandgap for the top cell is 1.7 eV and that of bottom cell is 1.1 eV for a two-cell arrangement. Alloys of CdTe, like CdZnTe, CdMnTe, have been suggested as suitable materials for top cell applications (5). But these materials have not yet been developed sufficiently for top cell applications.

Growth techniques like MBE, MOCVD have been successful in growing good quality single crystal films of these alloys with all compositions. Though many other growth techniques have been used to grow CdTe films for solar cell applications (6), very limited attempts have been made to grow CdTe films by MOCVD for solar cell applications. Recently, an efficiency of 9.2% was reported for MOCVD-grown CdTe films where CdTe films were grown at atmospheric pressure at a substrate temperature of 410 C (7). In order to improve MOCVD-grown CdTe cell efficiency, growth optimization and device analysis are necessary. In this study, polycrystalline CdTe films were grown by MOCVD at substrate temperature in the range of 300 to 400 C, in an attempt to improve the efficiency by understanding the loss mechanisms in MOCVD CdTe solar cell. We were able to achieve 9.7% efficiency, which is the highest reported efficiency for MOCVD-CdTe cell today. Model calculations were performed on the highest efficiency (9.7%) MOCVD-CdTe cell to investigate the carrier loss mechanisms and provide guidelines for achieving greater than 15% efficient

CdTe cells.

2.4.2. Experimental

Polycrystalline CdTe films were grown by MOCVD on CdS/SnO_2/glass substrates using a Cambridge MR102 system. CdS/SnO_2/glass substrates were supplied by AMETEK Materials Research Laboratory. Dimethylcadmium was used as a source for Cd and diallyltellurium (DATe) and diisopropyltellurium were used as Te sources. The substrate temperature was varied from 300 to 360 C for diallyltellurium source and 360 to 400 C was maintained for diisopropyltellurium source. The inlet ratio of partial pressures of Cd to Te was 0.025, resulting a growth rate of ~ 1.5 um/hr. As-grown CdTe films were characterized by surface photovoltage spectroscopy and Auger electron spectroscopy for composition and uniformity. The thicknesses of these films were estimated from interference fringes observed in infrared reflection spectra. To fabricate cells, as-grown CdTe films were treated in $CdCl_2$ solution for a short time and annealed in air at 400 C. After the heat treatment, CdTe surface was etched in a mild solution of $Br:CH_3OH$. N-i-p cells were fabricated by depositing a 0.06 um thick Cu doped ZnTe layer on top of the etched CdTe surface. Nickel contacts of area 0.08 cm^2 were used as back contacts. Cell efficiencies were measured under 100 mW-cm^2 AM1.5 illumination. Bias dependent spectral response measurements were performed in the wavelength range of 350 to 900 nm under reduced light intensity.

2.4.3. Results and discussion

In order to grow CdTe films in the temperature range of 300 to 350 C, DATe was used since DATe cracks efficiently between 260 to 350 C. For the conditions used, maximum growth rate occurred at a growth temperature of 300 to 320 C. However, Auger depth profile showed uniform composition for films grown at all substrate temperatures. For CdTe growth temperatures higher than 350 C diisopropyltellurium was used because of higher cracking temperature.

N-i-p cells were fabricated on CdTe films grown at various substrate temperatures and on CdTe films with thicknesses varying from 1.5 to 2.6 um. Efficiencies in the range of 8-9% were obtained on films grown at all temperatures with very little efficiency dependence on growth temperature. The maximum observed efficiency was 9.7 % with V_{oc} of 720 mV, J_{sc} of 22.47 mA/cm^2, and fill factor of 0.60. This is the

highest efficiency reported so far on MOCVD-grown CdTe films. Figure 1 shows the light I-V data of 9.7% efficient cell. The J_{sc} value is comparable with the values obtained (22 mA/cm^2) on high efficiency polycrystalline CdTe solar cells grown by other techniques. (6) However, the observed V_{oc} and fill factor values are lower than the values obtained on electrodeposited CdTe films (3) (which has 11% efficiency) grown on identical substrates. This suggests that an improvement in MOCVD growth process is necessary. In general, series resistance and non-ohmic back contacts can affect the fill factor and interface state recombination at the heterojunction can reduce V_{oc}. In order to identify the dominant loss mechanisms in the MOCVD-CdTe cell, bias-dependent spectral response measurements were performed on the 9.7% efficient MOCVD-CdTe cell, figure 2. In the wavelength range of 500 to 800 nm, the external quantum efficiency (EQE) is greater than 0.85, which is consistent with the observed high J_{sc} value. On the other hand, electrodeposited CdTe films on identical substrates showed lower J_{sc} (20.8 mA/cm^2) and EQE, but higher V_{oc} and fill factor. The EQE of MOCVD CdTe cell showed a strong voltage dependence (figure 2), decreases with increasing forward bias and the magnitude of decrease is more pronounced at higher voltages. Furthermore, the magnitude of decrease in spectral response with applied bias is wavelength independent. In general, wavelength independent decrease in spectral response is attributed to recombination of carriers at the interface since bulk recombination reduces the diffusion length and makes the spectral response wavelength dependent. Similar results have been observed for $CuInSe_2$/CdS solar cells and the effect has been explained on the basis of interface recombination. (8,9) However, a recent report (10) showed that series resistance of the cell also could explain the decrease in spectral response with the applied forward bias.

In order to identify whether the observed bias dependent spectral response in MOCVD CdTe cells can be explained by series resistance of the cell, calculations were performed following the series resistance model. (10) According to this model, the bias dependent spectral response can be written as

$$SR(J_{sc}, \lambda)/SR(J, \lambda) = 1 + [(q/AKT)(R_L + R_S)] (J_{sc} - J) \qquad [1]$$

where $SR(J_{sc}, \lambda)$ is the spectral response at zero bias, $SR(J, \lambda)$ is the spectral response at various voltages, A, the diode quality factor, R_L, load resistance, R_s, series resistance of the cell, and J the total current under

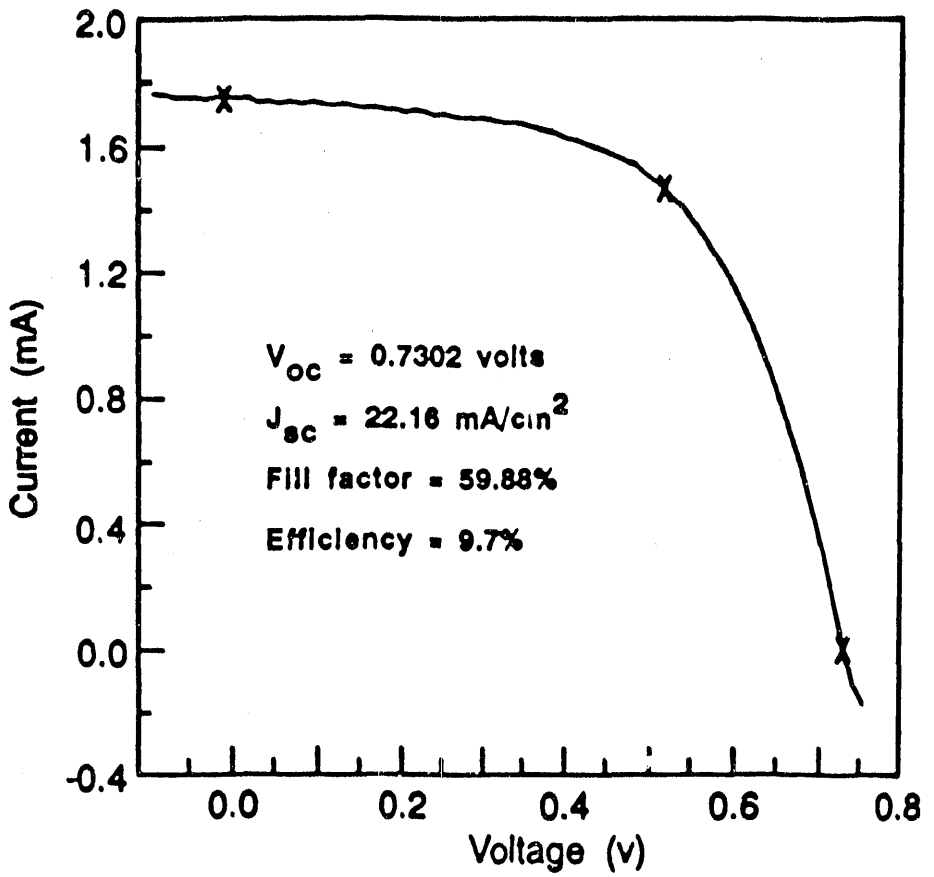

Figure 1. Lighted I-V behavior of MOCVD-grown CdTe/CdS solar cell.

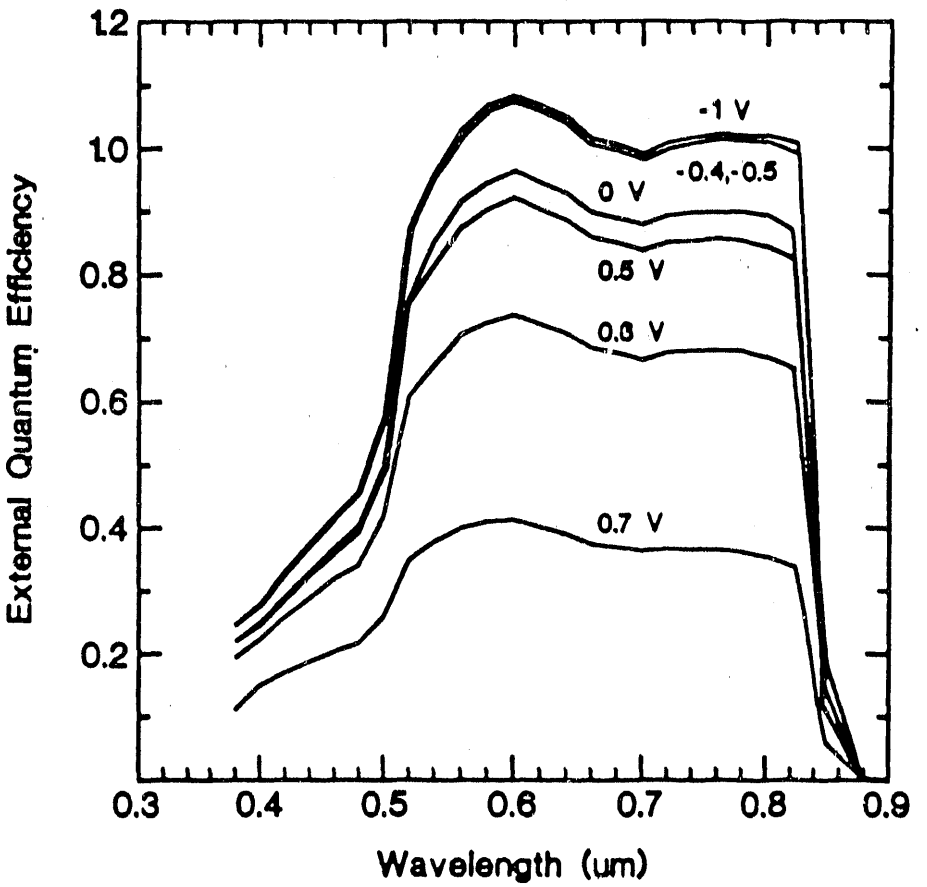

Figure 2. Bias-dependent spectral response data of 9.7% MOCVD-grown CdTe/CdS cell under a light bias equivalent to 0.85 mA current.

light. According to the above equation, the spectral response of the device should decrease linearly with R_s regardless of the wavelength. The magnitude of the decrease is related to the series and load resistance of the cell. The plot of $SR(J_{sc})/SR(J)$ -1 versus J_{sc}-J was a straight line for $CuInSe_2$/CdS solar cells. (10) From the slope of the line, $(R_s + R_L)$ was calculated which agreed well with light I-V data of $CuInSe_2$ cells. Similar calculations were performed from bias dependent spectral response data of 9.7% efficient cell and the results are shown in figure 3. It is clear that the plot is not a straight line, which suggests that the wavelength independent decrease in spectral response with increasing voltage is not caused exclusively by the series resistance of the cell. Hence, the interface recombination model (8) was considered for analysis. This model was originally proposed to explain Cu_2S/CdS solar cell data. (11,12)

According to this interface recombination model, the photocurrent is voltage dependent and can be written as

$$I(V) = I_d(V) - I_{sc}\eta(V) \qquad [2]$$

Here $\eta(V)$ is the collection function term which is defined as

$$\eta(V) = QE(V)/QE(0) \qquad [3]$$

where QE(0) is the J_{sc} at V=0 and QE(v) is the J_{sc} at different voltages. The collection function modifies the V_{oc} as

$$V_{oc} = AKT/q\ [\ln(I_{sc}/I_o) + \ln \eta(V_{oc})] \qquad [4]$$

and the fill factor as

$$\Delta FF = (V_{mp}/V_{oc})\ [1-\eta(V_{mp})] \qquad [5]$$

In order to estimate losses due to collection function, ratio of (QE(V)/QE(0)) was calculated as a function

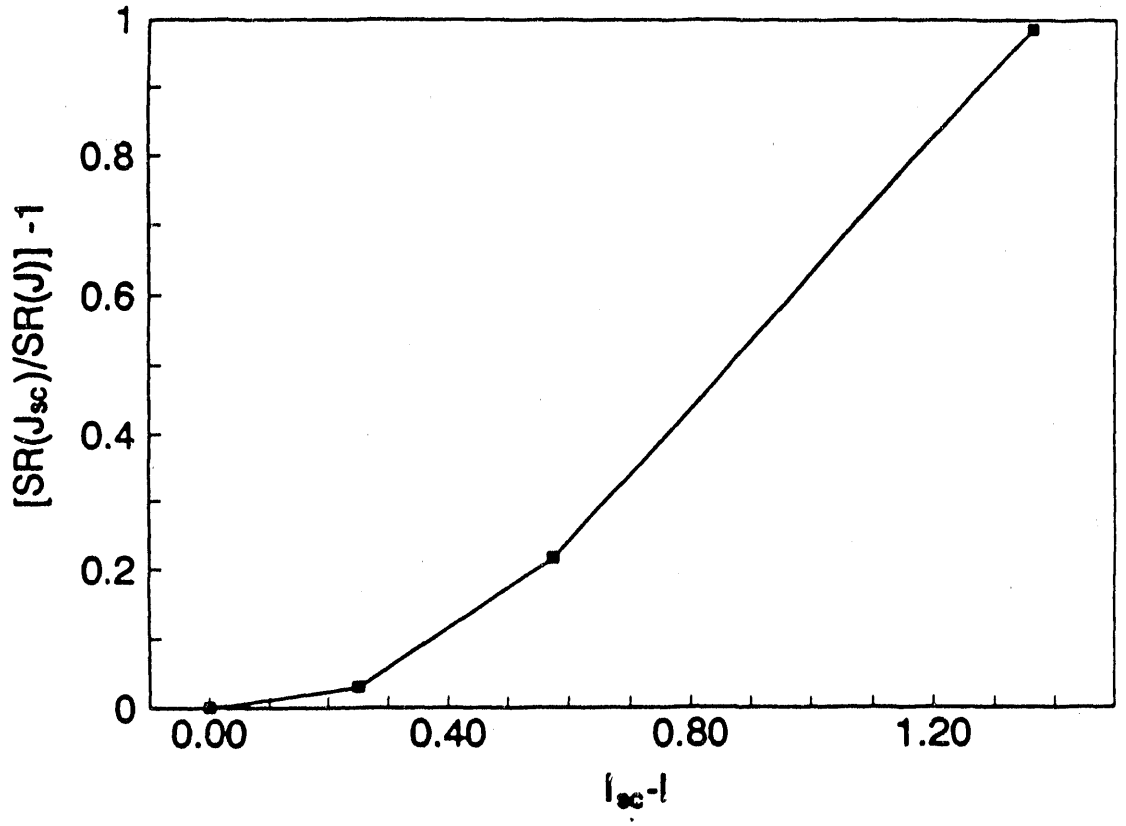

Figure 3. Spectral response ratio of 9.7% MOCVD-CdTe cell, calculated from bias-dependent spectral response data, at a wavelength of 500 nm.

of voltage at different wavelengths. Figure 4 is the plot of collection function versus voltage calculated from bias dependent spectral response data of 9.7% cell. It is clear from the figure that under forward bias the J_{sc} is significantly lower than J_{sc} at 0 V. If the loss of carriers at the interface affects the V_{oc} and fill factor, then the loss should be directly proportional to the value of collection function. The loss in V_{oc} due to the collection function was calculated from the knowledge of diode parameters, A and I_o. Figure 5 shows dark I-V data of 9.7 % efficient cell. A multivariable regression analysis was performed to fit the measured dark I-V data to a single exponential diode given by

$$I = I_o [\exp\{q(V-IR_s)/AKT\} -1] + (V-IR_s)/R_{sh} \qquad [6]$$

to obtain A, the diode ideality factor, R_s, the series resistance and R_{sh}, the shunt resistance of the diode. The analysis gave A = 1.81, J_0 = 1.1x 10^{-10} A, R_s = 87.8 ohms and R_{sh} = 4.2x 10^6 ohms. Using J_o, A, and the collection function at V_{oc}, the V_{oc} was calculated using equation 4. The calculated value of 730 mV agrees well with the measured value of 726 mV supporting the fact that the interface recombination is the cause for low V_{oc}. Notice that if $\eta(V) = 1$, then V_{oc} = 780 mV. Similarly the reduction in fill factor due to collection function term was calculated (from equation 5) which showed that the collection function reduced the fill factor by 0.12. In order to improve the efficiency, the CdTe/CdS interface has to be improved.

By improving or eliminating the interface recombination, the V_{oc} can be improved from 726 mV to 780 mV and the fill factor can be improved from 0.6 to 0.72. The improvement in J_{sc} can be estimated from reverse bias spectral response measurements. Figure 2 shows that under 1 V reverse bias the spectral response increases, suggesting a possible increase of at least 10% in J_{sc}, from 22.46 mA/cm^2 to 24 mA/cm^2. By combining all these improvements the efficiency of MOCVD- CdTe cell can be improved to 13.5%. Further improvement may require design modifications in the CdTe solar cell. For example we have found that 1500 A CdS used in this study absorbs significant amount of high energy photons and the loss of current due to CdS absorption was estimated to be 4 mA/cm^2 (3). By replacing CdS window by a wider bandgap material like CdZnS, at least part of the current loss can be recovered and the efficiency of the MOCVD CdTe cell can be improved to ~15%,.

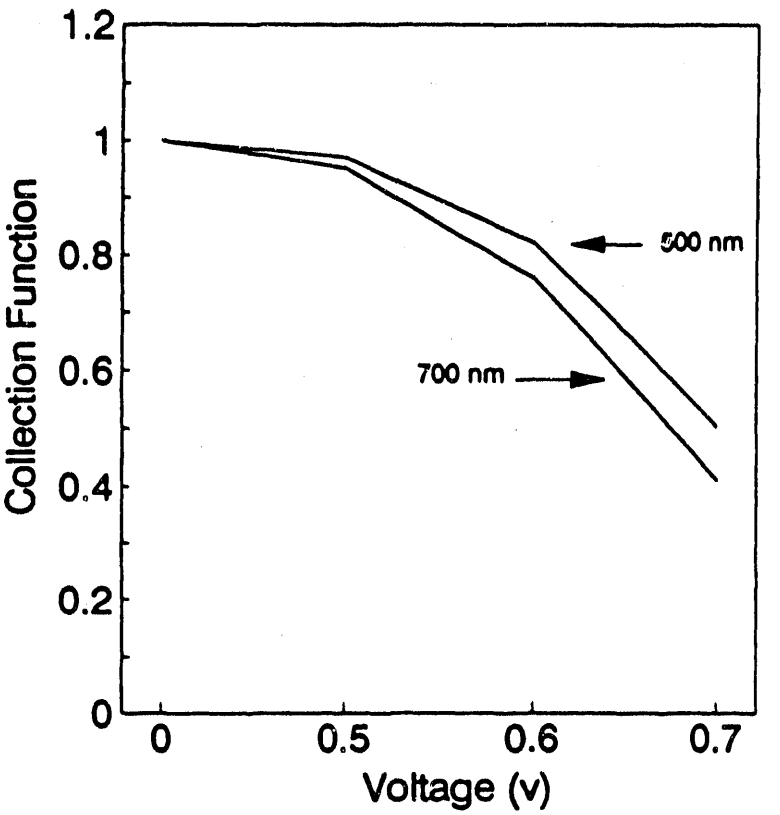

Figure 4. Plot of collection function versus applied bias, calculated from bias-dependent spectral response data of 9.7% MOCVD-CdTe cell.

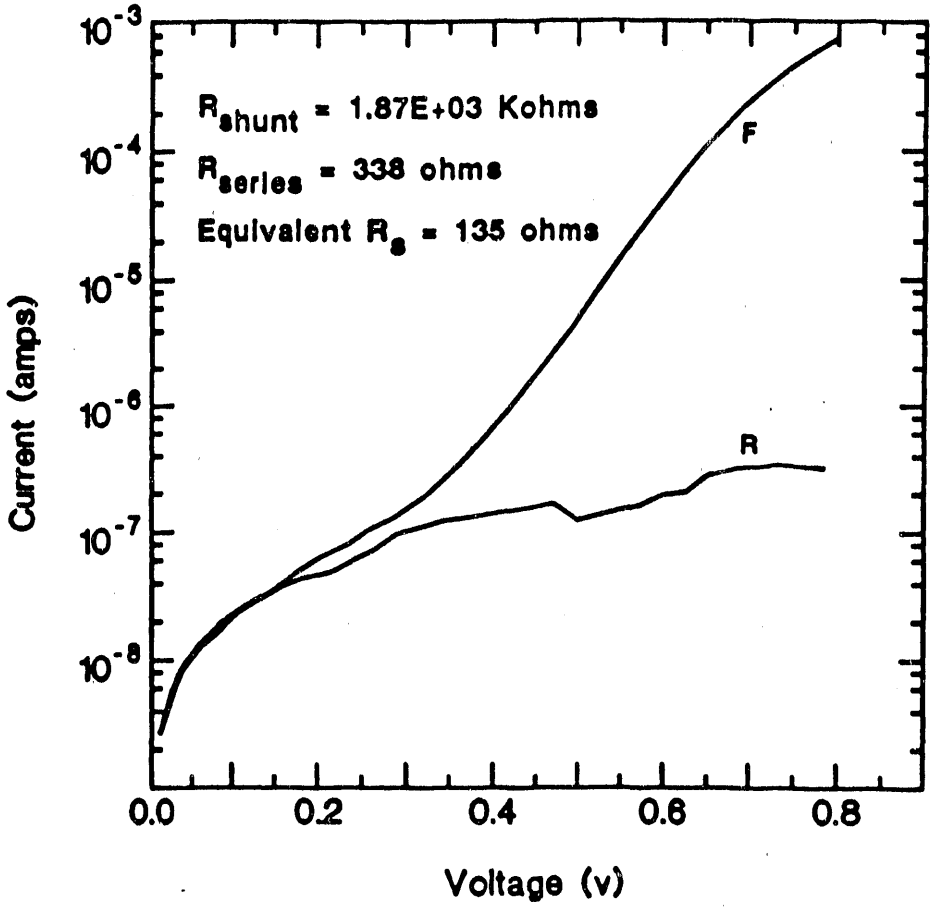

Figure 5. Dark I-V data of 9.7% MOCVD-CdTe cell.

2.4.5. Conclusions

Polycrystalline CdTe films were grown by MOCVD on CdS/SnO_2/glass substrates in order to fabricate frontwall CdTe/CdS solar cells. The CdTe films grown at different temperatures (300 to 400 C) using two different Te alkyls showed uniform composition. The cells fabricated on these films showed efficiencies in the range 8-10% and the maximum efficiency of 9.7%. This is the highest efficiency reported for MOCVD-grown CdTe/CdS cells. The observed J_{sc} in MOCVD cells was higher than the electrodeposited cells on identical substrates but the V_{oc} and fill factor values were lower. Bias-dependent spectral response measurements showed that MOCVD CdTe cell had a higher external quantum efficiency at zero bias, but lower external quantum efficiency at V_{oc}. This is because the external quantum efficiency of MOCVD cells decreases significantly with increasing forward bias voltages. These results suggest that a voltage dependent interface recombination is the dominant mechanism which reduces the V_{oc} and fill factor in MOCVD-grown CdTe/CdS cells. Model calculations were performed to estimate the losses in V_{oc} and fill factor due to interface recombination which were found to be 60 mV and 0.1, respectively. By improving CdTe/CdS interface and thus reducing the collection function effects, the efficiency of MOCVD CdTe cell efficiency can be improved to ~13.5%.

2.5. INVESTIGATION OF POLYCRYSTALLINE CdZnTe, CdMnTe, AND CdTe FILMS FOR PHOTOVOLTAIC APPLICATIONS

(This paper was published in Solar Cells, 27, 219 (1989)).

2.5.1. INTRODUCTION

CdTe is a promising material for high efficiency thin film solar cells due to its near optimum 1.45 eV bandgap, ease of deposition, and strong optical absorption. Polycrystalline thin film heterojunction solar cells have been fabricated using CdTe films on CdS/SnO_2/glass substrates with efficiencies of 10-11% (1-3) with a potential of exceeding 15%. (4) It is well known that cell performance can be increased significantly by fabricating a tandem cell structure with a wide bandgap cell (E_g = 1.65-1.75 eV) on top of a low bandgap cell (E_g = 1.0 eV). A greater than 10% efficient top cell with ~80% subgap transmission coupled with a 12-15% bottom cell can produce a combined cell efficiency of 15-20%. (5) Polycrystalline $CuInSe_2$ cells are well suited for the bottom cell because of its 1 eV bandgap with efficiencies approaching 15%. (6) However, the top cell material has not yet been established. CdZnTe and CdMnTe are two of the promising materials for the top cell application because their bandgaps can be tailored between 1.45-2.26 eV (CdTe-ZnTe) and 1.45-2.85 eV (CdTe-MnTe), respectively, by controlling the film composition.

This paper presents the progress of polycrystalline CdZnTe and CdMnTe solar cells. CdZnTe and CdMnTe films were grown by MBE and MOCVD, respectively, on CdS/SnO_2/glass substrates for solar cell applications. Polycrystalline CdTe cells with efficiencies of 9-10% were fabricated first by both techniques to establish a high efficiency baseline process for II-VI solar cells. The Zn and Mn content was varied to tailor the bandgap to ~ 1.7 eV. Electrical and optical properties of the ternary films were measured before and after annealing in different ambients. Ternary solar cells were fabricated and analyzed. Ternary cell performance was lower than the CdTe cells. Therefore, a combination of measurements were performed to investigate the bulk and interfacial properties of the ternary films in the ZnTe/Cd(Zn,Mn)Te/CdS/SnO_2/glass cell structure to provide guidelines for achieving high efficiency CdZnTe and CdMnTe solar cells.

2.5.2. EXPERIMENTAL PROCEDURE

2.5.2a. Film Growth

CdZnTe and CdTe films were grown by molecular beam epitaxy (MBE) using a Varian Gen II MBE system. Elemental sources of 5N purity or better were used for all constituents. The films were grown on CdS/SnO_2/glass substrates that were baked in vacuum at 250 C for 1-2 hours before commencing film growth. Films were grown in an excess of Te and at a substrate temperature of 275 C for the first 30 min to achieve uniform nucleation which was then increased to 325 C for the remainder of the run. Growth rates were typically ~ 1 um/hr, regardless of film composition. Film purity was monitored using in-situ Auger measurements.

CdTe and CdMnTe films were grown by metalorganic chemical vapor deposition (MOCVD) on CdS/SnO_2/glass substrates using dimethylcadmium, diethyltellurium and diallyltellurium, and BIS (isopropylcyclopentadienyl) manganese as source materials for Cd, Te, and Mn, respectively. The CdMnTe films were grown at a substrate temperatures of 420 C while CdTe films were grown in the range of 300 C to 400 C.

2.5.2b. Cell Fabrication

Front wall solar cells were fabricated with a glass/SnO_2/CdS/CdTe or Cd(Zn,Mn)Te/ZnTe/Ni structure. The ~ 0.15 um n-type CdS layer was deposited on SnO_2 coated glass in a pyrolytic reactor from an aerosol containing $CdCl_2$ and thiourea. Polycrystalline CdTe, CdZnTe, or CdMnTe films were grown on the CdS. No attempts were made to intentionally dope the films. The structure was subsequently annealed under various conditions as described later. The anneal was followed by a mild surface etch of $Br:CH_3OH$ to remove any oxides prior to p-type ZnTe (Cu-doped) evaporation to complete the p-i-n structure. Finally Ni was evaporated to form ohmic contacts on the ZnTe film.

2.5.2c. Material and Device Characterization

Surface photovoltage and depth-resolved Auger measurements were performed to confirm the

bandgaps and compositional uniformity, respectively. X-ray photoelectron spectroscopy (XPS) measurements were performed to investigate the chemical nature of the CdZnTe film surfaces after various heat treatments and surface etching to shed some light on the subsequently formed CdZnTe/ZnTe interface behavior. Selected photoluminescence measurements were performed to investigate defect states of the film. Dark I-V-T measurements were performed in the temperature range of 80 K to 400 K and the data was analyzed using a multivariable regression analysis to determine the pertinent device parameters such as leakage current, diode factor, series and shunt resistances. Spectral response measurements were made using an Optronics Laboratory phase sensitive detection system in which the samples were illuminated through the glass substrate. Lighted I-V measurements were performed under 100 mW AM1.5 conditions to determine the cell efficiency.

2.5.3. RESULTS AND DISCUSSION

2.5.3a. CdTe Solar Cells

CdTe films were grown by both MOCVD and MBE on CdS/SnO_2/glass substrates. P-i-n solar cells were fabricated by depositing p^+-ZnTe capped by Ni to establish a baseline process for the ternary cell development. No attempts were made to intentionally dope the CdTe films. Figure 1 shows the lighted I-V data for our best CdTe cell, grown by MOCVD. The 9.7% efficiency achieved is the highest reported efficiency for MOCVD-grown CdTe. Compared to the best reported CdTe thin film cell to date (11%), fabricated by electrodeposition [7] our cell has a higher J_{sc} (22.16 mA/cm^2) and a lower V_{oc} (0.730 V), Table 1. Spectral response and I-V measurements were performed to understand this difference and to obtain guidelines for improving the CdTe cell performance further.

The spectral response shown in Figure 2 indicates that a true p-i-n heterojunction (rather than a buried homojunction) was formed for this 2.6 um thick CdTe film since the response is not only flat for all the wavelengths ranging from the CdS cutoff (0.5 um) to the CdTe cutoff (0.83 um), but the cutoffs are sharp also. Note that the external quantum efficiency values are over 90% throughout the usable spectrum which is better than the quantum efficiency of the highest efficiency (11%) CdTe cell, Figure 2. [7] This explains the higher J_{sc} value for the MOCVD cell and suggests that under short circuit conditions, the

Table 1 Compilation of cell data for p-i-n CdTe, CdZnTe and CdMnTe cells. All data is for 100 mW/cm^2 AM1.5 illumination. ** Entry is ZnTe/CdZnTe/0.1 um CdTe/CdS structure.

CdTe Cells

ID	Rs (ohm-cm^2)	Jsc (mA/cm^2)	Voc (volts)	Fill Factor	Efficiency (%)
Ga. Tech.	0.72	22.16	0.730	0.59	9.7
Ametek	0.40	20.7	0.760	0.72	10.8

CdZnTe Cells

anneal ambient	Eg (eV)	Rs (ohm-cm^2)	Jsc (mA/cm^2)	Voc (volts)	Fill Factor	Efficiency (%)
air	1.70	2.68	4.00	0.429	0.580	1.0
forming gas	1.70	6.25	5.37	0.566	0.376	1.1
forming gas	1.70	15.5	3.21	0.646	0.298	0.62
air	1.55	1.2	14.4	0.511	0.48	3.6
air**	1.66	2.0	6.2	0.462	0.55	1.6

CdMnTe Cells

anneal ambient	Eg (eV)	Rs (ohm-cm^2)	Jsc (mA/cm^2)	Voc (volts)	Fill Factor	Efficiency (%)
air	1.55	2.0	12.5	0.609	0.427	3.6
none	1.70	9.6	1.82	0.392	0.402	0.3

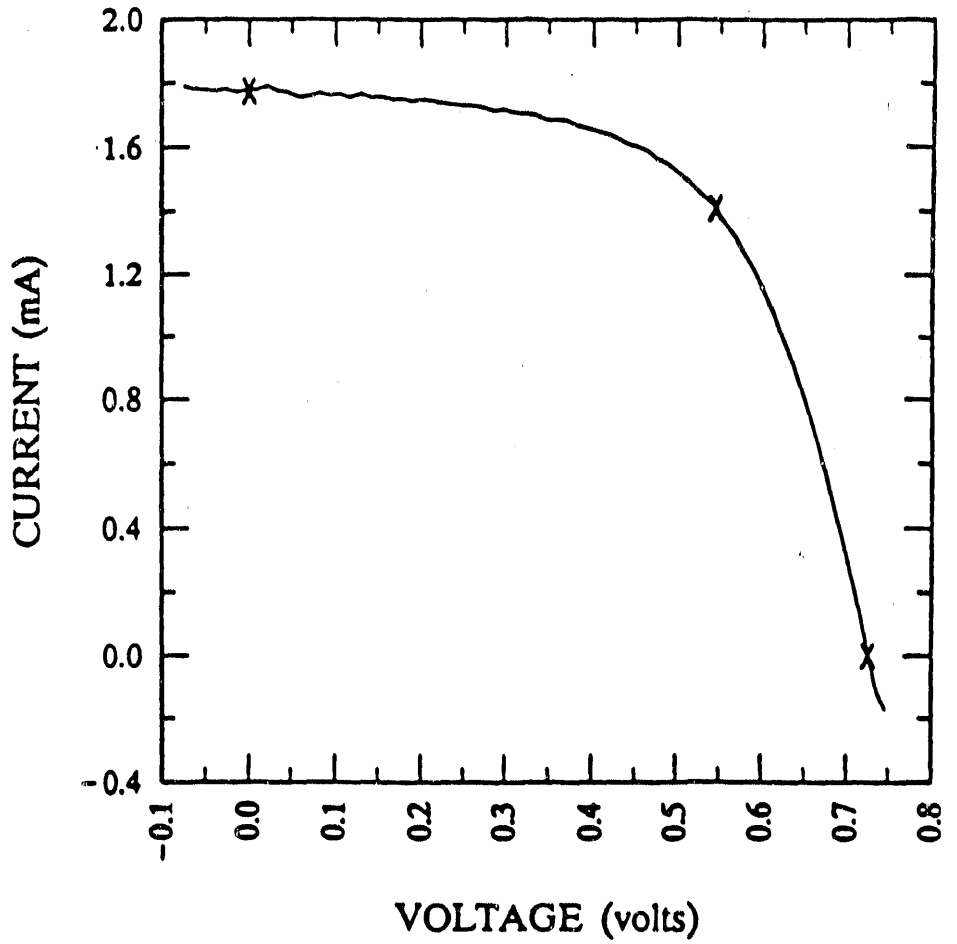

Figure 1. Measured lighted I-V characteristic of 9.7% MOCVD-grown CdTe p-i-n cell having a J_{sc} of 22.16 mA/cm^2, a V_{oc} of 0.730 V, and a fill factor of 0.59.

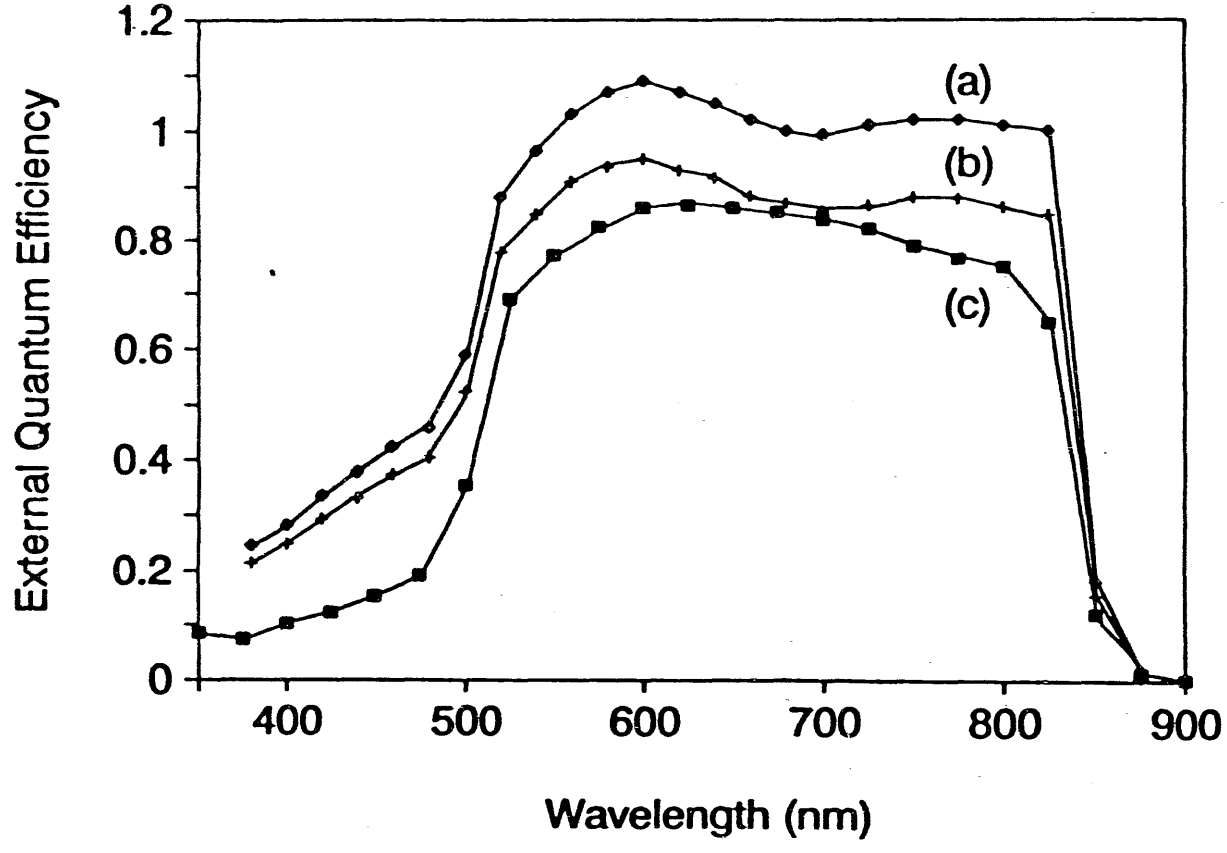

Figure 2. Spectral response of the 9.7% MOCVD-grown CdTe cell for two external bias conditions: (a) no externally applied bias, and (b) 1 volt externally applied reverse bias. The spectral response (no applied bias) of an 11% CdTe cell (7) is shown for comparison.

MOCVD cell has a lower interface recombination velocity. The p-i-n behavior in our cells is supported by C-V measurements which showed that the CdTe is fully depleted at zero bias. Since the bulk CdTe is fully depleted, the interface must play an important role in limiting the cell performance. In order to evaluate the interface quality, bias-dependent spectral response measurements were performed which showed about a 10% uniform increase in the quantum efficiency at 1 volt reverse bias, Figure 2. It has been shown that this type of behavior can be attributed to changes in interface recombination through a field-dependent collection function term which modifies the light-generated current. [4] The 10% increase in quantum efficiency under reverse bias indicates that J_{sc} can be improved significantly to > 24 mA/cm^2 in our cells by lowering the interface recombination velocity. Furthermore, similar measurements on the highest efficiency 11% CdTe cell [7] (Figure 2) showed less than a 5% increase in quantum efficiency under 1 volt reverse bias. It is apparent that the interface state behavior can be different for the MOCVD and electrodeposited CdTe cells. This can result in a different field dependence of carrier collection because of different rate of increase in the interface recombination velocity as the bias condition changes from short circuit to open circuit. I-V and bias dependent spectral response data indicate that compared to electrodeposited cells, MOCVD cells have a lower interface recombination velocity at short circuit but higher interface recombination velocity as the voltage approaches V_{oc}. This explains why the MOCVD cell has a superior J_{sc} but lower V_{oc} and fill factor.

Dark I-V measurements were performed to reveal and understand the loss mechanisms in more detail in these cells. Figure 3a shows the I-V behavior of a ~10% cell over a temperature range of 170-310 K. A multivariable regression analysis was used to fit the I-V curves to an equivalent circuit response consisting of two diodes with a shunt and series resistance so that the current density can be described as a function of the applied voltage by

$$J = J_1 + J_2 = J_{01}[\exp(B_1(V-JR_s) - 1] + J_{02}[\exp(B_2(V-JR_s) - 1] + (V-JR_s)/R_{sh} \quad (1)$$

where

$$B_{1,2} = q/(n_{1,2}kT) \quad (2)$$

At 310 K, the I-V behavior was dominated by one diode (J_2) with a J_{02} value of 1.5 x 10^{-8} A/cm^2, a diode factor n of 1.75, a series resistance (dark) of 5.28 ohm-cm^2, and a 18 kohm-cm^2 shunt resistance, Figure 3b.

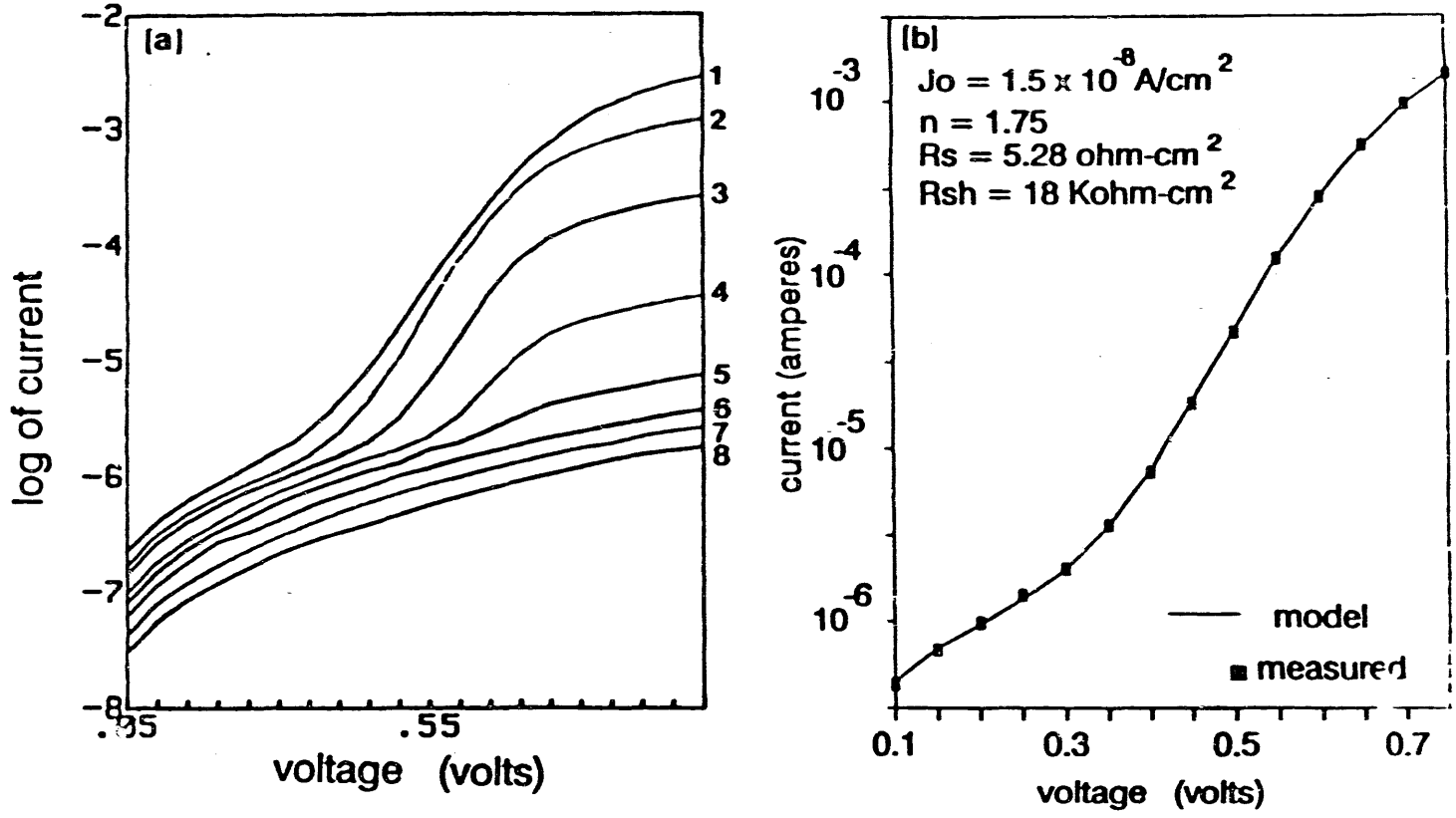

Figure 3. (a) Forward bias dark I-V characteristics measured for the temperature range of 310K (curve 1) to 170 K (curve 8) in steps of 20K, as indicated in the figure (b). An example (310 K) of the theoretical fit to the actual I-V data used to determine the transport parameters.

We also found that as the temperature is lowered from 310 K to 250 K, J_{02} decreases and the diode factor remains close to 1.75, suggesting a space-charge recombination controlled transport mechanism. At temperatures below 250 K, this transport becomes less important and other mechanisms (like tunneling, in addition to increased series resistance) become important, Figure 3. These changes are being analyzed further to shed more light on the characteristics and importance of the interface states. CdTe/CdS cells were also fabricated using MBE-grown CdTe films with efficiencies as high as 9%.

2.5.3b. <u>CdZnTe and CdMnTe Solar Cells</u>

The bandgaps of polycrystalline CdZnTe films grown by MBE and CdMnTe films grown by MOCVD on CdS/SnO_2/glass substrates were successfully tailored to any desired value. However, most emphasis was placed on 1.7 eV bandgap films for tandem cell applications. Based on the success of our CdTe films, ZnTe/CdZnTe/CdS and ZnTe/CdMnTe/CdS p-i-n cells were fabricated using the CdTe cell process. A summary of selected results are shown in Table 1. A post-deposition anneal was found to be necessary to obtain measurable cell data. However, the 410 C annealing procedure used for CdTe cells resulted in a significant decrease in the bandgap, from 1.7 eV to 1.55 eV, with cell efficiencies of 3-4%, Table 1. [8] Annealing in air was performed for various combinations of temperatures and times to determine optimum conditions and to retain the bandgap. A 30 min. anneal at 350 C gave the highest efficiency while maintaining the bandgap for CdZnTe, Table 1. Obviously, a significant decrease in cell performance is observed for the CdZnTe-based devices compared to the CdTe-based cells.

Various measurements were performed to understand the loss mechanisms in ternary cells. C-V measurements made on the CdZnTe cells showed a doping density of ~ $5x10^{15}$ cm^{-3} (p-type) which is about an order of magnitude greater than the measured doping in the MBE-grown CdTe films. This could result in incomplete depletion of the CdZnTe film. This was confirmed by spectral response measurements, Figure 4, which showed a strong wavelength dependence with reduced carrier collection at longer wavelengths. This suggests that, unlike the CdTe cells, these cells are behaving like p-n instead of p-i-n devices and hence are suffering from recombination in the undepleted bulk. Attempts are being made to reduce the film thickness to 1.0-1.5 um to achieve p-i-n-like behavior. However, the undepleted bulk does not explain the very large decrease in the absolute spectral response (Figure 4) compared to CdTe. This drop in response

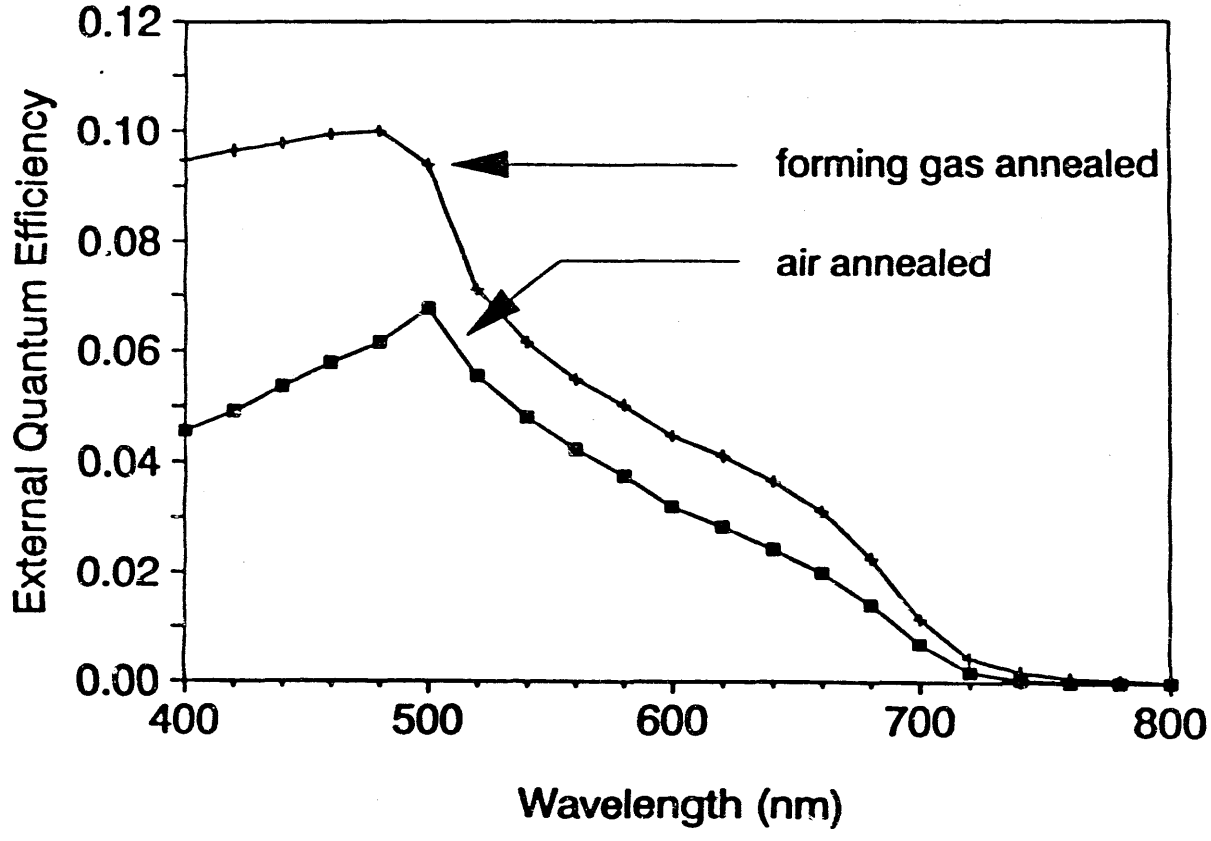

Figure 4. Spectral response of air annealed ZnTe/CdZnTe/CdS and forming gas annealed ZnTe/CdZnTe/CdS p-i-n cells for same CdZnTe thickness.

can only be due to a combination of CdZnTe/CdS interface and back contact region (Ni/ZnTe on CdZnTe) effects.

The most glaring difference between the two types of cells is in the values of series resistance and J_{sc}. Average R_s values (under illumination) were 2-3 ohm-cm^2 for the air annealed CdZnTe cells compared to 0.5-0.8 ohm-cm^2 for CdTe cells. In order to understand the source of high R_s, CdZnTe films were grown intentionally with different bandgaps but the same thickness. Figure 5 shows room temperature dark I-V data taken on three CdZnTe p-i-n cells with different bandgaps (compositions). As seen in the inset of the figure, the dark series resistance increased by a factor of ~4 compared to the CdTe regardless of the CdZnTe composition. The undepleted bulk resistance (~.01 ohm-cm^2) cannot account for the observed high R_s value (2-3 ohm-cm^2), therefore, the back contact region (Ni/ZnTe on CdZnTe) and the CdZnTe/CdS interface were investigated to find the cause of R_s.

Dark I-V and photoluminescence (PL) measurements were performed to analyze the bulk and interface defect states. Figure 5 shows that the value of J_0 steadily increased with increasing Zn concentration suggesting that the interface quality declines for higher Zn concentrations. This is consistent with previous reports on crystalline CdS/CdZnTe junctions in which this kind of degradation was attributed to an increase in interface states resulting from increased distortion of the CdZnTe lattice. [9] This poor interface quality can also explain the low V_{oc} observed in these air annealed films. Furthermore, preliminary photoluminescence measurements show broader luminescence peaks for CdZnTe and CdMnTe compared to CdTe which indicates a more defective bulk for the ternary films compared to CdTe. In order to modify the interface without changing the bandgap, an attempt was made to grow a very thin (~0.1 um) CdTe interlayer between the CdS and CdZnTe. This structure gave a higher J_{sc} but V_{oc} and R_s did not change appreciably suggesting that the high R_s, which is limiting the cell performance, is not due to the CdZnTe/CdS interface.

Since the CdZnTe devices showed poor performance using the air annealing process, various annealing ambients, including forming gas (10% hydrogen + 90% nitrogen) and argon were investigated to see if the performance could be improved by lowering J_0 by passivating bulk and interfacial defects and reducing R_s by avoiding surface oxide formation. Films were subjected to anneals using combinations of temperatures (100-400 C) and times (10 - 50 min) prior to ZnTe and Ni depositions. Surface photovoltage

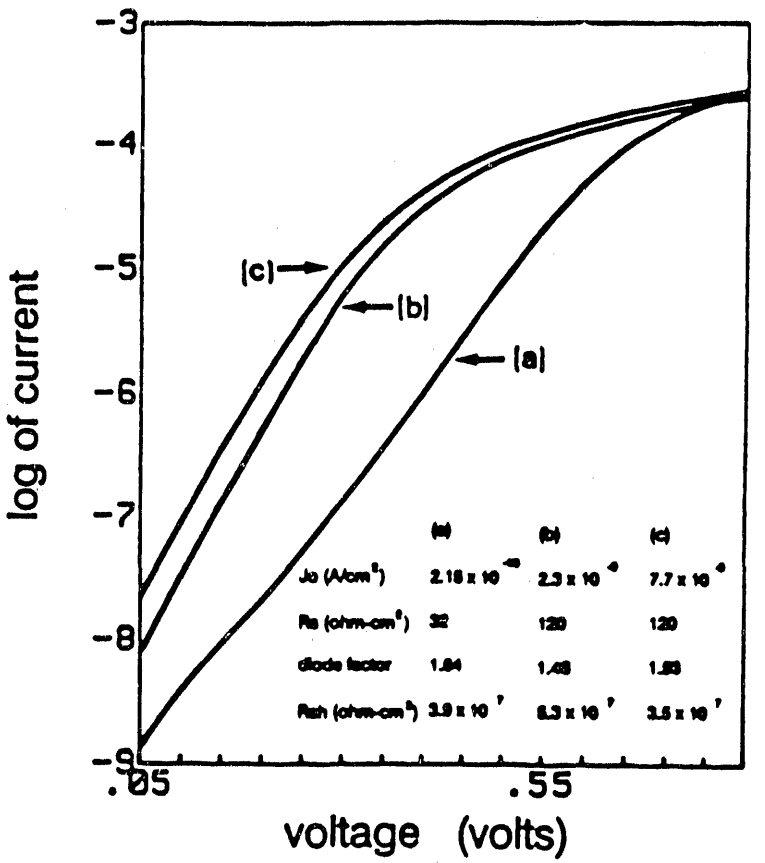

Figure 5. Forward bias dark I-V characteristics for (a) CdTe, (b) CdZnTe (E_g = 1.7 eV), and (c) CdZnTe (E_g = 1.8 eV) cell structures.

measurements showed that the bandgaps were not affected by these annealing conditions. No measurable cell data was obtained for either unannealed or argon annealed CdZnTe cells. In contrast, forming gas annealed films showed the highest V_{oc} values (0.646 V) reported for any CdZnTe/CdS junction. In addition, the J_{sc} values were as high or higher than those for the air annealed cells. However, the series resistance of the forming gas annealed cells was 3-5 times higher than the air annealed CdZnTe cells and about one order of magnitude higher than the CdTe cells. This is also reflected in the extremely low values of fill factor for the forming gas annealed cells (Table 1). Figure 4 shows that the forming gas anneal increases the quantum efficiency almost uniformly over the entire spectrum absorbed in the CdZnTe film as well as on either side of the CdZnTe/CdS junction. This combined with the high V_{oc} indicates that the forming gas anneal improves the interface quality, however the increase in quantum efficiency does not fully depict the huge improvement in V_{oc} because the higher R_s in the forming gas annealed cell lowers the overall spectral response. This also confirms that the high R_s in the CdZnTe cells is not due to the CdS/CdZnTe interface quality which leaves only the back contact region (NI/ZnTe on CdZnTe) as the primary suspect.

In order to investigate if the series resistance is mainly due to the back contact region, the annealed CdZnTe films were analyzed by optical transmission and x-ray photoelectron spectroscopy (XPS). Figure 6 shows the subgap transmission of CdZnTe films on CdS/SnO_2/glass substrates after air, forming gas, and argon anneals for 20 min at 350 C. The as-grown film transmission is also shown for comparison. Air annealing results in about 20% decrease in absolute transmission while the forming gas and argon anneals cause no degradation in transmission. In addition, the transmission of the air annealed CdZnTe/CdS structure decreases even further (~35% decrease in absolute transmission for 30 min at 350 C) with increased time and temperature while the forming gas and argon anneals showed no such tendency. XPS measurements indicate that the surface of the air annealed CdZnTe is rich in Zn content (Table 2) which is mostly oxidized. A 10 sec. etch in .02% $Br:CH_3OH$ removes all of the oxides (and forms a Te-rich surface (Te/(Cd + Zn) = 1.56). However, the CdZnTe surface is not quite as rich in Te as a $Br:CH_3OH$ etched p-CdTe surface where the Te/Cd ratio is typically 2-3. [10,11] Forming gas annealed CdZnTe films, which had the highest R_s, showed an even lower Te/(Cd + Zn) ratio of 1.33. This suggests that the Te rich surface, which makes the surface more p-type, may be important in lowering Rs by increasing the transport of carriers across the CdZnTe/ZnTe interface and improving the current in the external circuit. Attempts are

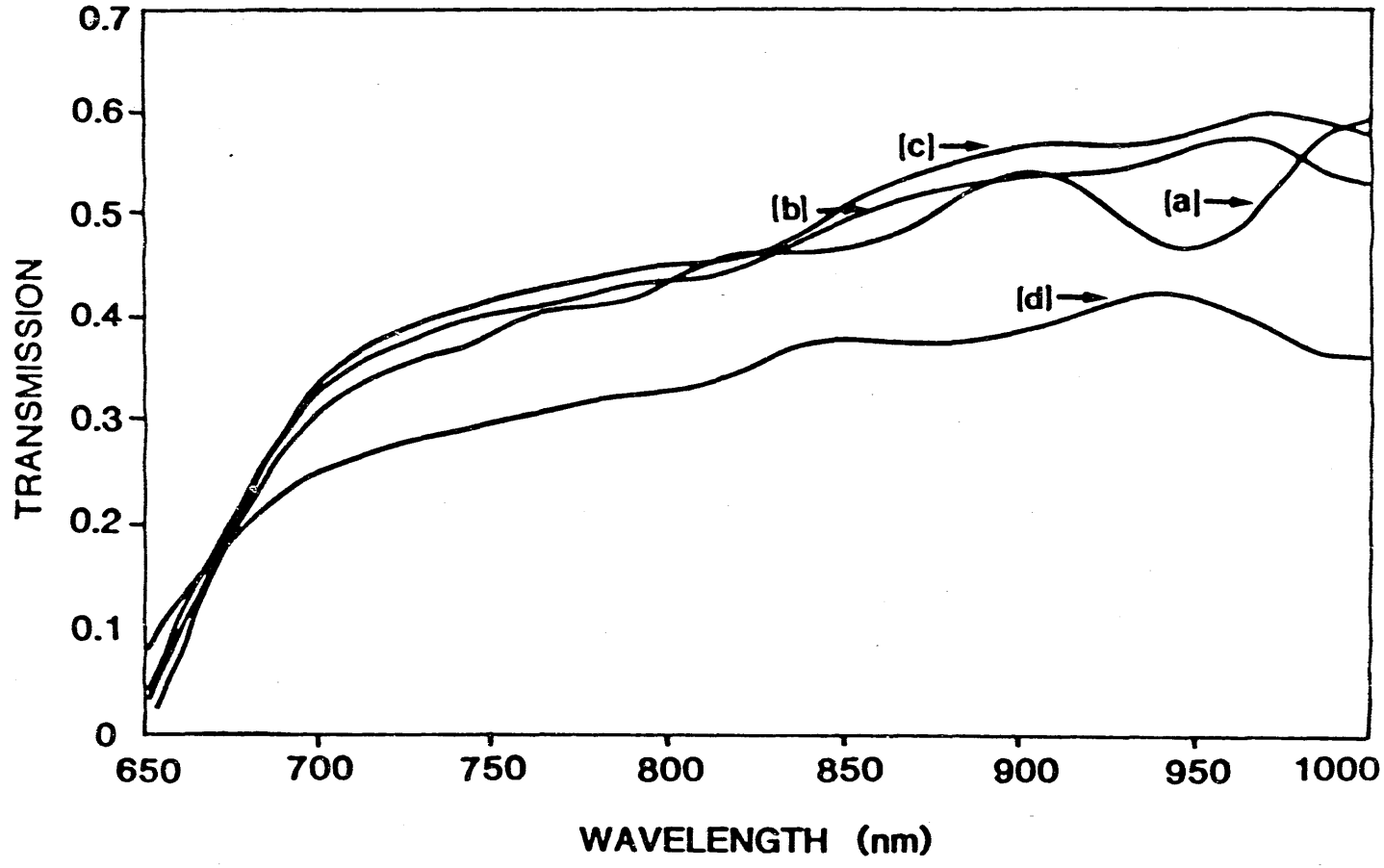

Figure 6. Visible-near IR transmission of CdZnTe, films that have undergone (a) no anneal, (b) argon anneal, (c) forming gas anneal, and (d) air anneal, all for 20 minutes at 350 C.

Table 2 Relative concentrations of Cd,Zn and Te in CdZnTe films processed as indicated in the table. Oxidized species are indicated.

element	as-grown	air annealed	Br:CH_3OH etch	H_2 + N_2 anneal	Br:CH_3OH etch	argon anneal	Br:CH_3OH etch
Cd	.56	.29	.66	.50	.67	.43	.67
Zn	.44	.71	.34	.50	.33	.57	.33
Te	1.1	.57	1.56	1.0	1.33	.86	1.5

being made to investigate various etching techniques to make the CdZnTe surface more Te-rich and to improve the CdZnTe/ZnTe interface. This combined with a forming gas anneal to reduce interface states, and thinning the CdZnTe film to obtain true p-i-n devices is expected to give a significant improvement in the cell performance.

2.5.4. CONCLUSIONS

Front wall polycrystalline thin film solar cells with Ni/ZnTe/CdTe/CdS/SnO_2/glass structures were fabricated with efficiencies in the range of 9-10%. CdTe films were grown by MBE and MOCVD techniques. Spectral response and dark I-V analyses showed that these cells behave like p-i-n diodes and their response is limited in part by high interface recombination velocity.

CdZnTe and CdMnTe films of 1.7 eV bandgap were grown by MBE and MOCVD, respectively, for tandem cell applications. The standard CdTe process was not optimum for ternary films and resulted in a decrease in the bandgap. A 350 C, 30 min anneal in air was found to improve the efficiency of CdZnTe cells while still maintaining the bandgap. However, the air annealed CdZnTe cells showed both high series resistance and high J_0 values compared to the CdTe cells resulting in low cell performance. It was found that annealing the CdZnTe films in forming gas increased the V_{oc} to ~ 0.65 V, the highest reported value for CdZnTe/CdS junctions, as compared to ~ 0.4 V for air annealed CdZnTe by improving the interface quality. However, the series resistance increased by an additional factor of ~ 3 which resulted in low cell performance in spite of the high V_{oc} on the CdZnTe cells. Spectral response measurements suggest that the CdZnTe cells do not behave as a true p-i-n diode but instead as a p-n cell, probably due to a higher doping level. The series resistance contribution due to the undepleted CdZnTe region was not found to be a major factor in the observed high series resistance of the cell. Thus, the back contact region and the CdZnTe/CdS interface states together may be responsible for limiting the cell performance. Hence, a combination of forming gas anneal and proper surface etching prior to contact formation is being investigated to achieve low R_s, high fill factor, and better cell performance. In addition, novel structures are also being studied which involve a thin (.1 um) interlayer of CdTe between the CdZnTe and CdS to increase the quality of the CdZnTe/CdS interface. Preliminary results have shown higher J_{sc} values for this structure than for the conventional CdZnTe device, without any significant change in the observed cutoff of the

CdZnTe.

SUMMARY

Polycrystalline $Cd_{1-x}Zn_xTe$ and $Cd_{1-x}Mn_xTe$ films with a bandgap of 1.7 eV were successfully grown on glass/SnO_2/CdS substrates by MBE and MOCVD techniques, respectively. Polycrystalline $Cd_{1-x}Zn_xTe$ films grown by MBE resulted in uniform composition and sharp interfaces, which are important for high performance devices. However, polycrystalline $Cd_{1-x}Mn_xTe$ films grown by MOCVD had nonuniform composition and showed evidence of Mn accumulation at the $Cd_{1-x}Mn_xTe$/CdS interface. It was found that Mn interdiffuses and replaces Cd in the CdS film. A CBE system for the growth of HgZnTe has been designed and constructed The growth of CdTe, HgTe, and HgZnTe has been demonstrated.

Frontwall CdTe/CdS solar cells fabricated on MOCVD-grown CdTe films showed efficiencies in the range 8-10% and the maximum efficiency of 9.7%. This is the highest efficiency reported for MOCVD-grown CdTe/CdS cells. Bias-dependent spectral response measurements showed that MOCVD CdTe cell had a higher external quantum efficiency at zero bias, but lower external quantum efficiency at V_{oc}. These results suggest that a voltage dependent interface recombination is the dominant mechanism which reduces the V_{oc} and fill factor in MOCVD-grown CdTe/CdS cells. Model calculations were performed to estimate the losses in V_{oc} and fill factor due to interface recombination which were found to be 60 mV and 0.1, respectively. By improving CdTe/CdS interface and thus reducing the collection function effects, the efficiency of MOCVD CdTe cell efficiency can be improved to ~ 13.5%. MBE-grown CdTe cells also gave efficiency in the range 8-9%.

Standard processing procedures used in the successful fabrication of high efficiency polycrystalline CdTe solar cells such as air annealing were found to provide the desired p-type enhancement of the CdZnTe bulk, however it resulted in extensive oxidation of Zn into the bulk and accumulation of Zn near the film surface. Subsequent etching in a standard Bromine-Methanol etch which was successfully used for CdTe cells removed only the surface oxides of Te and Cd from the CdZnTe surface but could not remove the Zn-O or the Zn-rich surface region to create a p^+ Te-rich surface which is necessary for low contact resistance to the CdZnTe surface. It was found that the removal of the thin surface layer of oxidized Te and Cd by the B-M etch reduced the series resistance of In/CdZnTe Schottky barrier diodes and yielded a diode-like I-V characteristic with a barrier height of ~1.2 eV. An alternate etch consisting of a concentrated dichromate

B-M etch reduced the series resistance of In/CdZnTe Schottky barrier diodes and yielded a diode-like I-V characteristic with a barrier height of ~1.2 eV. An alternate etch consisting of a concentrated dichromate solution was found to remove all oxides and resulted in a highly Te-enriched surface with a thickness of ~0.25 um and with a doping level of ~$2x10^{17}$ cm^{-3} compared to ~$3x10^{15}$ cm^{-3} doping concentration within the bulk of the CdZnTe film. These results suggest that an air anneal followed by a dichromate etch of the CdZnTe solar cell structure should siginificantly improve the ohmic behavior of the back contact which is necessary to increase present-day CdZnTe cell efficiency.

The standard CdTe process was not optimum for ternary films and resulted in a decrease in the bandgap. Efficiency as high as 4% was obtained on both CdZnTe and CdMnTe films with reduced bandgaps while poor efficiency was obtained on ternary films with 1.7 eV bandgap. CdZnTe cells showed both high series resistance and high J_0 values compared to the CdTe cells resulting in low cell performance. Spectral response measurements suggest that the CdZnTe cells do not behave as a true p-i-n diode but instead as a p-n cell, probably due to a higher doping level. Recent results indicate that $CdCl_2$ + $ZnCl_2$ chemical treatment may prevent the bandgap reduction, while chromate etch, instead of bromine-methanol etch, may provide the solution to high contact resistance in the ternary cells.

In future, we plan to apply the basic understanding developed through materials characterization, process development, and device analysis to improve the CdTe and CdZnTe cell performance. We intend to a). investigate preheat treatments of CdS, prior to CdTe deposition, to improve interface quality, b). Optimize $CdCl_2$ + $ZnCl_2$ chemical treatment to improve the CdZnTe cell efficiency and to understand the exact role of chloride treatment, c). optimize $K_2Cr_2O_7$:H_2SO_4 treatment to reduce the series resistance of ternary cells, and d). investigate carrier transport mechanisms to develop a better qualititative and quantitative understanding of interface recombination mechanisms in CdTe and CdZnTe devices.

ACKNOWLEDGEMENTS

The authors would like to thank Dr. P.V. Meyers, Dr. C.H. Liu, Dr. V. Ramanathan, and Laurie Russell of AMETEK applied materials laboratory for their help in depositing CdS and fabrication of cells, Dr. Pat Gillis and Dr. Owens of chemistry for XPS measurements, Dr. Brent Carter of Material Science Department for his help in AES measurements, K.T. Pollard for the help in MOCVD growth, D. Rajavel for the help in MBE growth, and Dr. E.A. Meeks and M.H. MacDougal for the help in experimental work.

We would like to thank K. Zweibel, R.L. Mitchell and K. Emery of SERI for helpful discussions and cell measurements.

4. REFERENCES

Section 2.1

1. P.K. Raychaudhuri, J. Appl. Phys., 62, 3025 (1987).
2. S.P. Albright, J.F. Jordan, B. Ackerman, and R.R. Chamberlin, Proc. Polycrystalline Thin Film Program Review Meeting, 17 (1989).
3. J.C.C. Fan, Proc. of SPIE, 30, 543 (1985).
4. M.G. Peters, A.L. Fahrenbruch, and R. Bube, J. Vac. Sci. Technol., A6, 3098 (1988)
5. B.M. Basol, V.K. Kapur, R.C. Kullberg, and R.L. Mitchell, Proc. 20th IEEE Photovoltaic Spec.Conf., 1500 (1988).
6. T.L. Chu, S.S. Chu, F. Firszt, and C. Herrington, J. Appl. Phys., 59, 1259 (1986).
7. J. Nelson, D. Riley, Proc. Phys. Soc. (London), 57, 160 (1945).
8. J.C. Wooley and B. Ray, J. Phys. Chem. Solids, 13, 151 (1960).
9. A. Nouhi and R.J. Stirn, Appl. Phys. Lett., 51, 2251 (1987).
10. P. Rhood, J. Appl. Phys., 58, 2288 (1985).
11. S.A. Ringel, A. Rohatgi, and S.P. Tobin, IEEE Trans. Electron Dev., 36 (7), 1230 (1989).
12. M. Migita, O. Kanehisa, M. Shiiki, and H. Yamamoto, J. Cryst. Growth, 93, 686 (1988).
13. I. Brian and O. Knacke, Thermochemical Properties of Inorganic Substances, Supplement (Springer, Berlin, 1977).
14. A. Rohatgi, C.J. Summers, A. Erbil, R. Sudharsanan, S.A. Ringel, P.V. Meyers, and C.H. Liu, Proc. Polycrystalline Thin Film Program Review Meeting, 45 (1989).

Section 2.2.

1. W.T.Tsang, Appl. Phys. Lett. 45, 1234 (1984).
2. M. Boukerche, P.S. Wijewarnasuriya, S. Sivananthan, I.K. Sou, Y.J. Kim, K.K. Mahavadi, and J.P. Faurie, J. Vac. Sci. Technol. A6, 2380 (1988).
3. P.S. Wijewarnasuriya, I.K. Sou, Y.J. Kim, K.K. Mahavadi, S. Sivananthan, M. Boukerche, and J.P. Faurie, Appl. Phys. Lett. 51, 2025 (1987).
4. D.J. Peterman, M.L. Wroge, B.J. Morris, D.J. Leopold, and J.G. Broerman, J. Appl. Phys., 63 1951

(1988).

5. M. Boukerche, J. Reno, I.K. Sou, C. Hsu, and J.P. Faurie, Appl. Phys. Lett. 48, 1973 (1986).

6. R.N. Bicknell, N.C. Giles, and J.F. Schetzina, Appl. Phys. Lett. 49, 1735 (1988).

7. J.D. Benson, D. Rajavel, B.K. Wagner, R.G. Benz II, and C.J. Summers, J. Crystal Growth 95, 543 (1989).

8. J.T. Cheung, Appl. Phys. Lett. 51, 1940 (1987).

9. D. Rajavel, J.D. Benson, R.G. Benz II, B.K. Wagner, and C.J. Summers, Tenth MBE Workshop, Raleigh, NC Sept. 1989 (to be published in J. Vac. Sci. Technol.).

10. B.K. Wagner, R.G. Benz II, and C.J. Summers, J. Vac. Sci. Technol. A7, 295 (1989).

11. H. Heinecke, K. Werner, M. Weyers, H. Luth, and P. Balk, J. Crystal Growth 81, 270 (1987).

12. D.J. Santeler, J. Vac. Sci. Technol. A4 348 (1986).

13. A. Sher, D. Egan, A. Zemel, H. Feldstein, and A. Ratzman, J. Vac. Sci. Technol. A4 2024 (1986).

Section 2.3.

1. S.P. Albright, J.F. Jordan, B. Ackerman, and R.R. Chamberlain, Proc. Polycryst. Thin Film Prog. Rev. Meeting, 17 (1989).

2. B.M. Basol, J. Appl. Phys. 58 (10), 3809 (1985).

3. T.C. Anthony, A.L. Fahrenbruch, R.H. Bube, J. Electron. Mat. 11(1), 89 (1982).

4. P.V. Meyers, Solar Cells 24, 35 (1988).

5. H. Matsumoto, K. Kuribayarshi, H. Uda, Y. Komatsu, A. Nakano, and S. Ikegami, Solar Cells 11, 367 (1984).

6. Y.S.Tyan and E.A. Perez-Albuerne, Proc. 16th IEEE Photovoltaic Spec. Conf., 794 (1982).

7. A. Rohatgi, C.J. Summers, A. Erbil, R. Sudharsanan, S.A. Ringel, P.V. Meyers, and C.H. Liu, Proc. Polycryst. Thin Film Prog. Rev. Meeting, 45 (1989).

8. J.C.C. Fan, Proc. of SPIE 30, 543 (1989).

9. K.W. Mitchell, C. Eberspacher, J. Ermer, and D. Pier, Proc. 20th IEEE Photovoltaic Spec. Conf., 1384 (1988).

10. W.J. Danaher, L.E. Lyons, M. Marychurch, and G.C. Morris, Appl. Surf. Sci. 27, 538 (1986).

11. W.J. Danaher, L.E. Lyons, G.C. Morris, Appl. Surf. Sci. 22/23, 1083 (1985).

12. J.C. Werthen, J.P. Haring, A.L. Fahrenbruch, R.H. Bube, J. Phys. D. Appl. Phys. 16, 2391 (1983).

13. J.C. Werthen, J.P. Haring, A.L. Fahrenbruch, R.H. Bube, J. Appl. Phys. 54 (10), 5982 (1983).

14. S.A. Ringel, R. Sudharsanan, A. Rohatgi, and W.B. Carter, submitted to J. Electron. Mat. (1989).

15. D. Briggs and M.P. Seah, "Practical Surface Analysis by Auger and Photoelectron Spectroscopy," Wiley and Sons (1983).

16. S.S. Choi and G. Lucovsky, J. Vac. Sci. Technol. B6 (4), 1198 (1988).

17. T. Taguchi, T. Sasaki, T. Terada, M. Ekawa, and A. Hiraki, J. Cryst. Growth 86, 819 (1988).

18. M.G. Peters, A.L. Fahrenbruch, and R.H. Bube, J. Appl. Phys. 64, 3106 (1988).

19. M. Nakamura, T. Kato, and N. Oi, Jap. J. Appl. Phys. 7 (5), 512 (1968).

20. M.G. Peters, Ph.D. Thesis, Stanford University (1987).

Section 2.4.

1. S. P. Albright, B. Ackerman, R. R. Chamberlin, and J. F. Jordan, Proc. of the Polycrystalline Thin Film Program Meeting, 17, (1989).

2. J. R. Sites, Proc. 20th IEEE Photovoltaic specialists conference, 1604, (1989).

3. P. V. Meyers and C. H. Liu, Proc. 4th International Photovoltaic Specialists Conference, 881, 1989.

4. J. C. C. Fan, Proc. SPIE, 543, 30, (1985).

5. K. Zweibel and A. Hermann, Proc. SPIE, 543, 119, (1985).

6. R. H. Bube, Solar Cells, 23, 1, (1988).

7. A. Nouhi, R. J. Stirn, P. V. Meyers, and C. H. Liu, J. Vac. Sci. Technol. A7, 833, (1989).

8. M. Eron and A. Rothwarf, Appl. Phys. Lett. 44, 131, (1984).

9. R. R. Potter, C. Eberspacher, and L. B. Fabick, Proc. 18th IEEE Photovoltaic Specialists Conference, 1659 (1985).

10. J. E. Phillips and M. Roy, Proc. 20th IEEE Photovoltaic Specialists Conference, 1614, (1989).

11. A. Rothwarf, Solar Cells, 2, 115, (1980).

12. M. Eron and A. Rothwarf, J. Appl. Phys. 57, 2275, (1985).

Section 2.5.

1 T.L. Chu, S.S. Chu, S.T. Ang, K.D. Han, Y.Z. Liu, K. Zweibel, and H.S. Ullal, Proc. IEEE 19th

Photovolt. Spec. Conf., 1466, (1987).

2 Y.S. Tyan and E.A. Perez-Alburee, Proc. 15th IEEE Photovolt. Spec. Conf., (1982) 794.

3 P.V. Meyers, Solar Cells, 24, 35 (1988).

4 K.W. Mitchell, A.L. Fahrenbruch, and R.H. Bube, J. Appl. Phys. 48, 4365 (1977).

5 J.C.C. Fan, Proc. SPIE, 30, 543 (1985).

6 K.W. Mitchell, C. Eberspacher, J. Ermer, and D. Pier, Proc. 20th IEEE Photovolt. Spec. Conf.,

7 P.V. Meyers and C.H. Liu, Proc. 4th Int. Photovolt. Sci. Eng. Conf. (1989).

8 A. Rohatgi, R. Sudharsanan, S.A. Ringel, P.V. Meyers, and C.H. Liu, Proc. 20th IEEE Photovolt. Spec. Conf., .

9 M.G. Peters, A.L. Fahrenbruch, and R.H. Bube, J. Appl. Phys., 64, 3106 (1988).

10 Z. Sobiesierski, I.M. Dharmadasa, and R.H. Williams, Appl. Phys. Lett., 53, 2623 (1988).

11 B.M. Basol, S.S. Ou, and O.M. Stafsudd, J. Appl. Phys., 58, 3809 (1985).

LIST OF PUBLICATIONS AND PRESENTATIONS

Journal Papers

1. A. Rohatgi, S. A. Ringel, J. Welch, E. Meeks, K. T. Pollard, A. Erbil, C. J. Summers, P. V. Meyers, and C. H. Liu, "Growth and Characterization of CdMnTe and CdZnTe Polycrystalline Thin Films For Solar Cells", Solar Cells, 24, 185-194, 1988.

2. Z. C. Feng, R. Sudharsanan, S. Perkowitz, A. Erbil, K. T. Pollard, and A. Rohatgi, "Raman Scattering Characterization of High-Quality CdMnTe Films Grown by Metalorganic Chemical Vapor Deposition", J. Appl. Phys., 64, 6861-6863, 1988.

3. R. Sudharsanan, Z. C. Feng, S. Perkowitz, A. Rohatgi, K. T. Pollard, and A. Erbil, "Characterization of Thin CdMnTe Films by Infrared Spectroscopy", J. Electronic Materials. 18, 453-455, 1989.

4. Z. C. Feng, S. Perkowitz, R. Sudharsanan, A. Erbil, K. T. Pollard, and A. Rohatgi, "Photoluminescence of CdMnTe Films Grown by Metalorganic Chemical Vapor Deposition", J. Appl. Phys., 66, 1711-1716, 1989.

5. S. A. Ringel, R. Sudharsanan, A. Rohatgi, and W. B. Carter, "A Study of Polycrystalline Cd(Zn,Mn)Te/CdS Films and Interfaces," J. Electronic materials (In Print).

6. A. Rohatgi, S. A. Ringel, R. Sudharsanan, C. J. Summers, P. V. Meyers, C.H. Liu, and V. Ramanathan, "Investigation of CdZnTe and CdMnTe Polycrystalline films for Photovoltaic applications," Solar Cells, 27, 219-230 (1989).

7. S. A. Ringel, R. Sudharsanan, A. Rohatgi, M. S. Owens, and H. P. Gillis, "Effects of Annealing and Surface Preparation on the Properties of MBE-grown Polycrystalline CdZnTe Films," Submitted to J. Vacuum Science and Tech. (In Print).

8. R. G. Benz II, B. K. Wagner, and C. J. Summers, "Growth of CdTe and Hg-based alloys by chemical beam epitaxy," J. Vac. Sci. Tech. (In Print).

9. R. Sudharsanan and A. Rohatgi, "Investigation of MOCVD-grown CdTe/CdS solar cells," Submitted to J. Appl. Phys.

Conference Presentations with Proceedings (refereed)

1. A. Rohatgi, R. Sudharsanan, S. A. Ringel, P. V. Meyers, and C. H. Liu, "Wide Bandgap Thin Film Solar Cells From CdTe," Proceedings of the 20th IEEE Photovoltaic Specialists Conference, 1477-1481, 1988.

2. S. Perkowitz, Z. C. Feng, A. Erbil, R. Sudharsanan, K. T. Pollard, and A. Rohatgi, "Raman and Photoluminescence Analysis of CdMnTe Thin Films", Proceedings of SPIE Vol. 1055, Raman and Luminescence Spectroscopies in Technology, (In Print).

Conference Presentations (Oral Presentation Only)

1. R. Sudharsanan, S. Perkowitz, and A. Rohatgi, "Characterization of Thin CdMnTe Films by Infrared Spectroscopy," Bulletin of the American Physical Society, 33, 398, 1988.

2. R. Sudharsanan, Z. C. Feng, S. Perkowitz, A. Rohatgi, K. T. Pollard, and A. Erbil, "Characterization of MOCVD-Grown CdMnTe Films by Infrared, Raman, and Photoluminescence Spectroscopy," 35th National Symposium of the American Vacuum Society, Atlanta, GA, Oct. 2-7, 1988.

3. A. Rohatgi and S. A. Ringel, "Characterization and Modeling of High-Efficiency GaAs Heteroface Solar Cells." Joint Crystalline Cell Research and Concentrating Collector Projects Review Meeting, Sandia National Laboratories, Albuquerque, NM, July 19-21, 1988.

4. A. Rohatgi, R. Sudharsanan, S. A. Ringel, C. J. Summers, P. V. Meyers, and C. H. Liu, "Investigation of CdZnTe and CdMnTe Polycrystalline Films for Photovoltaic Applications", Proc. PVAR and D 9th Review Meeting, 55, 1989.

5. A. Rohatgi, C. J. Summers, A. Erbil, R. Sudharsanan, S. A. Ringel, P. V. Meyers, and C. H. Liu, "Current Status and Future Directions of Cd(Zn, Mn)Te/CdS Solar Cells", Proc. Polycrystalline Thin Film Program Meeting, 45-50, 1989, SERI/CP -211-3550.

6. R. Sudharsanan, K. T. Pollard, A. Erbil, A. Rohatgi, "MOCVD Growth of CdTe and CdMnTe Films for Photovoltaic Applications", Fourth Biennial Workshop on Organometallic Vapor Phase Epitaxy, Monterey, CA, Oct. 8-11, 1989.

7. A. Rohatgi, "CdTe and ZnTe Based Solar Cells", DOE Peer Review of Photovoltaic Research, held at Denver, CO, 1989.

8. S. A. Ringel, R. Sudharsanan, A. Rohatgi, M. S. Owens, and H. P. Gillis, "Effects of Annealing and Surface Preaparation on the Properties of MBE-grown Polycrystalline Films", 36th National Symposium of the American Vacuum Society, Boston, MA, Oct. 23-27, 1989.

Document Control Page	1. SERI Report No. SERI/TP-211-3952	2. NTIS Accession No. DE91002112	3. Recipient's Accession No.
4. Title and Subtitle High-Efficiency Cadmium and Zinc Telluride-Based Thin Film Solar Cells			5. Publication Date October 1990 6.
7. Author(s) A. Rohatgi, C. J. Summers, A. Erbil, R. Sudharsanan, and S. Ringel			8. Performing Organization Rept. No.
9. Performing Organization Name and Address School of Electrical Engineering Georgia Institute of Technology Atlanta, Georgia 30332			10. Project/Task/Work Unit No. PV040301 11. Contract (C) or Grant (G) No. (C) XL-7-06031-1 (G)
12 Sponsoring Organization Name and Address Solar Energy Research Institute 1617 Cole Blvd. Golden, CO 80401			13. Type of Report & Period Covered Technical report 14.

15. Supplementary Notes
SERI technical monitor: R. Mitchell

16 Abstract (Limit: 200 words)

Polycrystalline $Cd_{1-x}Zn_xTe$ and $Cd_{1-x}Mn_xTe$ films with a band gap of 1.7 eV were successfully grown on glass/SnO_2/CdS substrates by molecular beam epitaxy (MBE) and metal-organic chemical vapor deposition (MOCVD), respectively. Polycrystalline $Cd_{1-x}Zn_xTe$ films grown by MBE resulted in uniform composition and sharp interfaces. However, polycrystalline $Cd_{1-x}Mn_xTe$ films grown by MOCVD showed nonuniform compositions and evidence of manganese accumulation at the $Cd_{1-x}Mn_xTe$/CdS interface. We found that manganese interdiffuses and replaces cadmium in the CdS film. By improving the CdTe/CdS interface and, thus, reducing the collection function effects, the efficiency of the MOCVD CdTe cell can be improved to about 13.5%. MBE-grown CdTe cells also produced 8%-9% efficiencies. The standard CdTe process was not optimum for ternary films and resulted in a decrease in the band gap. Recent results indicate that $CdCl_2$ + $ZnCl_2$ chemical treatment may prevent the band-gap reduction, and that chromate etch (rather than bromine etch) may provide the solution to contact resistance in the ternary cells.

17. Document Analysis
a. Descriptors
photovoltaics ; solar cells ; thin films ; cadmium telluride ; graded band gap ; high efficiency

b. Identifiers/Open-Ended Terms
zinc telluride

c. UC Categories
270

18. Availability Statement	19. No. of Pages
National Technical Information Service U.S. Department of Commerce 5285 Port Royal Road Springfield, VA 22161	90 20. Price A05

Form No. 0069E (6-30-87)

END

DATE FILMED

12/10/90